

Exploring the biosynthesis and
physiological function of gibberellin-
related compounds in the liverwort
Marchantia polymorpha

SUN, Rui

Table of Contents

Abstract	1
Abbreviations	3
Chapter 1 Introduction	5
The phytohormone gibberellin	5
GA metabolism in flowering plants.....	6
Evolution of GA biosynthesis.....	7
GA signaling and evolution	8
Involvement of GA in light responses	10
R/FR responses in <i>M. polymorpha</i>	11
Chapter 2 Results	13
Evolution history of KO and KAO homologs in <i>M. polymorpha</i>	13
MpKOL1 and MpKAOL1 catalyzes the biosynthesis of KA and GA ₁₂	17
Subcellular localization of GA biosynthesis enzymes.....	19
FR enrichment promoted the biosynthesis of GA ₁₂ in <i>M. polymorpha</i>	21
MpCPS loss-of-function altered thallus growth under FR-enriched conditions	23
MpCPS is required for gemma dormancy in the gemma cup.....	27
MpCPS participates in the regulation of gametangiophore formation	28
Mp <i>cps</i> ^{ld} can be rescued by KA but not canonical GAs	33
KA is a crucial intermediate in GA _{Mp} biosynthesis	34
Genetic redundancy of GA _{Mp} biosynthesis enzymes.....	38
Transcriptional response to FR enrichment is modulated by GA _{Mp}	41
Chapter 3 Discussion	46
GA _{Mp} serves as a phytohormone in <i>M. polymorpha</i>	46
GA _{Mp} modulates growth anisotropy in response to FR enrichment.....	46
The biosynthetic route of GA _{Mp}	47
Evolution of GA-related phytohormones in land plants.....	48
Chapter 4 Materials and Methods	50
Bibliography	62
Acknowledgments	79

Abstract

The emergence of land plants from streptophyte algae brought about many evolutionary innovations, including the biosynthesis of several plant hormones. Gibberellins (GAs) are a group of diterpenoid hormones that was likely evolved within the land plant lineage. Despite the chemical diversity of GA-related compounds, vascular plants synthesize a few bioactive GAs through a conserved pathway. Meanwhile, the other clade of land plants, i.e., bryophytes, only possess genes to produce GA precursors such as *ent*-kaurenoic acid (KA) and GA₁₂. It has been shown that in the moss *Physcomitrium patens*, KA and its derivative act as a plant hormone to regulate protonema differentiation, blue light avoidance and spore germination. Yet in other bryophyte species, the function of GA precursors is still unclear.

The liverwort *Marchantia polymorpha* encodes four types of evolutionarily conserved GA biosynthesis enzymes: *ent*-copalyl diphosphate synthase (CPS), *ent*-kaurene synthase (KS), *ent*-kaurene oxidase (KO) and *ent*-kaurenoic acid oxidase (KAO). Enzymatic assay from a previous study identified MpCPS and MpKS as functional homologs of CPS and KS, respectively. In this research, the evolutionary history of land plant KO and KAO homologs was resolved through phylogenetic analysis, and enzymatic assay confirmed that MpKOL1 and MpKAOL1 exhibit conserved catalytic activities.

Consistent with previous findings, far-red light (FR) enriched conditions induced the expression of GA biosynthesis genes in a manner dependent on the FR signaling regulator, MpPHYTOCHROME INTERACTING FACTOR (MpPIF). Disruption of MpCPS caused only a mild change in thallus morphology under regular culture conditions, but completely inhibited the hyponastic and slender thallus growth induced by FR enrichment. Moreover, MpCPS loss-of-function drastically promoted thallus growth under FR-enriched conditions, which suggested a growth inhibition activity for the downstream product of MpCPS. In addition, FR-induced sexual reproduction was delayed in *Mpcps* mutants, and the morphology of sexual branches known as gametangiophores was distorted.

Next, the bioactivity of several GA-related compounds was evaluated in wild-type and *Mpcps* plants. Application of KA but not any canonical bioactive GAs fully rescued the phenotypes of *Mpcps*, but none of the compounds evoked clear morphological changes in wild-type plants. Further genetic mutations of MpKS, MpKOL1 or MpKAOL1 confirmed that KA is a critical biosynthetic intermediate. While GA₁₂ biosynthesis was disrupted in all these mutants, the mild influence of *Mpkaol1* on sexual reproduction suggested that GA₁₂ is not absolutely required.

Taken together, it is likely that *M. polymorpha* produces one or more bioactive compounds from KA, which is distinctive from canonical bioactive GAs in vascular plants. For convenience, the bioactive compound is referred to as GA_{Mp}. GA_{Mp} acts as a growth hormone that facilitates responses to FR enrichment. Remarkably, more than half of the FR-induced transcriptome changes were dependent on GA_{Mp}, especially those related to stress responses and secondary metabolism. Since the canonical GA receptor GIBBERELLIN INSENSITIVE DWARF1 (GID1) is not conserved in *M. polymorpha*, the perception mechanism for GA_{Mp} is yet unknown. It is possible that the biosynthesis of GA precursors emerged in the common ancestor of all land plants, but independently derived into different growth regulators in bryophyte and vascular lineages during the past 450 million years of evolution.

Abbreviations

2ODD	2-oxoglutarate-dependent dioxygenase
3OH-KA	<i>ent</i> -3 β -hydroxy-kaurenoic acid
7OH-KA	<i>ent</i> -7-hydroxy-kaurenoic acid
ATR1	ARABIDOPSIS THALIANA CYTOCHROME REDUCTASE1
bHLH	basic helix-loop-helix
cFR	continuous far-red light
Cit	Citrine
CK	cytokinin
CKX	CYTOKININ OXIDASE
CPR	CYTOCHROME P450 REDUCTASE
CPS	<i>ent</i> -copalyl diphosphate synthase
cW	continuous white light
CXE	carboxylesterase
CYP	cytochrome P450 monooxygenase
DAPI	4',6-diamidino-2-phenylindole
DEG	differentially expressed gene
DEX	dexamethasone
EdU	5-ethynyl-2'-deoxyuridine
<i>ent</i> -CDP	<i>ent</i> -copalyl diphosphate
EOD-FR	far-red light treatment at the end of day
FR	far-red light
GA	gibberellin or gibberellic acid
GA20ox	gibberellin 20-oxidase
GA2ox	gibberellin 2-oxidase
GA3ox	gibberellin 3-oxidase
GA ₉ -Me	gibberellin A ₉ methyl ester
GAI	GIBBERELIC-ACID INSENSITIVE
GAMT	gibberellin methyl transferase
GC-MS	gas chromatography–mass spectrometry
GGDP	[<i>E, E, E</i>]-geranylgeranyl diphosphate
GID1	GIBBERELLIN INSENSITIVE DWARF1
GO	gene ontology
GUS	β -glucuronidase
IPT	ISOPENTENYLTRANSFERASE
KA	<i>ent</i> -kaurenoic acid
KA2ox	<i>ent</i> -kaurenoic acid 2-oxidase
KAN	KANADI
KAO	<i>ent</i> -kaurenoic acid oxidase
KO	<i>ent</i> -kaurene oxidase
KS	<i>ent</i> -kaurene synthase
LC-MS/MS	liquid chromatography with tandem mass spectrometry

LEA	LATE EMBRYOGENESIS ABUNDANT
LFR	low fluence response
LOG	LONELY GUY
MEP	2-C-methyl-D-erythritol-4-phosphate
MRM	multiple reaction monitoring
MVA	mevalonic acid
PBS	phosphate buffer saline
PFA	paraformaldehyde
phy	phytochrome
PIF	PHYTOCHROME INTERACTING FACTOR
POD	peroxidase
R	red light
RGA	REPRESSOR OF GIBBERELLIC-ACID INSENSITIVE
RNA-seq	RNA sequencing
RT-qPCR	reverse transcription–quantitative polymerase chain reaction
SCR	SCARECROW
SD	standard deviation
SLiCE	the seamless ligation cloning extract
SPL	SQUAMOSA PROMOTER BINDING PROTEIN-LIKE
TF	transcription factor
TOF	time-of-flight
TPS	terpene synthase

Chapter 1 Introduction

The phytohormone gibberellin

Plants use hormones, i.e., small signaling molecules, to coordinate growth, development and responses to the environment. Gibberellins (GAs) are a group of diterpenoid compounds broadly produced by many plants and plant-associated microbes (MacMillan, 2001; Bömke and Tudzynski, 2009; Nett et al., 2017). First discovered from the rice pathogen fungus *Fusarium fujikuroi* (previously known as *Gibberella fujikuroi*), GAs contribute to the excessive growth symptoms in the bakanae disease caused by the fungus (Kurosawa, 1926). Later in 1950s, GAs were isolated from the bean *Phaseolus coccineus* and other plants, establishing their role as endogenous plant hormones (MacMillan and Suter, 1958). The most prominent activity of GA in flowering plants is growth promotion. Deficiency in GA biosynthesis or signaling often leads to severe dwarfism and organ growth defects, e.g., affecting leaf expansion, floral development and fruit growth (Brian and Hemming, 1955; Phinney, 1956; Koornneef and van der Veen, 1980; Sakamoto et al., 2004; Wenzel et al., 2000; Yu et al., 2004; Fuentes et al., 2012). During seed germination, GA accumulation is required for the elongative growth of the embryo and eventual rupture of the endosperm (Urbanova and Leubner-Metzger, 2016).

As a group of chemical compounds, GAs are defined by their molecular structure instead of physiological activity. Typical GAs have a tetracyclic skeleton containing 19 or 20 carbon atoms, as exemplified by the structure of *ent*-gibberellane (Figure 1-1). More than 130 GAs have been identified from plants and microbes, but only a few (including GA₁, GA₃, GA₄ and GA₇) are highly active in angiosperms (MacMillan, 2001; Sponsel, 2016).

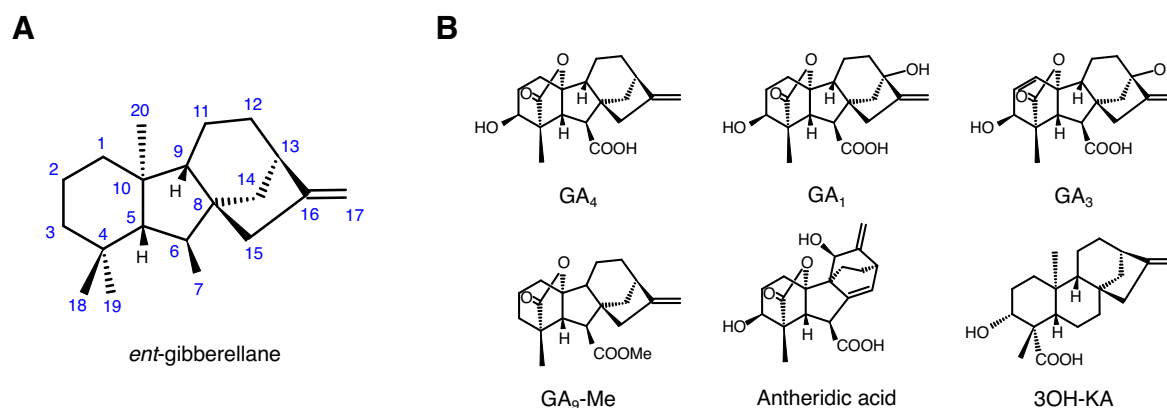


Figure 1-1 Chemical structure of GA and GA-related compounds. (A) The structure of *ent*-gibberellane, showing the skeleton and numbering of carbon atoms in GAs. (B) Representative GAs and GA-related compounds. GA₁ and GA₄ are typical bioactive GAs produced by seed plants. GA₃ is a major product from the fungus *F. fujikuroi*. GA₉ methyl ester (GA₉-Me) and antheridic acid are identified from ferns (Yamane, 1998; Tanaka et al., 2014). *ent*-3 β -Hydroxy-kaurenoic acid¹ (3OH-KA) is a bioactive compound from the moss *Physcomitrium patens* (Miyazaki et al., 2018).

¹ There are conflicts between the traditional nomenclature of GAs and the name of this compound in previous literatures regarding the orientation of the hydroxyl group. Following the GA nomenclature, this compound should be named as “*ent*-3 α -hydroxy-kaurenoic acid”. However, to keep consistency with (Miyazaki et al., 2018), the name “*ent*-3 β -hydroxy-kaurenoic acid” was used in this thesis.

GA metabolism in flowering plants

Despite the chemical diversity of GAs, a major GA biosynthesis pathway has been revealed by intensive studies in flowering plants (Figure 1-2). Similar to other diterpenoid compounds, the biosynthesis of GAs requires the formation of the general precursor, [*E, E, E*]-geranylgeranyl diphosphate (GGDP), through sequential condensation of four five-carbon isoprenyl precursors. In plants, the isoprenyl precursors could be produced through either the 2-*C*-methyl-D-erythritol-4-phosphate (MEP) pathway in the plastid, or the mevalonic acid (MVA) pathway in the cytosol. In *Arabidopsis* (*Arabidopsis thaliana*), the MEP pathway is predominantly utilized for GA biosynthesis (Kasahara et al., 2002). In the plastid, GGDP is converted to the bicyclic intermediate *ent*-copalyl diphosphate (*ent*-CDP) and then into the tetracyclic *ent*-kaurene by two terpene synthases (TPSs), the *ent*-CDP synthase (CPS) and the *ent*-kaurene synthase (KS) (Sun and Kamiya, 1994; Yamaguchi et al., 1998b; Hayashi et al., 2006). The conversion of *ent*-kaurene to bioactive GAs involves multiple processes of oxidation, starting with the action of two cytochrome P450 monooxygenases (CYPs). The CYP701 family member *ent*-kaurene oxidase (KO), which is mainly localized on the plastid outer membrane, catalyzes the three-step conversion of *ent*-kaurene to *ent*-kaurenoic acid (KA) (Helliwell et al., 1998, 1999, 2001b). Then in the endoplasmic reticulum, *ent*-kaurenoic acid oxidase (KAO) of the CYP88 family catalyzes three steps of oxidation to convert KA into GA₁₂, the first C₂₀-GA in the pathway. (Helliwell et al., 2001a, 2001b). The last steps are catalyzed by soluble 2-oxoglutarate-dependent dioxygenases (2ODDs) in the cytoplasm and nucleus (Helliwell et al., 2001b; Chen et al., 2014). GA 20-oxidase (GA20ox) catalyzes three rounds of oxidation on the C-20 methyl group, eventually removing this carbon to form C₁₉-GAs with γ -lactone (Lange et al., 1994; Lange, 1994; Phillips et al., 1995). Another 2ODD, GA 3-oxidase (GA3ox) introduces a hydroxyl group at C-3, which is essential for producing bioactive GAs such as GA₄ and GA₁ (Talon et al., 1990; Lester et al., 1997; Williams et al., 1998).

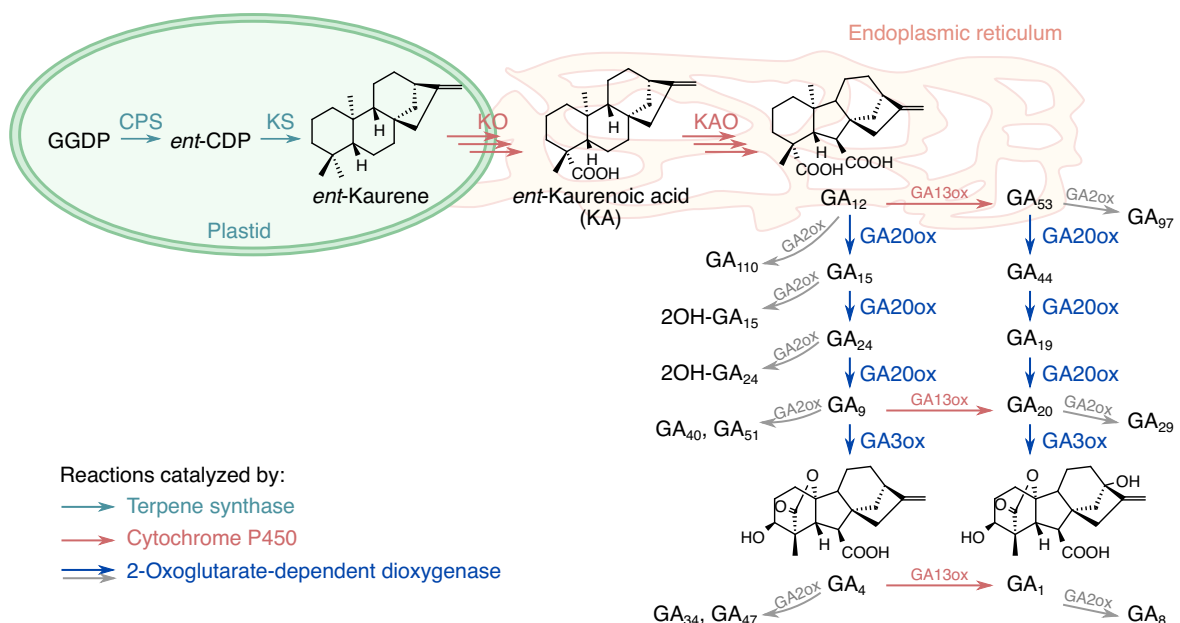


Figure 1-2 GA biosynthesis pathway in flowering plants. Arrows indicate enzymatic steps that have been experimentally characterized. For simplicity, several GA20ox products identified by (Lange et al., 2020) are omitted from the figure. GGDP, geranylgeranyl diphosphate; *ent*-CDP, *ent*-copalyl diphosphate; 2OH-GA₁₅, 2 β -hydroxy-GA₁₅; 2OH-GA₂₄, 2 β -hydroxy-GA₂₄; CPS, *ent*-copalyl diphosphate synthase; KS, *ent*-kaurene synthase; KO, *ent*-kaurene oxidase; KAO, *ent*-kaurenoic acid oxidase; GA13ox, GA 13-oxidase; GA20ox, GA 20-oxidase; GA3ox, GA 3-oxidase; GA2ox, GA 2-oxidase.

The activity of GAs is modulated by various modification/inactivation enzymes, including the 2ODD-family GA 2-oxidase (GA2ox), the SABATH-family GA methyl transferases (GAMT) and CYP714 family members (Lester et al., 1999; Martin et al., 1999; Thomas et al., 1999; Varbanova et al., 2007; Zhu et al., 2006; Magome et al., 2013; Nomura et al., 2013; Lange et al., 2020). In addition, GA 13-oxidases from various enzyme families catalyzes the C-13 hydroxylation of GAs, which leads to the generation of GA₁ as the bioactive compound (Gilmour et al., 1986; Magome et al., 2013; He et al., 2019).

Evolution of GA biosynthesis

Recent phylogenetic studies demonstrated that extant land plants are composed of two monophyletic groups: bryophytes including mosses, liverworts and hornworts; and vascular plants including lycophytes, ferns and seed plants (Puttick et al., 2018; Sousa et al., 2019; Su et al., 2021; Harris et al., 2022). Multiple sources of evidence support that GA biosynthesis is largely conserved in vascular plants. Apart from angiosperms, GA₁ and/or GA₄ have been identified in gymnosperms (Kamienska et al., 1976; Moritz et al., 1989; Moritz, 1995; Wang et al., 1996), ferns (Yamane et al., 1985, 1988; Tanaka et al., 2014) and lycophytes (Hirano et al., 2007; Aya et al., 2011). Homologs of all key GA biosynthesis enzymes are broadly identified from the genomes of vascular plants (Cannell et al., 2020; Yoshida et al., 2020). Moreover, physiological activity of GAs has been discovered in non-flowering vascular plants. GA treatment promotes shoot elongation of the gymnosperm *Pinus tabuliformis*, which is similar to the effect in angiosperms (Li et al., 2020b). Gametophytes of some fern species release GA-derived compounds as a pheromone, known as antheridiogens, to stimulate spore germination and male gametogenesis in the surrounding population (Yamane, 1998; Schneller, 2008; Tanaka et al., 2014; Hornych et al., 2021). In the lycophyte *Selaginella moellendorffii*, GA also contributes to the development of microspore outer walls (Aya et al., 2011).

In contrast to vascular plants, it is considered that bryophytes could not produce canonical bioactive GAs. Analyses of bryophyte genomes identified homologs of genes encoding CPS/KS, KO and KAO, but no bona fide members of the GA-related 2ODD families (Hayashi et al., 2006; Hirano et al., 2007; Miyazaki et al., 2011; Bowman et al., 2017; Yoshida et al., 2020; Li et al., 2020a). Given that these enzymes are all absent from the genomes of streptophyte algae (Cannell et al., 2020; Jia et al., 2022; Casey and Dolan, 2023), it is possible that the biosynthesis of KA and GA₁₂ emerged early in land plant evolution, while 2ODD enzymes are recruited to the pathway specifically in vascular plants (Figure 1-3B). Consistently, KA and its derivatives rather than GAs were detected in several liverworts and mosses (Nagashima et al., 2003; Nozaki et al., 2007; Hayashi et al., 2010; Miyazaki et al., 2015a). In the moss *Physcomitrium patens*, PpCPS/KS and PpKO sequentially catalyzes the production of *ent*-kaurene and KA, while no GA₁₂ is produced due to the absence of KAO. The Pp*cps/ks* and Pp*kao* mutants are defective in protonema differentiation, blue-light avoidance and spore germination, which could be rescued by KA treatment, suggesting that some KA derivative acts as a hormone (Hayashi et al., 2006, 2010; Miyazaki et al., 2014, 2015b; Vesty et al., 2016). Further analysis isolated *ent*-3 β -hydroxy-kaurenoic acid² (3OH-KA) as a putative bioactive compound, which serves a role distinct to GAs in angiosperms (Miyazaki et al., 2018).

In addition to the fungus *F. fujikuroi*, several other plant-associated fungi and bacteria can produce GAs bioactive in vascular plants (reviewed in Tudzynski et al., 2016). In these

² See the footnote on page 5.

species, *ent*-kaurene is also synthesized from GGDP, and subsequently oxidized at C-19, C-7, C-20 and C-3 to produce GAs (Tudzynski et al., 2016). However, the involvement of different enzymes suggested that these pathways emerged independently in different kingdoms through convergent evolution. In the fungal species *F. fujikuroi*, *Sphaceloma manihoticola* and *Phaeosphaeria* sp. L487, the oxidation steps are catalyzed by CYP503 and CYP68 family members (Tudzynski and Hölter, 1998; Tudzynski et al., 2001; Bömke et al., 2008; Kawaide, 2006). While in the bacteria *Bradyrhizobium japonicum* and *Sinorhizobium fredii*, CYP112, CYP114, CYP117 and other enzymes are responsible for producing GA₉ from *ent*-kaurene (Nett et al., 2017).

GA signaling and evolution

In angiosperms, bioactive GAs are mainly perceived by the soluble receptor GIBBERELLIN INSENSITIVE DWARF1 (GID1), which is localized in the cytoplasm and the nucleus (Ueguchi-Tanaka et al., 2005; Willige et al., 2007). After binding with GA, the transition or stabilization of GID1 conformation triggers the interaction between GID1 and nuclear-localized DELLA proteins, which are central transcriptional regulators that suppresses GA signaling (Peng et al., 1997; Silverstone et al., 1998; Ueguchi-Tanaka et al., 2005; Nakajima et al., 2006; Murase et al., 2008). Next, the GA-GID1-DELLA complex is recognized by the F-box protein GIBBERELLIN INSENSITIVE DWARF2 (GID2), which is a subunit of the E3 ubiquitin ligase known as the SKP1, CUL1, F-box protein (SCF) complex. The SCF^{GID2} complex mediates the ubiquitination and degradation of DELLA through the 26S proteasome pathway, which releases the downstream responses from DELLA suppression (Sasaki et al., 2003; Gomi et al., 2004) (Figure 1-3A).

DELLA proteins belong to the plant-specific GRAS family (named after family members GIBBERELLIC-ACID INSENSITIVE [GAI], REPRESSOR of GAI [RGA] and SCARECROW [SCR]) of transcriptional regulators and are composed of two conserved domains: the DELLA domain at the N-terminus, which mediates the GA-dependent interaction with GID1 and harbors transactivation activity; as well as the GRAS domain at the C-terminus (Dill et al., 2001; Itoh et al., 2002; Griffiths et al., 2006; Willige et al., 2007). Due to the lack of canonical DNA-binding motifs, DELLA proteins regulate downstream gene expression through protein-protein interactions with numerous transcription factors (TFs) and epigenetic regulators, which are associated with the GRAS domain (Briones-Moreno et al., 2023). In some cases, the interaction suppresses the activity of TFs, and GA-dependent DELLA degradation releases the target TF from suppression (Feng et al., 2008; de Lucas et al., 2008; Bai et al., 2012; Hou et al., 2010). In other cases, the interaction recruits DELLA as a transcriptional co-activator, and GA presence inhibits the expression of downstream genes (Lim et al., 2013; Yoshida et al., 2014; Fukazawa et al., 2014; Marín-de la Rosa et al., 2015). A recent research showed that DELLA proteins directly interact with the histone H2A, which stabilizes the binding of the DELLA-TF complex to the target chromatin (Huang et al., 2023). It is noteworthy that GA signaling might also be transduced in a DELLA-independent manner. In *Arabidopsis*, GA treatment induces a burst of cytosolic Ca²⁺ increase within a few minutes, which is neither influenced by the overexpression of degradation-resistant DELLA nor by the loss of all five DELLA homologs (Okada et al., 2017).

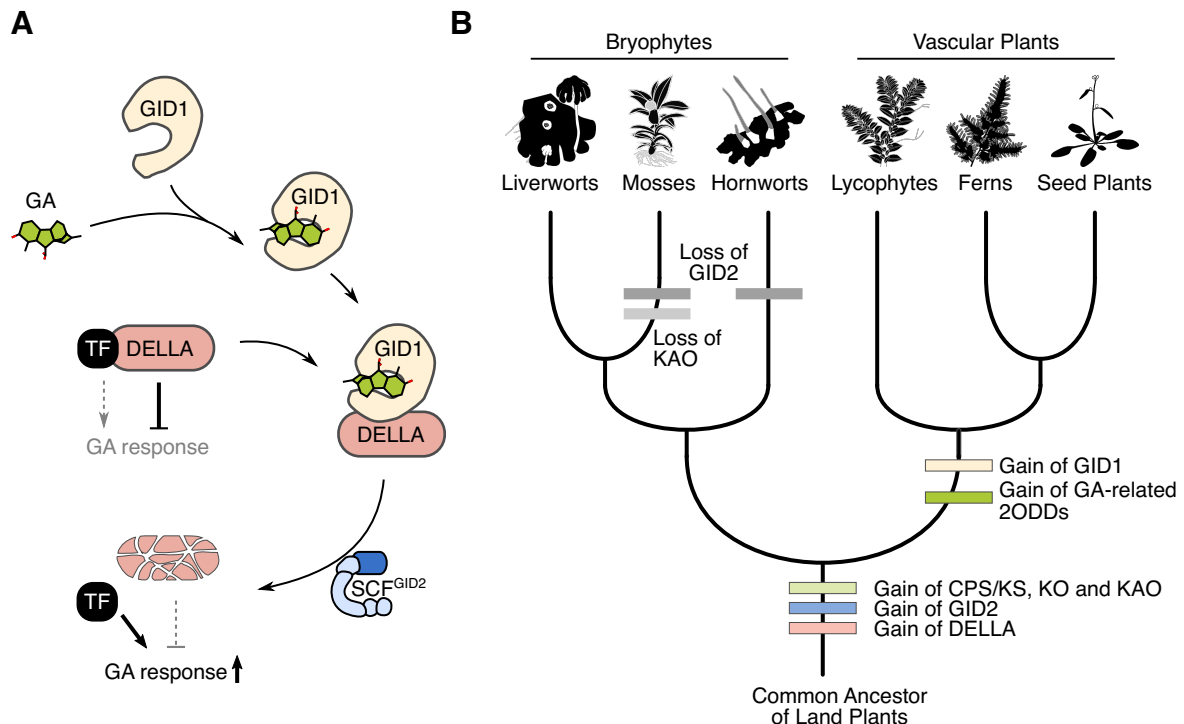


Figure 1-3 GA signaling perception mechanism and putative GA-related evolutionary events. (A) Model for GA signaling mediated by GID1, DELLA and GID2. (B) Hypothetical gain and loss events of genes related to GA biosynthesis and signaling during land plant evolution.

The evolution of GID1, DELLA and GID2 has been investigated through both computational and experimental approaches. GID1 proteins have a close relationship with carboxylesterases (CXEs) of the α/β hydrolase fold superfamily but lack the hydrolase activity (Ueguchi-Tanaka et al., 2005; Nakajima et al., 2006; Marshall et al., 2003). Three highly-conserved amino acid residues (Ser, His and Asp) in the catalytic center are essential for the enzymatic activity of CXEs, while in GID1s the replacement of His with Val or Ile facilitates GA binding in the deep pocket (Ueguchi-Tanaka et al., 2005; Nakajima et al., 2006; Shimada et al., 2008; Murase et al., 2008). In the phylogenetic analyses, the monophyletic clade of GID1 homologs consists of massive sequences from lycophytes, ferns and seed plants; none from mosses or liverworts; and only two partial sequences from hornworts. For bryophyte CXEs, the lack of residues critical for GA binding or GID1-DELLA interaction further distinguishes them from bona fide GID1s (Bowman et al., 2017; Yoshida et al., 2018; Hernández-García et al., 2019). GID1-like CXEs from the moss *P. patens* showed no binding affinity to GA₄, GA₉ or GA₁₂ in vitro. In contrast, both GID1 homologs from the lycophyte *Selaginella moellendorffii* were able to bind GA₄ in the presence of SmDELLA, and successfully rescued the dwarfism caused by GA deficiency in the rice *gidl-3* mutant, suggesting that GID1s are likely evolved with the emergence of vascular plants (Hirano et al., 2007; Yasumura et al., 2007).

Investigation of genomes and transcriptomes elucidated that DELLA-type GRAS family proteins broadly exist in all major lineages of land plants (Hernández-García et al., 2019). Yeast assays provided further insights into the ancestral function of DELLA proteins: both the transcriptional activating function of the N-terminus DELLA domain and the capacity for the GRAS domain to interact with dozens of transcription factors are well conserved among land plants (Hernández-García et al., 2019; Briones-Moreno et al., 2023). In the liverwort *M.*

polymorpha, overexpression of MpDELLA inhibited thallus growth, decreased gemma dormancy and delayed sexual reproduction (Hernández-García et al., 2021). In the moss *P. patens*, loss of PpDELLA function accelerated spore germination but impaired male fertility (Phokas et al., 2023). On the other hand, the potential to interact with GID1 upon GA stimulation is mostly confined to DELLAs from vascular plants, despite that a DELLA from the hornwort *Nothoceros vincentianus* could interact with Arabidopsis GID1s in a GA-dependent manner (Hirano et al., 2007; Yasumura et al., 2007; Hernández-García et al., 2019; Phokas et al., 2023). When expressed in Arabidopsis or rice, lycophyte DELLAs from two *Selaginella* species but not moss DELLAs from *P. patens* were prone to GA-dependent degradation, suggesting that the GA signaling function of DELLA is gained in vascular plants (Hirano et al., 2007; Yasumura et al., 2007).

Homologs for the F-box protein GID2 are found in vascular plants and a broad range of liverworts, but not in mosses or hornworts (Bowman et al., 2017; Hernández-García et al., 2019). Taken together, it seems that all the necessary components of GA signaling are assembled in the common ancestor of vascular plants, and the signaling mechanism has been conserved in this plant lineage (Figure 1-3B). In the moss *P. patens*, GA₉ methyl ester (GA₉-Me) or KA treatment could rescue spore germination and protonema differentiation phenotypes of the Pp*cps/ks* mutant, but showed no effect on PpDELLA stability (Vesty et al., 2016; Phokas et al., 2023). Mutation in both PpDELLAs did not change the promotive effect of GA₉-Me on spore germination, suggesting that GA-related hormonal diterpenoids might act independently of DELLAs in *P. patens* and other bryophytes (Phokas et al., 2023).

Involvement of GA in light responses

GAs participate in many processes of environmental responses in angiosperms (Colebrook et al., 2014). In particular, both GA metabolism and responsiveness are modulated in the light responses mediated by the photoreceptor phytochrome. Phytochromes are dimeric chromoproteins that perceive red and far-red lights by transitioning between two states, the inactive Pr state and the active Pfr state (reviewed in Li et al., 2011). Absorption of red light (R) activates phytochromes to the Pfr state, which could be reversed to the Pr state upon far-red light (FR) absorption or through thermal relaxation in the darkness (reviewed in Li et al., 2011). Arabidopsis encodes five phytochromes (phyA~phyE) that mediate distinct responses to different light intensity and composition (Sharrock and Quail, 1989; Clack et al., 1994). Arabidopsis phyA regulates the responses triggered by lights of very low intensity or that triggered by prolonged FR irradiation of relatively high intensity (Nagatani et al., 1993; Parks and Quail, 1993; Shinomura et al., 1996). Meanwhile, phyB is the dominant regulator for low fluence responses (LFR) that are reversibly activated by R and inhibited by FR (Shinomura et al., 1996). A class of basic helix-loop-helix (bHLH) transcription factors known as PHYTOCHROME INTERACTING FACTORS (PIFs) directly interact with Pfr state phytochromes and play a central role in transcription regulation downstream of phytochrome signaling (Ni et al., 1998, 1999; Leivar and Monte, 2014).

In Arabidopsis, seed germination is mainly regulated by phyB in a R/FR photo-reversible manner, but is also managed by phyA under prolonged FR irradiation (Shinomura et al., 1994; Reed et al., 1994; Shinomura et al., 1996). Under both conditions, light-activation of phytochromes acts through the protein PIF3-LIKE5 (PIL5/PIF1) to control GA metabolism genes, elevating the level of bioactive GAs by promoting the expression of GA3ox1 and GA3ox2 while suppressing the expression of GA2ox2 (Yamaguchi et al., 1998a; Ogawa et al., 2003; Oh et al., 2006). In addition, PIL5 directly regulates the expression of two DELLA genes in a positive manner, which fine-tunes the GA responsiveness (Oh et al., 2007).

In the seedlings, light regulation of GA levels occurs in an opposite manner. During seedling de-etiolation, dark-grown seedlings respond to light exposure by decreasing GA biosynthesis and promoting the inactivation, which reduces the level of bioactive GAs and suppresses hypocotyl growth (Toyomasu et al., 1992; Reid et al., 2002; Achard et al., 2007; Hirose et al., 2012). Furthermore, DELLA accumulation suppresses PIF function through physical interaction, which prevents PIF from binding to the target sites and sequesters PIF for degradation (de Lucas et al., 2008; Feng et al., 2008; Li et al., 2016). In phyB-dependent shade avoidance responses, enrichment of far-red light (FR) or end-of-day FR treatment triggers de novo GA biosynthesis to facilitate the elongation of stems and petioles, as well as the hyponastic growth of petioles (Beall et al., 1996; Devlin et al., 2003; Hisamatsu et al., 2005; Sessa et al., 2005; Djakovic-Petrovic et al., 2007; Küpers et al., 2023).

R/FR responses in *M. polymorpha*

Phytochromes exist in many lineages of prokaryotic and eukaryotic organisms, and it has been suggested that canonical plant phytochromes originated in streptophytes before the emergence of land plants (Ulijasz and Vierstra, 2011; Rockwell et al., 2014; Li et al., 2015). In the chlorophyte alga *Micromonas pusilla*, the sole phytochrome absorbs orange and far-red light and shows a light-dependent nuclear translocation (Duanmu et al., 2014). In the streptophyte alga *Spirogyra varians*, bending and aggregation of filaments is regulated reversibly by R and FR, which is typical of phytochrome-mediated response (Lee and Kim, 2019).

In the liverwort *M. polymorpha*, most responses to R and FR treatments are observed in the haploid thallus since the life cycle is dominated by the gametophyte generation. A series of studies in the 1960s discovered that when *M. polymorpha* plants were cultured under day/night cycles, a few minutes of FR irradiation at the end of day (EOD-FR) could efficiently induce the hyponastic growth of thallus tips and the decrease in chlorophyll content, which could be reversed if a short R irradiation was applied after FR (Fredericq, 1964; Ninnemann and Halbsguth, 1965; Fredericq and de Greef, 1966; Fredericq and Greef, 1968). Such a response depends on the active growth in the apical meristem region. The thallus tips would revert to flat growth when the EOD-FR treatment stopped after a few cycles. If the apexes were excised, the hyponastic response was observed in the newly-regenerated thallus tip, but not the basal fragment of the old thallus (Fredericq and Greef, 1968). Consistently, recent research observed similar morphological differences in the thalli regenerated under R pulse cycles or R/FR pulse cycles (Nishihama et al., 2015). The regenerants grown under R/FR cycles were slender and hyponastic, bearing elongated epidermal cells, while the regenerants grown under R cycles were wide and flat. Observations on sporelings grown under same conditions suggested that the phytochrome-inactive R/FR cycles inhibit cell division but favors cell elongation, which also explained the delay of cell-cycle re-entry during thallus regeneration (Nishihama et al., 2015). Besides, the germination of gemmae, i.e., asexual propagules of *M. polymorpha*, is reversibly induced by R and FR pulses in the darkness (Otto and Halbsguth, 1976; Inoue et al., 2016).

When *M. polymorpha* plants are cultured under full white light conditions, supplementation of FR with or without reducing the total light intensity also leads to a series of developmental changes. In addition to hyponasty, some apical meristems become dormant after dichotomous bifurcation, generating an asymmetric thallus architecture (Briginshaw et al., 2022; Streubel et al., 2023). Likewise, high FR irradiance under such conditions provokes the transition to sexual reproduction and differentiation of sexual branches called gametangiophores (Kubota et al., 2014; Inoue et al., 2016). All these responses are

antagonistically governed by the sole phytochrome (MpPHY) and the single PIF (MpPIF) in the *M. polymorpha* genome (Inoue et al., 2016, 2019; Briginshaw et al., 2022; Streubel et al., 2023). A liverwort-specific Mpo-MR13 miRNA and the transcription factor MpSQUAMOSA PROMOTER BINDING PROTEIN-LIKE1 (MpSPL1) contributes to the regulation of meristem dormancy downstream of MpPHY-MpPIF (Streubel et al., 2023). MpDELLA interacts with MpPIF and negatively regulates MpPIF function in an evolutionarily conserved manner (Hernández-García et al., 2021). Meanwhile, loss of the *M. polymorpha* KANADI ortholog (MpKAN) reduced FR-induced growth tropisms and transcriptome changes (Briginshaw et al., 2022).

Interestingly, several putative GA biosynthesis genes were up-regulated by FR in a MpKAN-dependent manner, suggesting that they may participate in the FR response of *M. polymorpha* (Briginshaw et al., 2022). This research aims to investigate the molecular function of these GA biosynthesis genes, elucidate the physiological role of GA-related compounds in *M. polymorpha*, and expand the understanding of GA metabolism in the context of land plant evolution.

Chapter 2 Results

Evolution history of KO and KAO homologs in *M. polymorpha*

To investigate the GA-related metabolic pathway in *M. polymorpha*, this research focused on evolutionarily conserved enzymes that catalyze the biosynthesis of GA precursors in vascular plants. Previous studies investigated the catalytic activity of all seven plant-type TPSs in *M. polymorpha* (Kumar et al., 2016; Jia et al., 2022) and found that MpDTPS3 (Mp2g07200, referred to as MpCPS) specifically catalyzes the production of *ent*-CDP from GGDP, which could be used by MpDTPS4 (Mp6g05950, referred to as MpKS) to produce *ent*-kaurene (Kumar et al., 2016). To find candidate enzymes that act downstream of *ent*-kaurene, phylogenetic analyses were performed to identify homologs of KO and KAO. Arabidopsis proteins were used as query sequences to search against publicly available genomes and transcriptomes, and phylogenetic relationships were inferred among initial hits to determine the outgroup and core set of sequences for a refined analysis.

Consistent with the previous research, KOs from the CYP701 family are well conserved in land plants but not found in streptophyte algae (Bowman et al., 2017). At least one homolog was identified from most analyzed genomes and transcriptomes, which covered all major taxonomy lineages. Liverwort homologs were grouped into two clades, each containing sequences from Haplomitriopsida, Marchantiopsida and Jungermanniopsida, suggesting that a duplication event took place at an early stage of liverwort evolution (Figure 2-1). Three copies of KO genes were found in *M. polymorpha*: MpKOL1 (Mp3g18320) from one clade, as well as MpKOL2 (Mp2g01950) and MpKOL3 (Mp2g01940) from the other clade. MpKOL2 and MpKOL3 locate next to each other on chromosome 2, implying that they originated from a tandem duplication event.

The phylogeny of CYPs related to KAOs is less clear (Figure 2-2), so pairwise sequence identity was calculated among the analyzed proteins, and the arbitrary rule of >40% identity (Nelson, 2006) was used to distinguish different CYP families (Figure 2-3). Following this rule, a monophyletic group of proteins containing all known plant KAOs and sharing high sequence identity were considered as CYP88 family members. These CYP88 members formed two major clades with high branch support, both containing sequences from bryophytes and vascular plants. However, it is hard to conclude about the gene divergence due to the limited overlap of species in the two clades. Compared to KOs, much fewer CYP88 proteins were identified from a smaller range of species, suggesting a frequent loss of this gene family in land plants, including a complete loss in the moss lineage. For liverworts and hornworts, multiple copies of CYP88s from the same species are dispersed in distinct clades, which might be results of deep divergence in the bryophyte lineage or poor maximum-likelihood inference based on amino acids. Two KAOs homologs were identified from *M. polymorpha*: MpKAOL1 (Mp4g23680) and MpKAOL3 (Mp2g10420). They are phylogenetically associated with different group of liverwort sequences and physically located on different chromosomes.

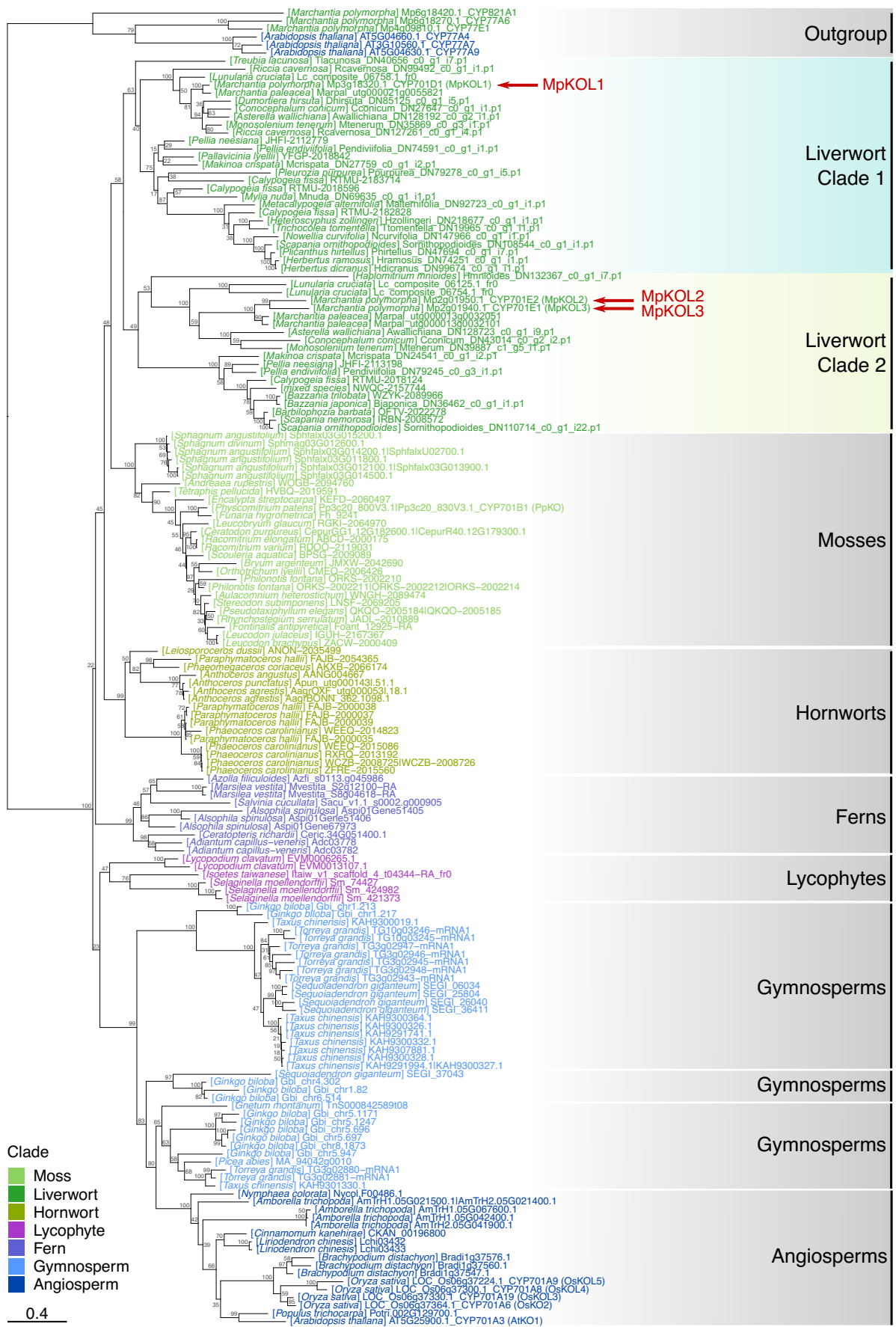


Figure 2-1 Phylogeny of CYP701(KO) homologs. The support values shown next to nodes were derived from 1000 standard non-parametric bootstraps using IQ-TREE 2. Branch length represents the number of substitutions per site. *M. polymorpha* KO homologs were highlighted by red arrows.

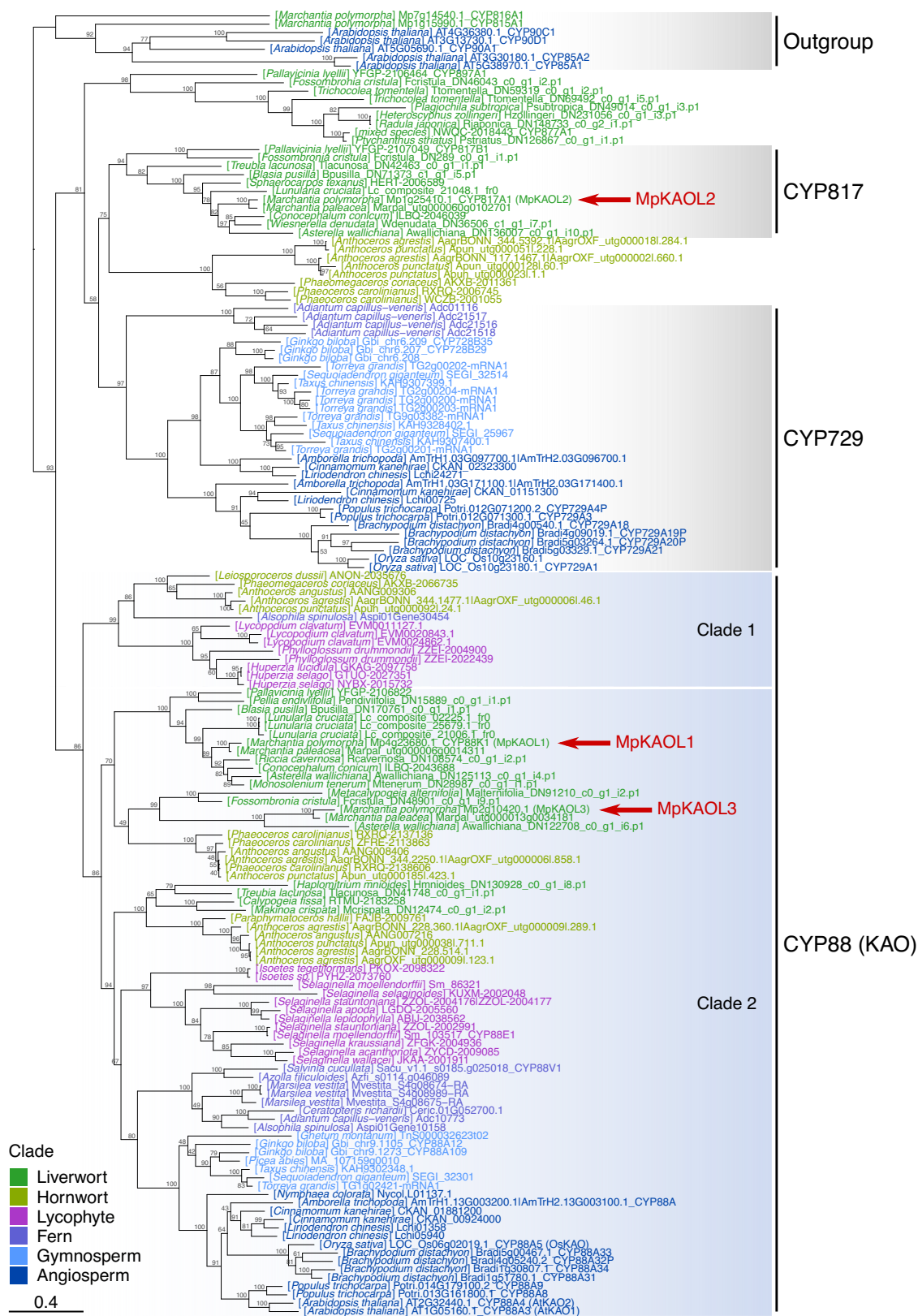


Figure 2-2 Phylogeny of CYP88(KAO) and closely-related proteins. The support values shown next to nodes were derived from 1000 standard non-parametric bootstraps using IQ-TREE 2. Branch length represents the number of substitutions per site. *M. polymorpha* proteins MpKAOL1, MpKAOL3 and MpKAOL2 are highlighted by red arrows.

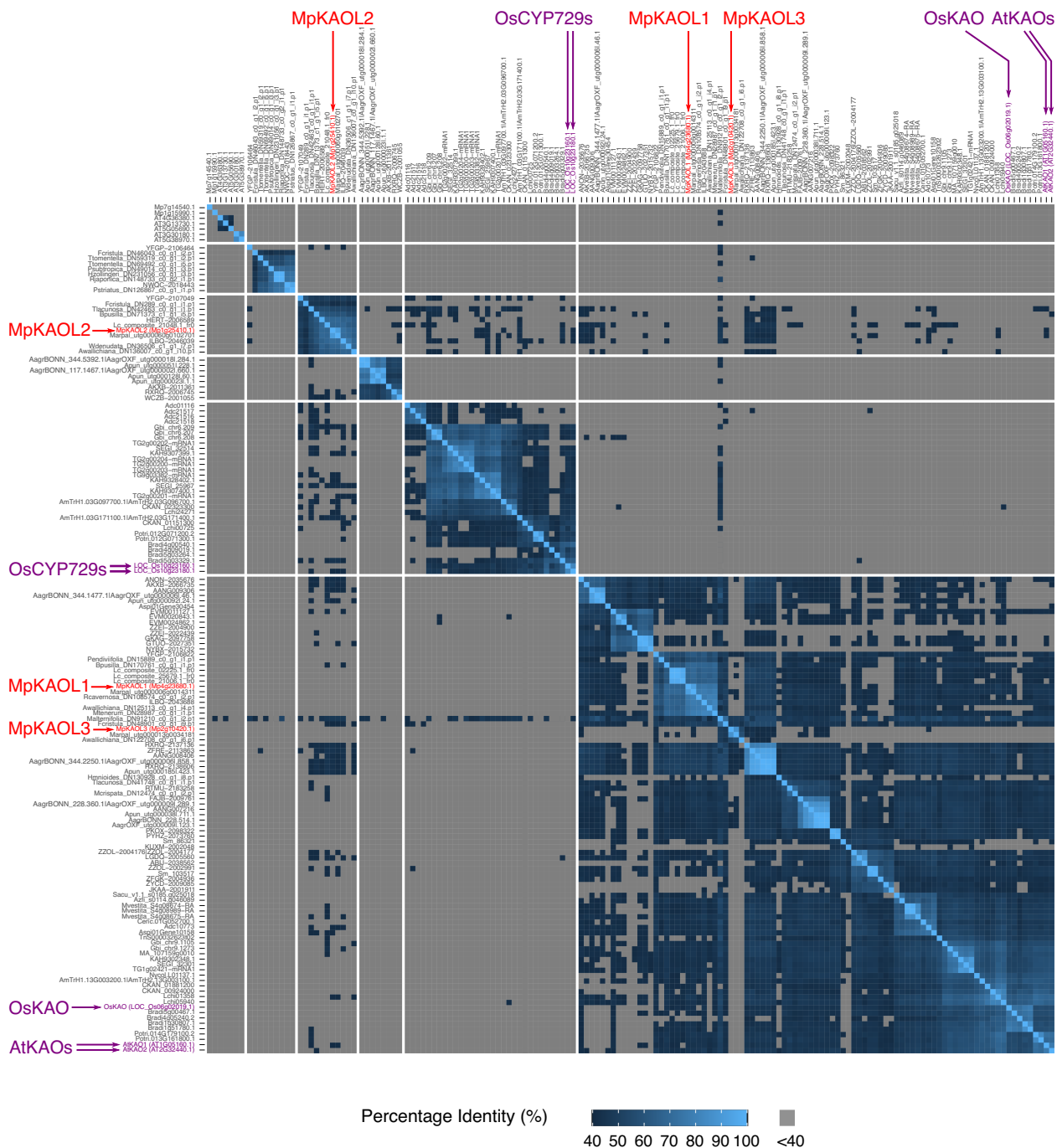


Figure 2-3 Heatmap showing percentage identity among CYP88(KAO) and closely-related proteins. Pairwise percentage identities were calculated among sequences shown in **Figure 2-2** by local alignment using BLAST. To highlight the threshold for defining membership in a CYP family (Nelson, 2006), sequence identities below 40% were omitted from the visualization. MpKAOL2 and its liverwort homologs showed limited similarity to CYP729 or KAO (CYP88) family members. *M. polymorpha* genes of interest are highlighted by red arrows, and their closely-related genes from Arabidopsis or rice are indicated with purple arrows.

Another CYP protein, MpKAOL2 (Mp1g25410), was previously considered as a KAO homolog (Bowman et al., 2017). When sequences from a broader range of species were analyzed, this protein showed neither close phylogenetic relationship nor >40% percentage identity with bona fide KAOs. In the phylogenetic tree, MpKAOL2s and its liverwort homologs formed a monophyletic group with several hornwort sequences and CYP729 family members from vascular plants, suggesting that they might share a common origin in evolution (Figure 2-2). Yet the low similarity of protein sequences rejected them to be classified into the same CYP family (Nelson, 2006). Instead, another previous report designated MpKAOL2 as MpCYP817A1 (Nelson, 2018).

MpKOL1 and MpKAOL1 catalyzes the biosynthesis of KA and GA₁₂

To test if *M. polymorpha* homologs of CYP701 and CYP88 possess KO or KAO activity, the enzymatic activity of these proteins is evaluated using a heterologous expression system in the methylotrophic yeast *Pichia pastoris*, which carries the *Arabidopsis* CYTOCHROME P450 REDUCTASE1 (AtCPR1, AT4G24520) to facilitate CYP function. After initial cell proliferation and protein induction, yeast cells were co-cultured with substrates in the growth medium for a duration of two days. Finally, the culture infiltrates were collected, extracted and analyzed with gas chromatography-mass spectrometry (GC-MS). When the three KO homologs were tested with 7 μg of *ent*-kaurene in 50-mL cultures, only the yeast cells expressing MpKOL1 produced KA as a major product (Figure 2-4). No KA was detected in cultures expressing MpKOL2 or MpKOL3, suggesting that they might have lost KO activity during evolution.

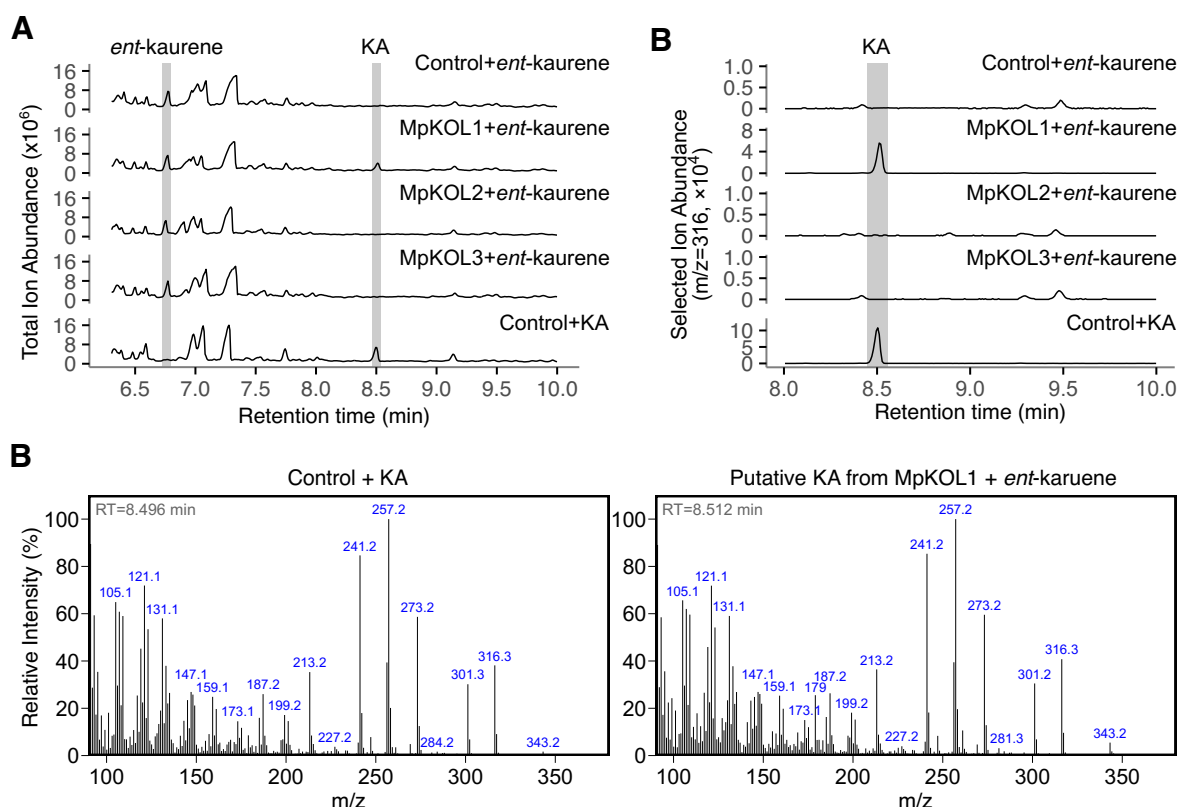


Figure 2-4 Functional characterization of KO homologs in *M. polymorpha*. (A-B) Total (A) and selected (B) ion chromatogram from GC, showing the production of KA by MpKOL1. (C) Mass spectra showing identical ion fragments between the MpKOL1 product and authentic KA from the control group. The data was collected by Wakako Fukuda and Sho Miyazaki at Tokyo University of Agriculture and Technology. Data of the “Control+KA” group was the same as in **Figure 2-5**.

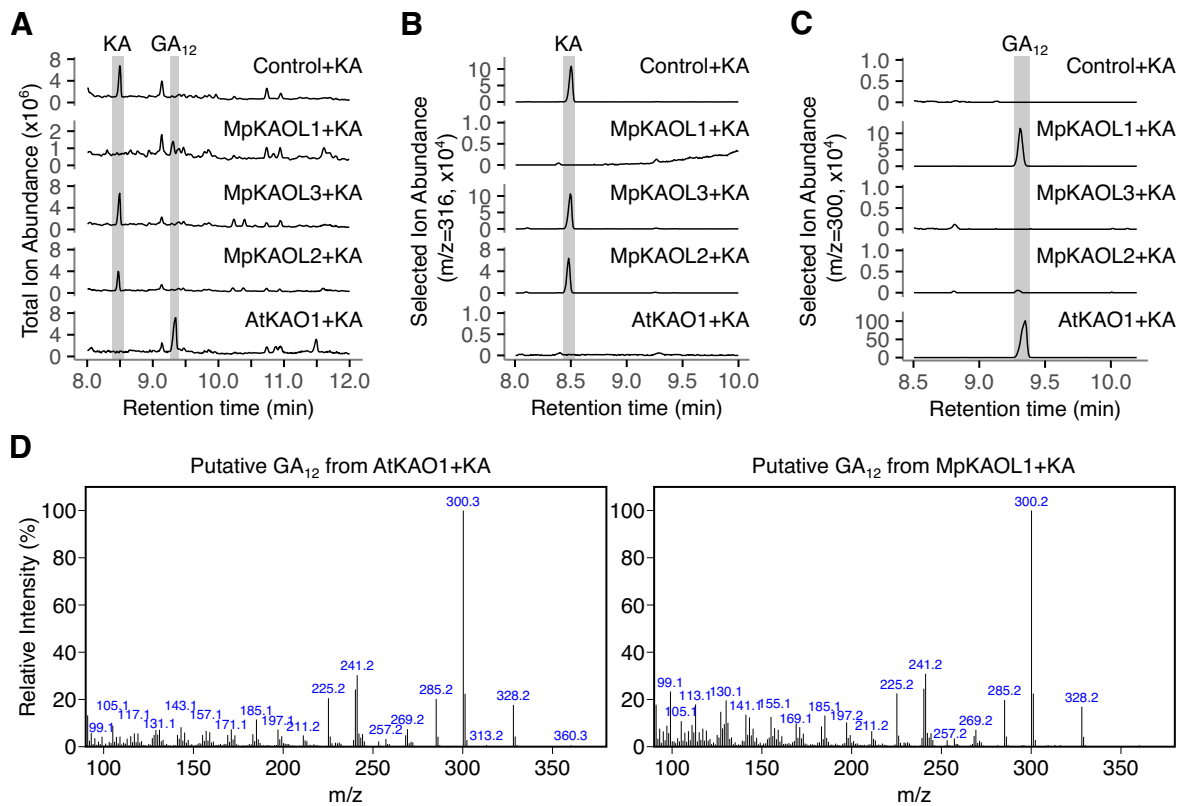


Figure 2-5 Functional characterization of KAO homologs in *M. polymorpha*. (A) Total ion chromatogram from GC, showing the consumption of KA and various product peaks. (B) Selected ion chromatogram at $m/z=316$, showing the consumption of KA. (C) Selected ion chromatogram at $m/z=300$, showing the production of GA_{12} . (D) Mass spectra showing identical ion fragments between the putative GA_{12} product of MpKAOL1 and the major product of AtKAO1. The data was collected by Wakako Fukuda and Sho Miyazaki at Tokyo University of Agriculture and Technology. Data of the “Control+KA” group was the same as in **Figure 2-4**.

In another set of experiments, yeast cells expressing MpKAOL1, MpKAOL3 or the CYP817 homolog MpKAOL2 were co-cultured with 15 µg of KA in 50 mL of growth medium. In parallel, cells expressing Arabidopsis KAO1 (AT1G05160) were tested as the positive control. After two days' incubation, KA was completely consumed in the yeast cultures harboring MpKAOL1 or AtKAO1, while remaining KA could be detected in the groups expressing MpKAOL2 or MpKAOL3 (Figure 2-5A-B). Multiple products seemed to be generated in all experiment groups, yet their identities remain unclear because there are no authentic compounds available for comparison (Figure 2-5A). Nevertheless, GA₁₂ was detected among the products from the MpKAOL1 group. Although no authentic GA₁₂ sample was included in the analysis, the putative GA₁₂ product peak from the MpKAOL1 group shared a similar retention time and mass spectrum signatures with the major product from the AtKAO1 group, as well as the previous literature (Nett et al., 2017) (Figure 2-5C-D).

Taken together, the results suggest that in addition to MpCPS and MpKS, MpKOL1 and MpKAOL1 possess evolutionarily conserved enzymatic activities. The four enzymes may function in a sequential manner to synthesize GA₁₂ in *M. polymorpha*.

Subcellular localization of GA biosynthesis enzymes

To inspect the subcellular localizations of MpCPS, MpKS, MpKOL1 and MpKAOL1 in vivo, stable transgenic plants were constructed to express each enzyme under the cauliflower mosaic virus 35S constitutive promoter with a C-terminal Citrine fusion (Figure 2-6). MpCPS-Cit and MpKS-Cit exhibited similar subcellular localization patterns, as the fluorescence signals emitted by both proteins co-localized with the autofluorescence of chlorophyll in the chloroplasts. Furthermore, the intensity of Citrine signals in these samples are complementary to that of thylakoid-enriched chlorophyll, suggesting that both enzymes might be abundant in the soluble stroma. The MpKOL1-Cit fluorescence signals were also localized in chloroplasts but showed highest intensity in the envelopes. A distinctive distribution pattern was observed for MpKAOL1-Cit, which did not overlap with chloroplasts or cell nuclei stained with 4',6-diamidino-2-phenylindole (DAPI). Signals surrounding the cell nuclei and the plasma membrane indicated that this protein might be localized in the endomembrane system. Overall, the localizations of all four proteins were similar to their homolog in Arabidopsis (Helliwell et al., 2001b), which is in line with the evolutionary conservation of their molecular functions.

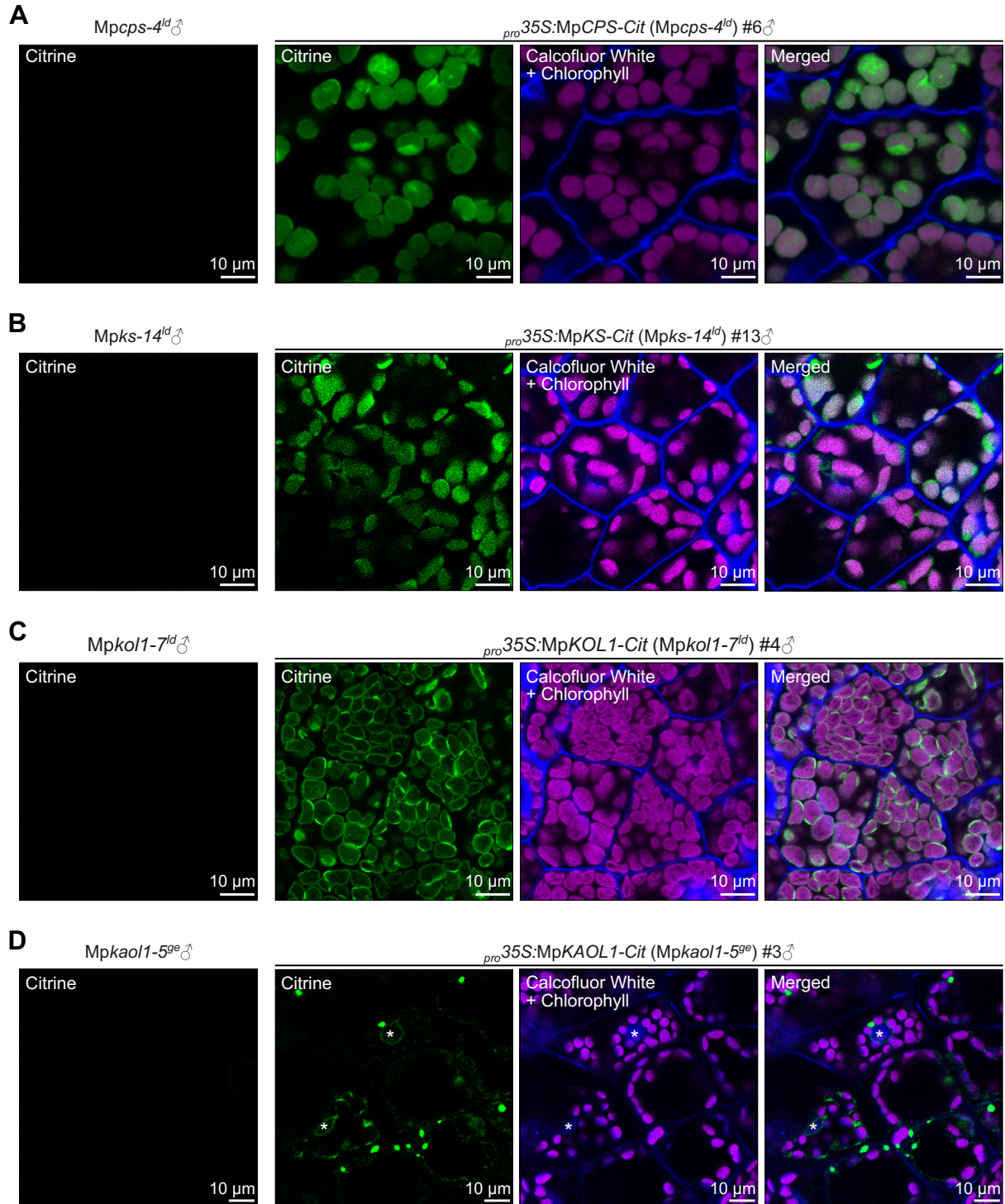


Figure 2-6 Subcellular localizations of MpCPS (A), MpKS (B), MpKOL1 (C) and MpKAOL1 (D). For the observation, 7-day-old plants cultured under cW+cFR were fixed and stained with calcofluor white to show the cell wall (A-C) or DAPI to show the cell nuclei (D, also indicated with asterisks). Signals from Citrine-labeled proteins were shown in green, while the chlorophyll autofluorescence was shown in magenta. Both calcofluor white and DAPI signals were shown in blue.

FR enrichment promoted the biosynthesis of GA₁₂ in *M. polymorpha*

Based on transcriptome profiles, Briginshaw et al. (2022) noticed that in *M. polymorpha*, putative GA biosynthesis genes were up-regulated under FR-enriched light conditions. Such observation was confirmed by an independent analysis of another previously published transcriptome data set (Hernández-García et al., 2021) (Figure 2-7A). When 7-day-old wild-type plants cultured under continuous R was irradiated with monochromatic FR, the expression of *MpKOLI* was significantly increased after 1 h, while *MpCPS* and *MpKAOLI* are also upregulated after 4 h. Disruption of *MpPIF* by homologous recombination (Inoue et al., 2016) completely inhibited the transcriptional expression changes, suggesting that this response is dependent on the MpPHY-MpPIF signaling module.

To further validate this conclusion, the relative gene expression levels of *MpCPS*, *MpKS*, *MpKOLI* and *MpKAOLI* were examined with reverse transcription–quantitative polymerase chain reaction (RT-qPCR). In this experiment, wild-type, *Mppi^{ko}*, or the complementation line of *Mppi^{ko}* (*gMpPIF/Mppi^{ko}*) were grown under continuous white light (cW) for 7 days, then irradiated with continuous FR as a supplemental light source (cW+cFR). The expression of all four genes was significantly increased by FR treatment in a *MpPIF*-dependent manner, but the dynamics were different between *MpKOLI* and the other three enzymes. After FR treatment, *MpKOLI* expression reached the highest point at the 8 h time point and slightly declined at 24 h, while *MpCPS*, *MpKS* and *MpKAOLI* showed a gradual increase over the 24-h induction period. Such difference indicated that there might be a different mechanism of transcriptional regulation on *MpKOLI* (Figure 2-7B).

In agreement with the elevated expression of biosynthetic genes, GA₁₂ was significantly accumulated under FR enriched conditions. When 10-day-old wild-type plants were cultured for another 4 days under the cW+cFR condition, the endogenous level of GA₁₂ reached 30.05±0.60 pg/g fresh weight, while the plants left in cW for the same duration only contained GA₁₂ of 8.54±1.29 pg/g fresh weight (Figure 2-7C) (Okabe, bachelor's thesis, 2022).

The sites of GA₁₂ biosynthesis were investigated by employing the promoters of the biosynthetic genes in conjunction with the β-glucuronidase (GUS) reporter. The observation was carried out in 7-day-old plants, which were cultured for one more day under cW or cW+cFR conditions. *MpCPS*, *MpKOLI* and *MpKAOLI* promoters showed almost ubiquitous expression in the young thallus, only slightly weaker near the apical meristems. The activity of *MpKS* promoter was relatively weak under the cW condition. Under the FR enriched cW+cFR condition, higher GUS activity was observed in all constructs. The elevated *MpKS* promoter activity became visible along the thallus edge (Figure 2-7D).

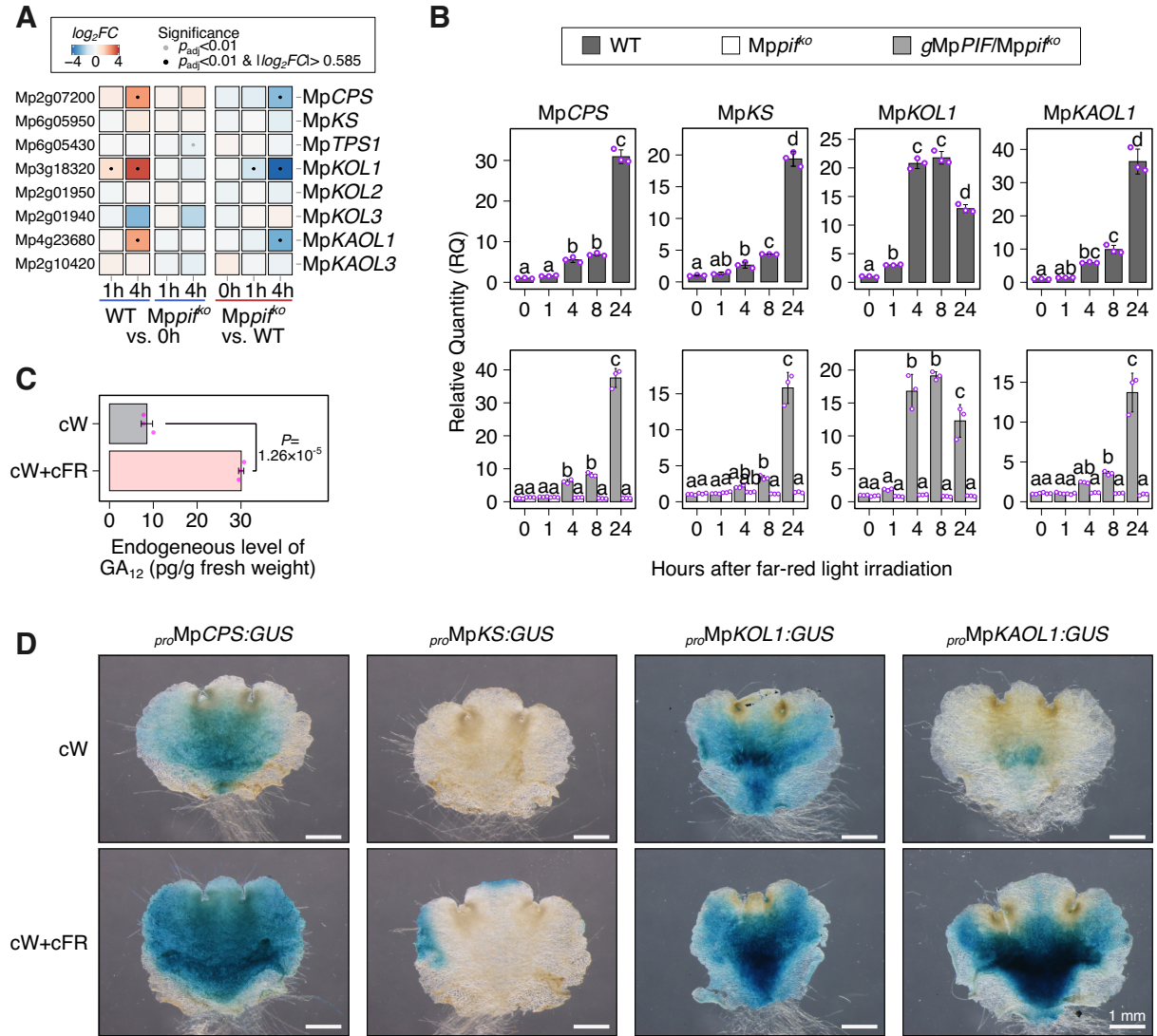


Figure 2-7 Upregulation of GA₁₂ biosynthesis by FR enrichment. (A) Heatmaps showing gene expression changes triggered by FR irradiation, using data from (Hernández-García et al., 2021). FC, fold change. P_{adj} , adjusted P -value. Wild-type (WT) plants refer to the Tak-1 male accession. (B) Relative expression level of GA₁₂ biosynthesis genes measured by RT-qPCR. (C) Endogenous levels of GA₁₂ measured from Tak-1 plants grown under different light conditions (data from Maiko Okabe, bachelor's thesis, 2022). (D) Promoter activity of GA₁₂ biosynthesis genes shown by the GUS reporter. The samples were stained overnight for GUS activity.

MpCPS loss-of-function altered thallus growth under FR-enriched conditions

To explore the physiological function of GA biosynthesis genes in *M. polymorpha*, large deletion mutants of MpCPS with complete loss of the coding sequence (CDS) were generated using the CRISPR/Cas9^{D10A} nickase technique (Hisanaga et al., 2019; Koide et al., 2020). As *M. polymorpha* is a dioicous liverwort, independent mutant alleles were generated in both the male Tak-1 (*Mpcps-4^{ld}*, *Mpcps-27^{ld}*) and the female Tak-2 (*Mpcps-120^{ld}*, *Mpcps-123^{ld}*) wild-type accessions (Figure 2-8).

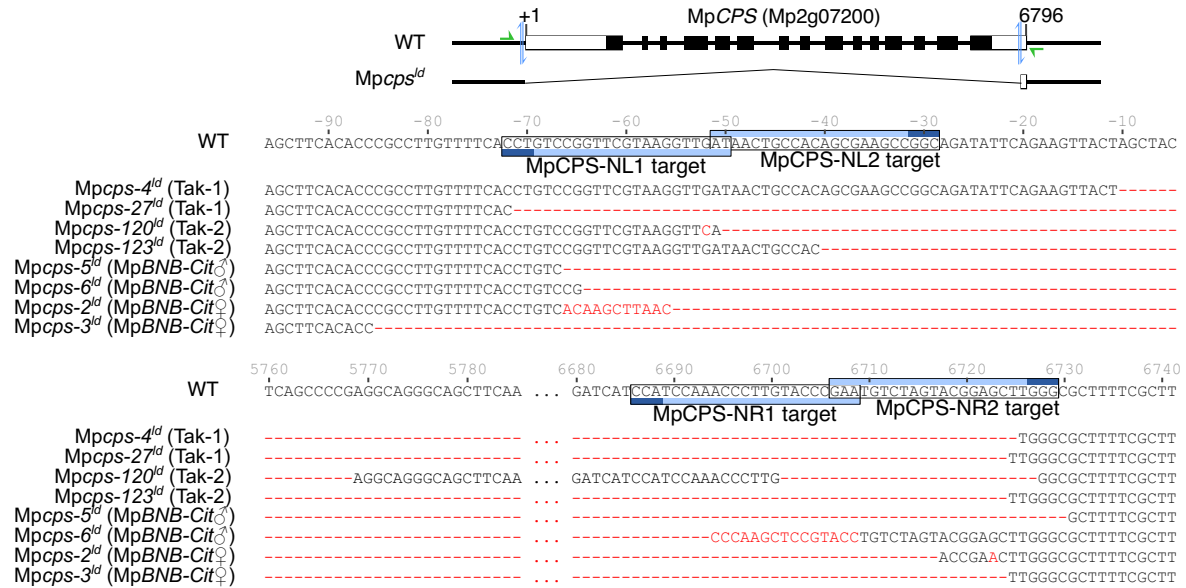


Figure 2-8 Genotype information of *Mpcps^{ld}* mutants in this research. The reference sequence (WT) was extracted from the MpTak_v6.1 genome assembly. In the gene structure diagram, untranslated regions in the transcript are depicted as white rectangles, while coding regions of exons are represented by black rectangles. Binding sites for genotyping primers are indicated by green arrows. Target sites for guide RNAs are denoted by blue arrows in the diagram and highlighted in the sequence with frames, with the protospacer adjacent motif (PAM) indicated in dark blue. Numbers above the sequence indicate their positions relative to the transcription start sites (+1). In the alignment, insertions and substitutions are highlighted using red letters.

Given that the biosynthesis of GA₁₂ and presumably other GA-related compounds is elevated under FR enriched conditions, the thallus morphology of the mutants was observed under both cW and cW+cFR conditions after 12 days of growth from gemmae. In most cases, both of the two apical meristems of a *M. polymorpha* gemma would independently develop into mature thallus tissue. The part that derived from a single gemma meristem was defined as a “half thallus”. Two half thalli developed from one gemmae were measured separately for size, shape and hyponasty.

When *Mpcps-4^{ld}* and *Mpcps-27^{ld}* mutants of the male Tak-1 background were grown under the cW condition, their morphology was only slightly different from that of wild-type plants. Smaller growth angles were observed between the thalli of *Mpcps^{ld}* mutants and the agar medium, and the thallus pieces were marginally larger and wider than those of wild-type plants (Figure 2-9). Meanwhile, Tak-1 plants exhibited a pronounced response to FR enrichment through hyponastic growth that drastically increased the growth angles, as well as anisotropic growth that resulted in slenderer thalli with increased length-width ratios. These morphological changes were absent in *Mpcps^{ld}* mutants, confirming that MpCPS is

essential for the growth responses to FR enrichment (Figure 2-9). In addition, *Mpcps^{ld}* mutants showed a substantial increase in thallus size compared to wild-type plants under cW+cFR (Figure 2-9A,D). This suggests that MpCPS potentially engages in a pathway generating growth-inhibiting compounds in *M. polymorpha*, which is opposite to the growth-promoting GAs in angiosperms. As a verification, two independent complementation lines were generated from *Mpcps-4^{ld}*, using the 35S constitutive promoter to express the CDS of MpCPS with a Citrine fused at the C-terminus (*pro35S:MpCPS-Cit*). Under both light conditions, this construct fully reversed the thallus shape, size and hyponasty of *Mpcps^{ld}*, confirming that these phenotypes were caused by MpCPS loss-of-function (Figure 2-9).

The female Tak-2 accession was less sensitive to FR enrichment, and no consistent difference was observed between *Mpcps^{ld}* mutants and wild-type plants under cW. Nevertheless, the female *Mpcps^{ld}* mutants developed significantly larger, wider and flatter thallus under cW+cFR, which could be complemented by the *pro35S:MpCPS-Cit* construct (Figure 2-10).

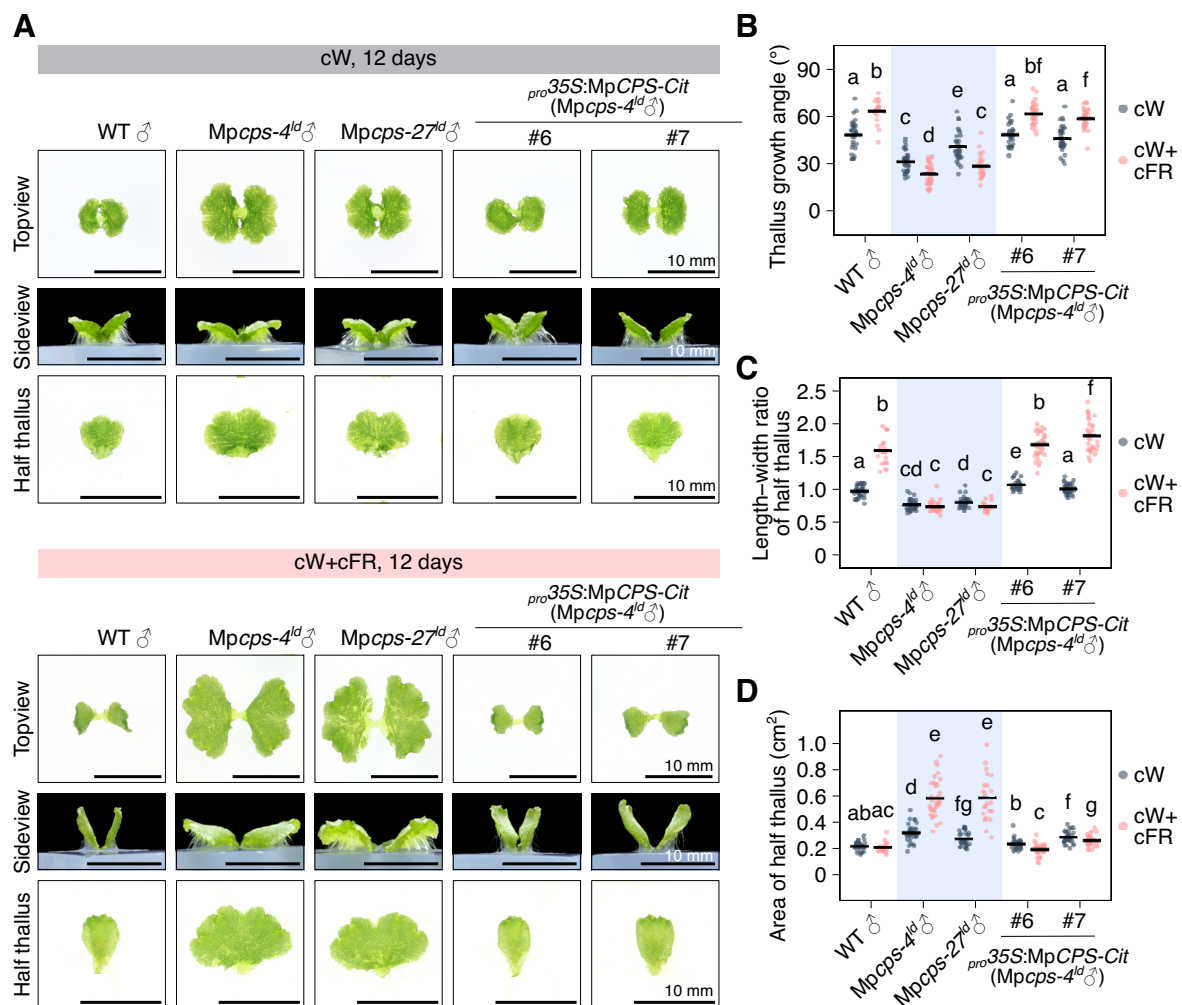


Figure 2-9 Thallus morphology of male *Mpcps^{ld}* mutants under cW and cW+cFR. (A) Representative images of 12-day-old plants. Different views were selected arbitrarily from different plants. (B-D) Quantification of thallus growth angles (B), length-width ratios (C) and thallus sizes (D) from half thalli shown in (A). Each dot represents data from a “half thallus” (n=21-36), and horizontal bars represent mean values. Letters represent statistical differences from non-pooled Welch’s *t*-test with Benjamini-Hochberg adjustment, and non-overlapping letter combinations were significantly different (adjusted $P < 0.05$).

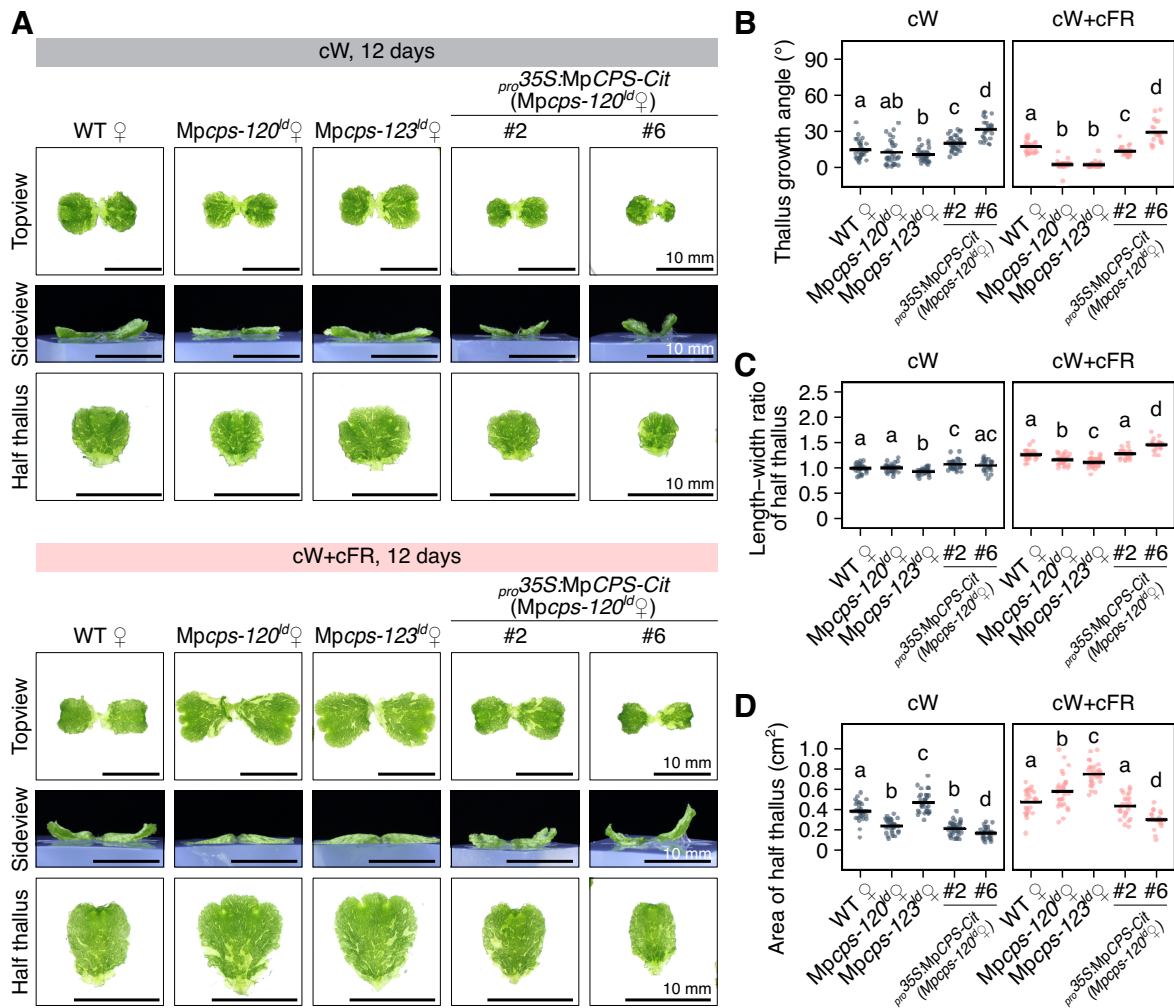


Figure 2-10 Thallus morphology of female *Mpcps*^{td} mutants under cW and cW+cFR. (A) Representative images of 12-day-old plants. Different views were selected arbitrarily from different plants. (B-D) Quantification of thallus growth angles (B), length-width ratios (C) and thallus sizes (D) from half thalli shown in (A). Each dot represents data from a “half thallus” (n=19-34), and horizontal bars represent mean values. Letters represent statistical differences from non-pooled Welch’s *t*-test with Benjamini-Hochberg adjustment, and non-overlapping letter combinations were significantly different (adjusted $P < 0.05$).

To assess the influence of *Mpcps^{ld}* on thallus growth at the tissue level, cell division activities were investigated in 7-day-old plants grown under cW+cFR using 5-ethynyl-2'-deoxyuridine (EdU). This thymidine analogue could be incorporated into the nuclei of S-phase cells and further conjugated with fluorophores through click chemistry (Salic and Mitchison, 2008). After image acquisition with confocal microscopy, signals acquired at different depth were color-coded to visually represent the three-dimensional distribution of actively dividing cells (Figure 2-11A). As expected, in all the samples cells actively proliferated around the apical meristems, and gradually ceased division in a basipetal manner. In the slender thalli of wild-type plants and *MpCPS* complementation lines, EdU-positive nuclei were restricted to a relatively narrow region near the midrib (Figure 2-11A-B). Interestingly, different distribution patterns were observed between dorsal and ventral signals in these samples. In the ventral side, EdU signals retained further along the midrib in the basal direction, while in the dorsal side EdU signals were distributed near the apical region. Such asymmetry in cell division activity could be a reason for the FR-induced hyponastic growth (Figure 2-11A). Compared to wild-type plants, the overall cell division was more active in *Mpcps^{ld}* mutants, as quantified by higher numbers of EdU-positive nuclei (Figure 2-11A,C). It was common to observe two fully separated apical meristems instead of one in these samples, suggesting a faster progress of bifurcation that might have benefited from and also contributed to the active cell divisions (Figure 2-11A,C). In *Mpcps^{ld}* mutants, the distribution patterns of EdU signals were similar between the dorsal and ventral sides, which might explain the horizontal thallus growth under FR enriched conditions (Figure 2-11A).

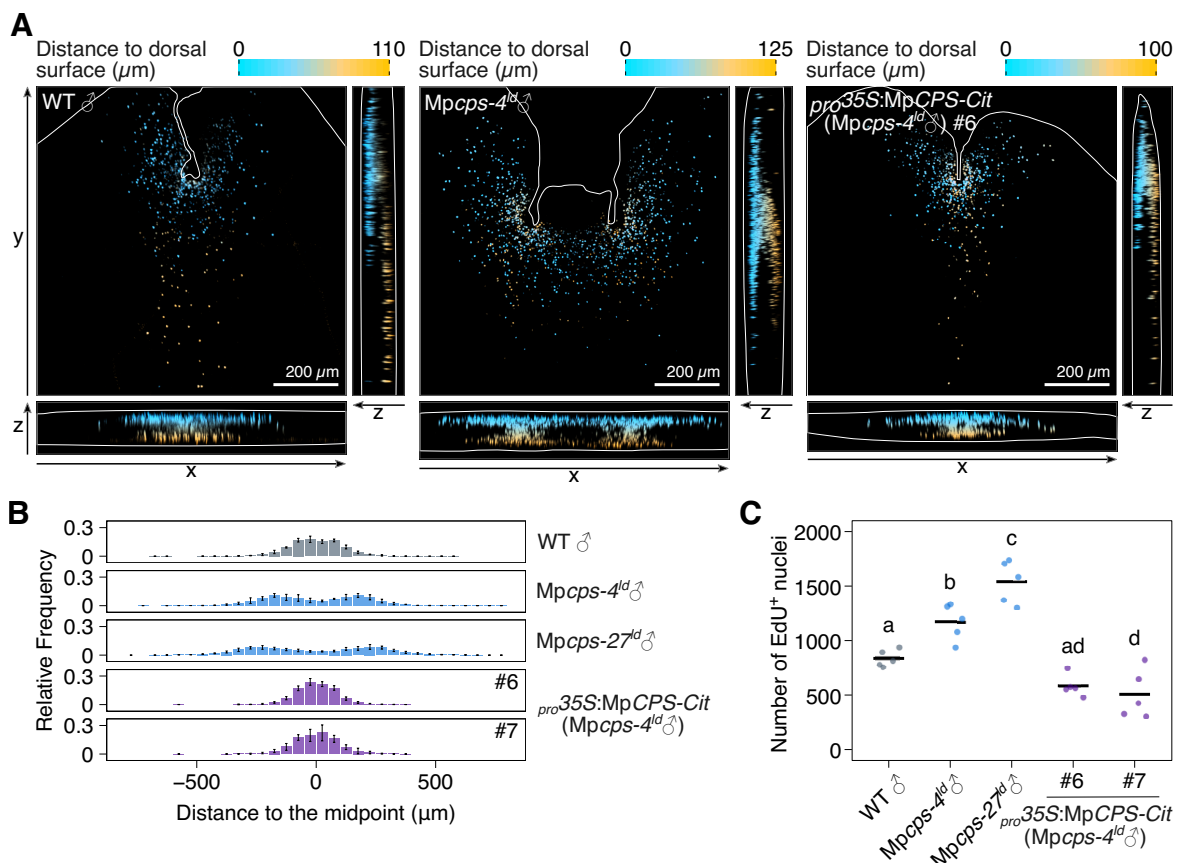


Figure 2-11 Cell division activities in thallus grown under cW+cFR. (A) Selected image stacks of apical regions from 7-day-old plants labelled with EdU, color-coded by z-direction depth and presented in two-dimensional projections from three directions. The margins of thalli or the borders of imaging areas are marked with white lines. (B) Distribution of EdU-positive (EdU⁺) nuclei along the x axis. (C) Total number of EdU⁺ nuclei in the apical regions (n=5). Letters represent statistical groups by Tukey's HSD test ($P < 0.05$ for non-overlapping letters).

MpCPS is required for gemma dormancy in the gemma cup

The observations above showed that MpCPS loss-of-function mildly enhanced thallus growth in 12-day-old plants even under the cW condition. When the plants were cultured for a longer duration under cW (25 days from gemmae), the increase in thallus sizes was no longer observed in male *Mpcps^{ld}* mutants. Instead, they were moderately smaller and developed fewer number of gemma cups than Tak-1 wild-type plants, possibly suffering from physical hinderance when the thallus tips were growing downwards into the agar medium (Figure 2-12A-B). Nevertheless, decreased gemma dormancy was observed in both *Mpcps-4^{ld}* and *Mpcps-27^{ld}*, as both lines harbored lower ratios of dormant gemma cups with no germinated gemma. The complementation of *Mpcps-4^{ld}* by *pro35S:MpCPS-Cit* did not rescue the thallus size or total number of gemma cups, but the ratio of dormant gemma cups was restored (Figure 2-12B-D). The reduction in gemma dormancy resembled that of *Mppif^{ko}* mutants (Hernández-García et al., 2021), which is consistent with the hypothesis that the biosynthesis of GA-related compounds acts downstream of MpPIF.

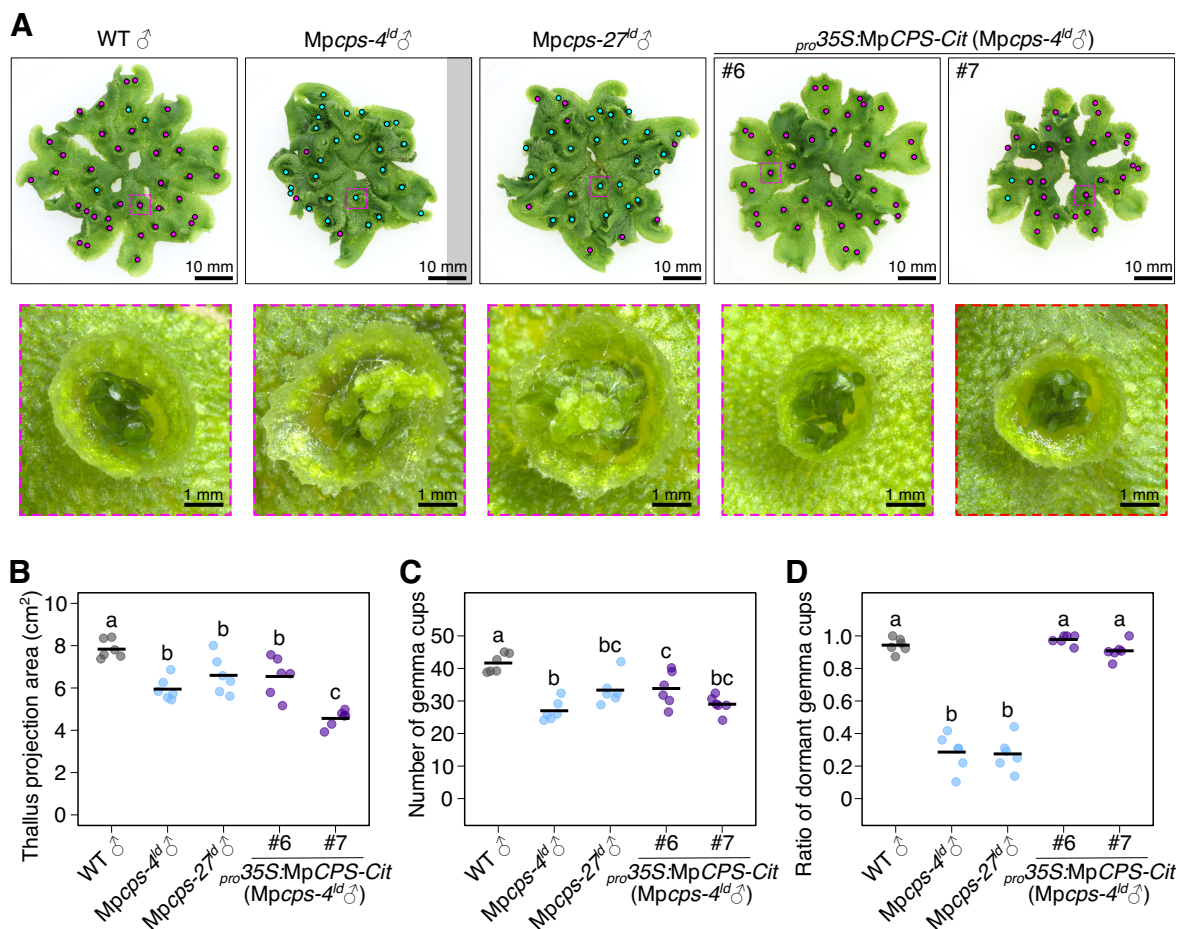


Figure 2-12 *Mpcps^{ld}* altered in-cup gemma dormancy under cW. (A) Representative images of 25-day-old plants grown from gemmae under cW. Cyan and magenta dots indicate dormant and non-dormant gemma cups, respectively. For the gemma cups indicated by dashed boxes, images were taken under stereoscopes to show gemma dormancy or germination in the bottom row. A gemma cup was defined as non-dormant if at least one gemma in the cup developed rhizoids or was enlarged in size. (B-D) Quantifications of thallus sizes (B), total numbers of gemma cups (C), or the ratio of dormant gemma cups (D) in different genotypes. Each dot represents data from a single plant (n=6), and horizontal bars represent mean values. Non-overlapping letters indicate significant statistical difference ($P < 0.05$ by Tukey's HSD test).

MpCPS participates in the regulation of gametangiophore formation

Sexual reproduction is one of the major FR responses in *M. polymorpha* (Inoue et al., 2019). Generally under cW, all the apical meristems of *M. polymorpha* undergoes indeterminate growth, bifurcating periodically to generate dichotomous branches. Conversely, under FR-enriched condition with sufficient FR irradiance, a proportion of apical meristems would enter dormancy, and another proportion of meristems would differentiate into sexual branches called gametangiophores (Streubel et al., 2023; Inoue et al., 2019). To determine if this process is affected by *Mpcps^{ld}*, experiments were carried out under FR-enriched conditions with different culturing methods. For quantitative analysis, plants were grown from gemmae in aseptic culture under cW for 7 days, then half thalli developed from single gemma meristems were transferred onto fresh medium and cultured under cW+cFR. Consistent with the results in the last section, *Mpcps^{ld}* showed faster growth under this condition (Figure 2-13A). During the induction period, both male and female *Mpcps^{ld}* mutants gradually developed higher total numbers of apical meristems than their wild-type parents and complementation lines (Figure 2-13B). It could be a result simply from faster bifurcation as observed in the EdU analysis, or it might suggest that fewer apical meristems adopted FR-induced determinate fates in *Mpcps^{ld}* mutants. In addition, the progress of gametangiophore formation was slower in *Mpcps^{ld}*, which was shown by both the delay in forming the first gametangiophores and fewer occurrence of gametangiophore formation throughout the 16 days of observation after FR irradiation (Figure 2-13A-B).

In addition, *MpCPS* loss-of-function distorted the gametangiophore morphology in both male and female plants. *M. polymorpha* is a dioicous plant that generates eggs and sperms on different gametophytes carrying different sex chromosomes, and the gametangiophores are sexually dimorphic. In wild-type plants, the male gametangiophores developed round, disc-like receptacles connecting to cylindrical stalks in the ventral center. In contrast, the receptacles of male *Mpcps^{ld}* mutants were fan-shaped, connecting to the stalks at the basal end (Figure 2-13C). Similarly, the female receptacles of wild-type plants were shaped like umbrellas, developing finger-like structures (digitate rays) in a circle. While for female *Mpcps^{ld}* plants, the receptacles were palm-like, with all the digitate rays arranged in a row (Figure 2-13C). Some of the *Mpcps^{ld}* female gametangiophores continued to bifurcate during development, which in extreme cases generated a large dichotomous branch (Figure 2-13D).

When the plants were grown on vermiculites in the open air, the morphology of gametangiophores were slightly different from that in petri dishes (Figure 2-14A-D). With no physical restriction in the vertical direction, the stalk length of gametangiophores could be easily evaluated. Compared to wild-type plants, the stalks of both male and female *Mpcps^{ld}* gametangiophores were shorter, thicker and wider (Figure 2-14A-B). In addition, the palm-like female receptacles of *Mpcps^{ld}* were more compact when grown in the open air, with little sign of clear bifurcation. Instead, more digitate rays were developed in *Mpcps^{ld}* receptacles (Figure 2-14D). Despite the morphological changes, the fertility of *Mpcps^{ld}* gametangiophores seemed to be unaffected. In the crossing experiments, mature spores could be generated in all combinations between wild-type plants and *Mpcps^{ld}* mutants, and no obvious difference was noticed between wild-type and *Mpcps^{ld}* sporophytes (Figure 2-14E-F).

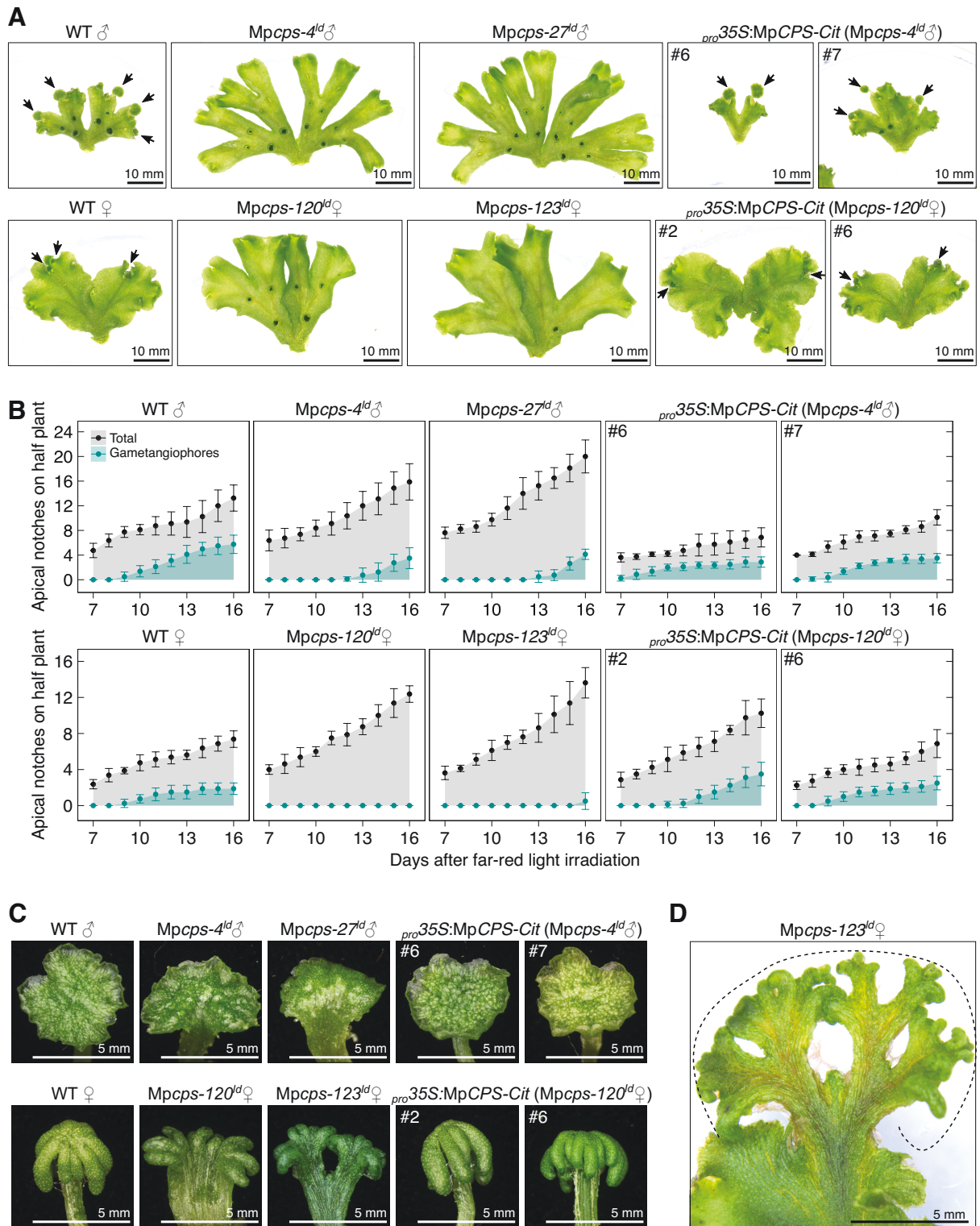


Figure 2-13 The influence of *Mpcps^{ld}* on gametangiophore formation in the aseptic culture. The plants were cultured for 7 days under cW and 16 days under cW+cFR. (A) Morphology of thallus fragments during gametangiophore induction. Arrows indicate gametangiophores that could be seen with naked eyes. (B) Progress of bifurcation and gametangiophore formation in apical notches. Dots and error bars represent mean \pm SD (n=8). (C) Morphology of young gametangiophore receptacles. (D) A female gametangiophore of *Mpcps^{ld}*, showing an extreme example of indeterminate bifurcation. The whole structure indicated by the dashed line is equivalent to a single gametangiophore in normal plants.

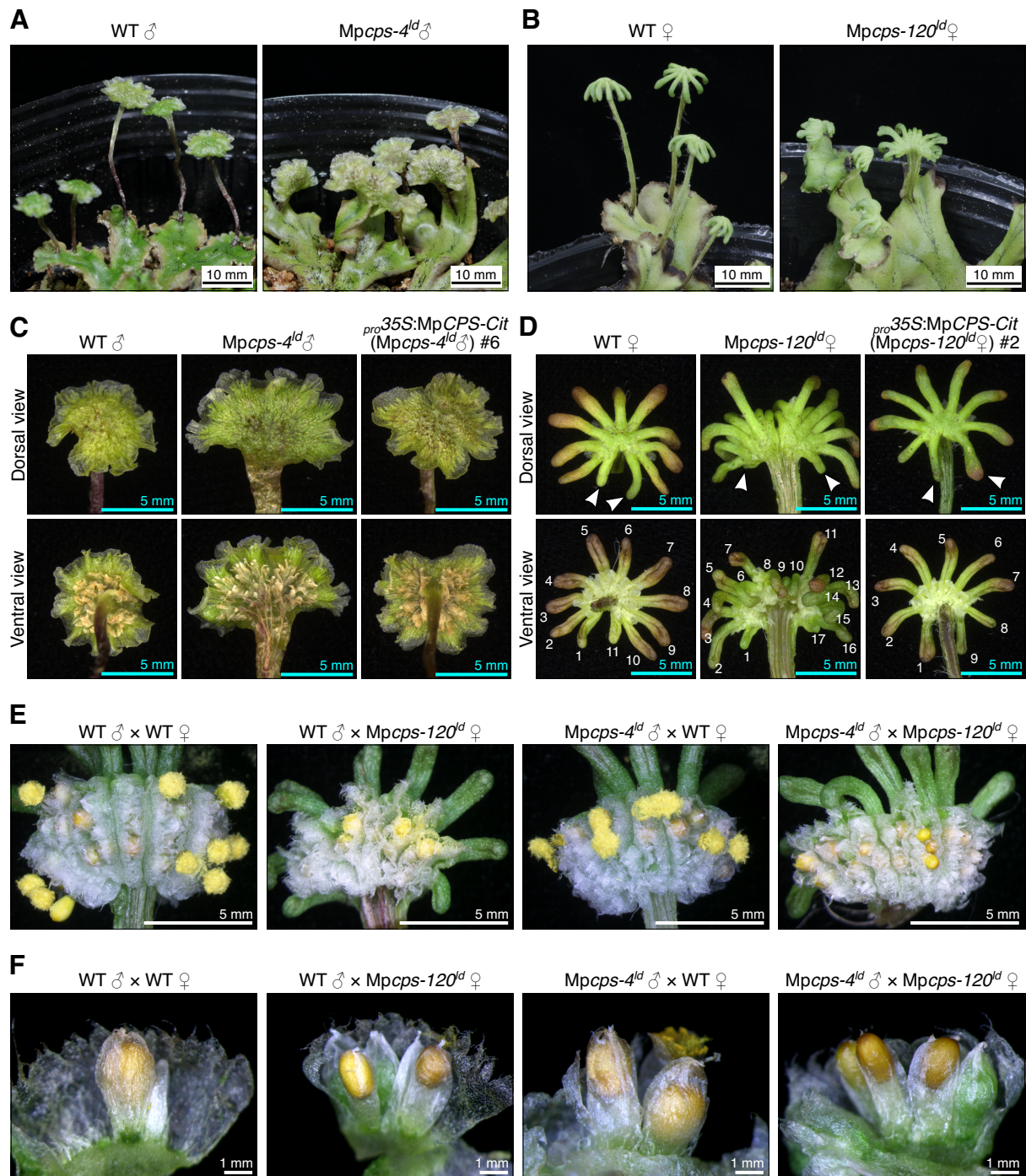


Figure 2-14 Morphology and fertility of *Mpcps^{ld}* gametangiophores when grown on vermiculites. (A) Morphology of male plants bearing gametangiophores, photographed after 81 days of growth under cW+cFR. (B) Morphology of female plants bearing gametangiophores, photographed after 63 days of growth under cW+cFR. (C-D) Morphology of male (C) and female (D) gametangiophores. Arrowheads in (D) indicate the marginal digitate rays. (E-F) Crossing experiments with all combinations between wild-type and *Mpcps^{ld}* mutants, showing the whole receptacle bearing spores (E) or individual sporophytes (F).

The anatomy of *Mpcps^{ld}* gametangiophores was further observed with cross sections, which revealed thallus-like features in the mutant stalks. In wild-type plants, the male gametangiophore stalk was nearly cylindrical, carrying no air chambers in the dorsal side. On the contrary, the thick, wide stalk of *Mpcps^{ld}* male gametangiophores had a flat dorsal surface, which developed air chambers with photosynthetic filaments (Figure 2-15A), similar to the thallus structure (Shimamura, 2016). The female gametangiophore stalks of wild-type plants also had air chambers in the dorsal side, which was separated from the ventral part by two side grooves. The grooves were shallower in the *Mpcps^{ld}* female stalk, connecting the dorsal and ventral surfaces in a relatively smooth manner (Figure 2-15B). In the ventral side, both male and female *Mpcps^{ld}* gametangiophore stalks tended to have more canals for pegged rhizoids, which might be resulted from excessive bifurcation during gametangiophore morphogenesis (Figure 2-15A-B). Consistent with the fertility test, no abnormalities were observed in antheridia or archegonia of *Mpcps^{ld}* mutants (Figure 2-15C-D).

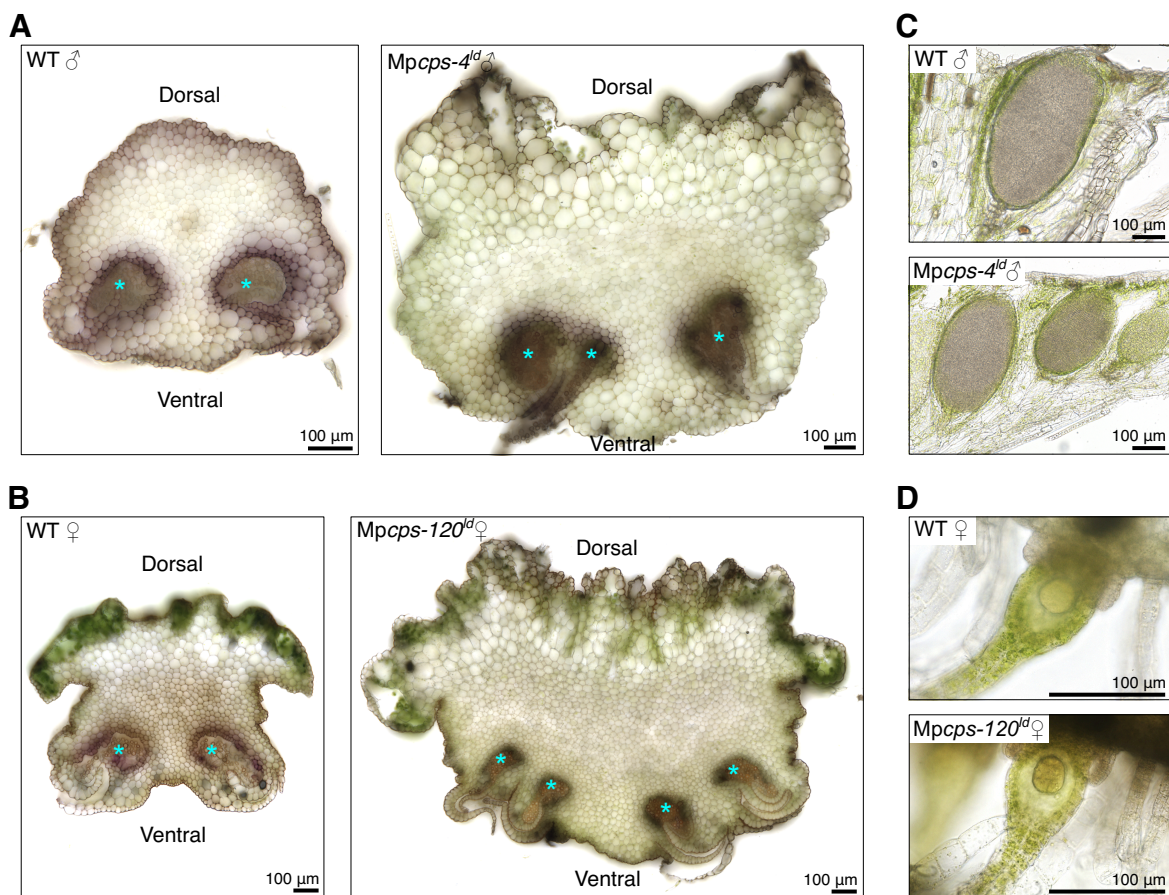


Figure 2-15 Cross-sections showing the anatomy of *Mpcps^{ld}* gametangiophores. (A-B) Transverse agar sections of male (A) and female (B) gametangiophore stalks. Bundles of pegged rhizoids were indicated with asterisks (*). Thickness: 200 μm. (C-D) Vertical agar sections of gametangiophores, showing the antheridia in male receptacles (C) or mature archegonia with egg cells in female receptacles (D). Thickness: 70 μm.

Among the regulatory genes for sexual reproduction, *MpBONOBO* (*MpBNB*) is a master regulator that is both sufficient and necessary for gametangium and gametangiophore initiation in *M. polymorpha* (Yamaoka et al., 2018). Furthermore, the specific accumulation of *MpBNB* proteins in the initial cells and young gametangia (Yamaoka et al., 2018) provided a tool for tracing the influence of *Mpcps^{ld}* on reproductive development. To avoid artifacts from variation in genetic background, the CDS region of *MpCPS* was completely removed from *MpBNB-Citrine* knock-in lines (*MpBNB-Cit*) through genome editing with the CRISPR/Cas9^{D10A} nickase system (Hisanaga et al., 2019; Koide et al., 2020). For observation, male and female plants were cultured from gemmae under cW+cFR for 11 and 14 days, respectively. At the time of sampling, dome-shaped gametangiophore primordia could be found in plants with the wild-type *MpCPS* allele. Moreover, clusters and arrays of cell nuclei accumulating *MpBNB-Cit* were visible in the primordia, which indicated the timely gametangium differentiation. In contrast, *Mpcps^{ld}* *MpBNB-Cit* plants of the same age produced no visible gametangiophores, and Citrine-positive nuclei with *MpBNB* accumulation rarely appeared in the apical regions (Figure 2-16). This result supported that *Mpcps^{ld}* negatively modulates FR-induced gametangium differentiation, which might be related to down-regulation of *MpBNB* activity.

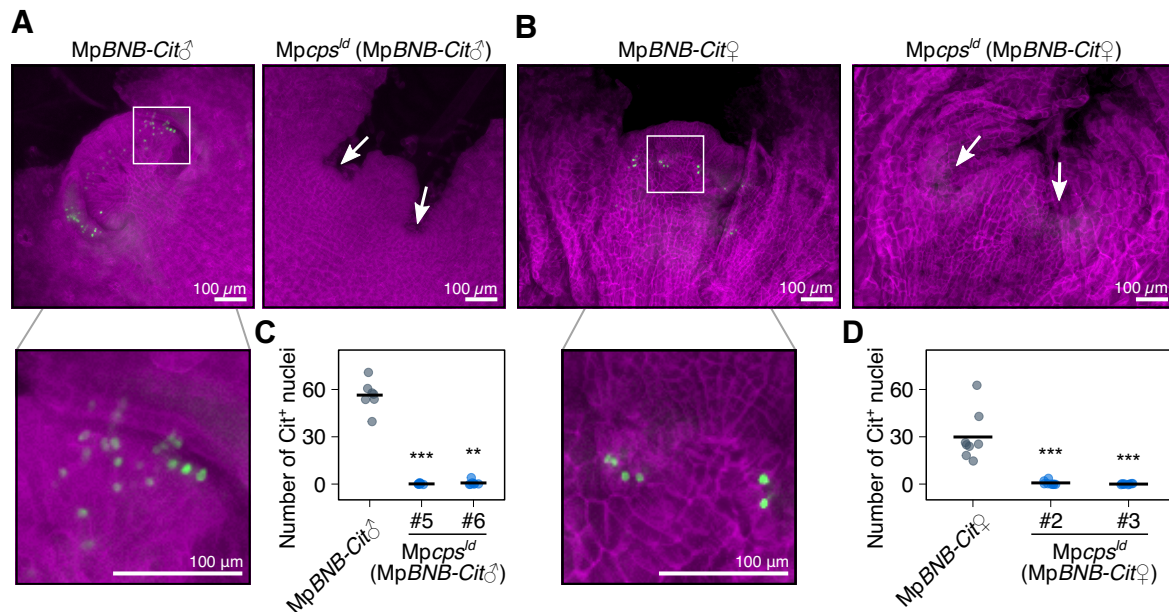


Figure 2-16 *Mpcps^{ld}* delayed gametangium differentiation under cW+cFR. (A-B) Z-stack projections of fluorescence microscopic images showing *MpBNB-Cit* accumulation (green signals) in 11-day-old male (A) or 14-day-old female (B) plants grown from gemmae under cW+cFR. Cell walls were stained with calcofluor white (shown in magenta). Arrows indicate apical meristems. Enlarged view of the boxed region was shown in the bottom. (C-D) Quantification of Citrine-positive (Cit⁺) nuclei in apical regions. Each dot represent data from a “half thallus” (C, n=7) or a quarter of the thallus (D, n=8). Horizontal bars represent mean values. Statistical difference compared to the control group is indicated by asterisks (Mann–Whitney *U* test; **, *P*<0.01; ***, *P*<0.001).

Mpcps^{ld} can be rescued by KA but not canonical GAs

Previous analysis in the laboratory showed that among 14 GAs commonly identified in angiosperms (GA₁, GA₃, GA₄, GA₉, GA₁₂, GA₁₅, GA₁₉, GA₂₀, GA₂₄, GA₂₉, GA₃₄, GA₄₄, GA₅₁ and GA₅₃), only GA₁₂ could be detected endogenously in Tak-1 plants (Okabe, bachelor's thesis, 2022) (see also Figure 2-7). It is highly probable that the bioactive compound in *M. polymorpha* is structurally different from canonical GAs in angiosperms. To test this hypothesis, several GA-related compounds were tested for their bioactivity in wild-type and Mpcps-4^{ld} plants.

In the first experiment, plants were culture for 12 days from gemmae under cW+cFR, on agar medium containing 2 μM of a GA-related compound or the solvent control (Figure 2-17A-B). Among the five compounds tested, 2 μM KA efficiently rescued the thallus morphology of Mpcps^{ld} mutants, while none of the canonical bioactive GAs (GA₁, GA₃ or GA₄) evoked a comparable response. GA₉-Me is one of the pheromone compounds released by *Lygodium* ferns, which could promote antheridia formation in young prothalli at 1 nM concentration (Yamane et al., 1979; Yamauchi et al., 1996; Tanaka et al., 2014). In the moss *P. patens*, 1 μM of GA₉-Me rescued protonema differentiation of the Ppcps/ks mutant. However, the Mpcps^{ld} mutant showed little response to 2 μM of GA₉-Me, rejecting its bioactivity in FR responses of *M. polymorpha*.

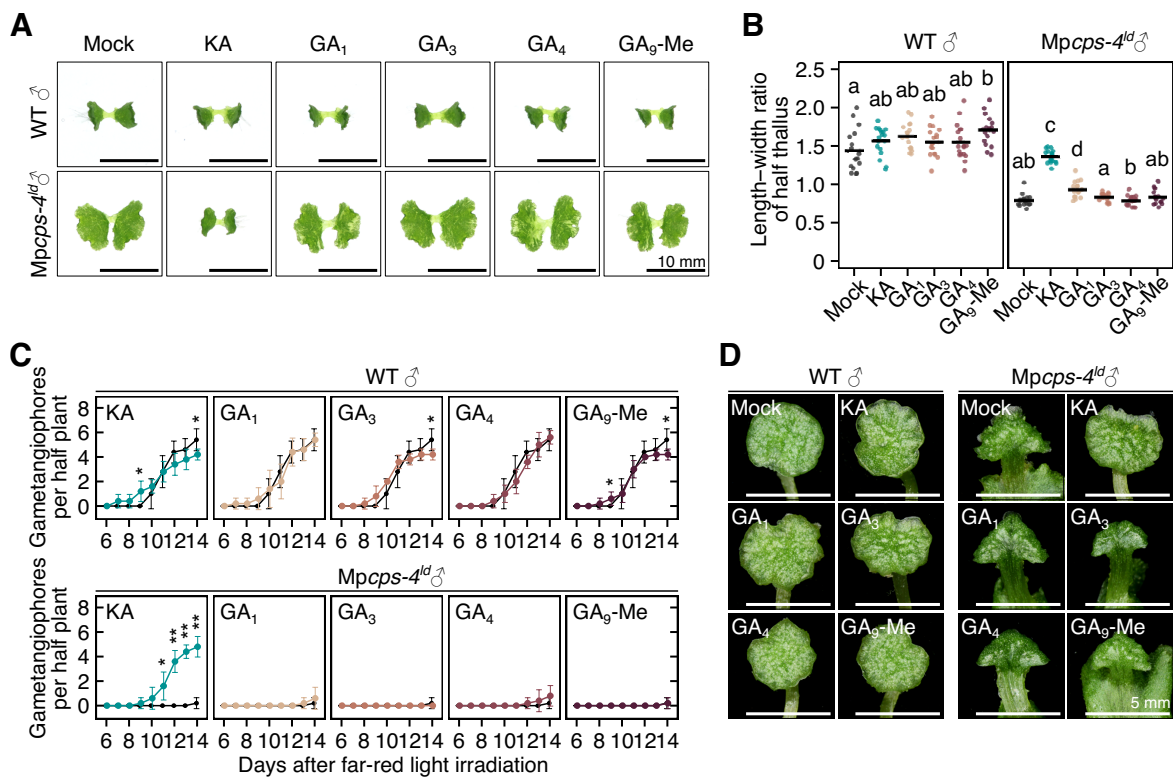


Figure 2-17 Effects of various GA-related compounds on FR responses of *M. polymorpha*. (A-B) Morphology of 12-day-old plants grown under cW+cFR with chemical treatments. Each dot in (B) represents data from a half thallus (n=16-18). Horizontal bars represent mean values, and non-overlapping letters represent significant statistical difference (non-pooled Welch's *t*-test with Benjamini-Hochberg adjustment, adjusted *P*<0.05). (C) Progress of gametangiophore formation with chemical treatment of GA-related compounds. Dots and error bars represent mean±SD (n=5). Asterisks indicate statistical difference by Kruskal-Wallis test (*, *P*<0.05; **, *P*<0.01). In each subplot, data from the mock group (black curves) was shown repetitively for comparison. (D) Morphology of male gametangiophore receptacles.

In a second experiment, plants were grown from gemmae under cW for 7 days, then transferred onto fresh agar medium containing GA compounds and placed under cW+cFR for observation of gametangiophore formation. Similar to the results above, 2 μ M of KA but not any other GAs rescued the delay in *Mpcps-4^{ld}* gametangiophore formation, as well as the morphology of male receptacles (Figure 2-17C-D). Such an observation supported that the phenotypes of *Mpcps^{ld}* mutant were caused by deficiency in one or more bioactive compounds derived from KA. For convenience, the putative bioactive compound(s) is referred to as “GA_{Mp}” in the following text. On the other hand, none of the chemicals induced any evident developmental changes in wild-type plants, including KA. KA might serve as a biosynthesis intermediate rather than being directly bioactive. Alternatively, GA_{Mp} responses might already be saturated in wild-type plants under FR-enriched conditions.

KA is a crucial intermediate in GA_{Mp} biosynthesis

To validate the biological function of other evolutionarily conserved GA biosynthesis enzymes, *Mpks^{ld}*, *Mpkol1^{ld}* and *Mpkaol1^{ge}* mutants were generated in the Tak-1 background. Genomic fragments were removed from the locus of *MpKS* or *MpKOL1* using the CRISPR/Cas9^{D10A} nickase system (Hisanaga et al., 2019; Koide et al., 2020) (Figure 2-18A-B). Frame-shift mutations were introduced into the CDS of *MpKAOL1* with regular CRISPR/Cas9 (Sugano et al., 2014) near the start codon (Figure 2-18C). As expected, all of the mutants inhibited the biosynthesis of GA₁₂ to a level below the detection limit, similar to the case in *Mpcps-4^{ld}* (Figure 2-19).

When the plants were grown under the cW+cFR condition for 12 days, all three mutants exhibited phenotypes that resembled *Mpcps^{ld}*. Compared to wild-type plants, the mutants exhibited significant decrease in thallus hyponasty and length-width ratio but drastic increase in plant size (Figure 2-20A-D), which suggested a reduced response to FR enrichment. Since *MpKS* and *MpKOL1* catalyze reactions upstream of KA production, it is expected that KA treatments could rescue *Mpks^{ld}* and *Mpkol1^{ld}*. As anticipated, the thallus hyponasty, size and shape of *Mpks^{ld}* and *Mpkol1^{ld}* was fully restored by 2 μ M KA. Similarly, as *MpKAOL1* uses KA as a substrate, *Mpkaol1^{ge}* plants should not be influenced by KA treatment. However, *Mpkaol1^{ge}* plants showed a weak but statistically significant response to 2 μ M KA (Figure 2-20A-D). To further examine this responsiveness to KA, *Mpkaol1-5^{ge}* and *Mpcps-4^{ld}* were treated using a series of KA concentrations lower than 2 μ M. Under the same growth conditions, 10 nM KA was sufficient to trigger a response in *Mpcps-4^{ld}*, and the response was robust at the dose of 100 nM. In contrast, *Mpkaol1^{ge}* was not sensitive to all concentrations of KA equal to or lower than 1 μ M (Figure 2-20E-H), indicating that the response occurs only at high KA concentration.

Gametangiophore formation was also observed for *Mpks^{ld}*, *Mpkol1^{ld}* and *Mpkaol1^{ge}* mutants (Figure 2-21). *Mpks^{ld}* and *Mpkol1^{ld}* delayed the formation of gametangiophores and developed fan-shaped antheridiophores, just like *Mpcps^{ld}*. In addition, both the delay and the morphology could be rescued by application of 2 μ M KA. Meanwhile, *Mpkaol1^{ge}* mutants formed normal gametangiophores with a moderate delay in the timing, regardless of the presence or absence of 2 μ M KA.

Taken together, it seems that KA is a critical intermediate for the biosynthesis of GA_{Mp}. Any mutant that blocks the generation of KA caused a severe defect in FR response, and KA can fully rescue these mutants. Based on the catalytic activity, it is not likely that KA biosynthesis is directly influenced by the *Mpkaol1^{ge}* mutation. Yet some aspects of FR responses were defective in *Mpkaol1^{ge}*, suggesting that KA itself is not sufficient to evoke all GA_{Mp} responses.

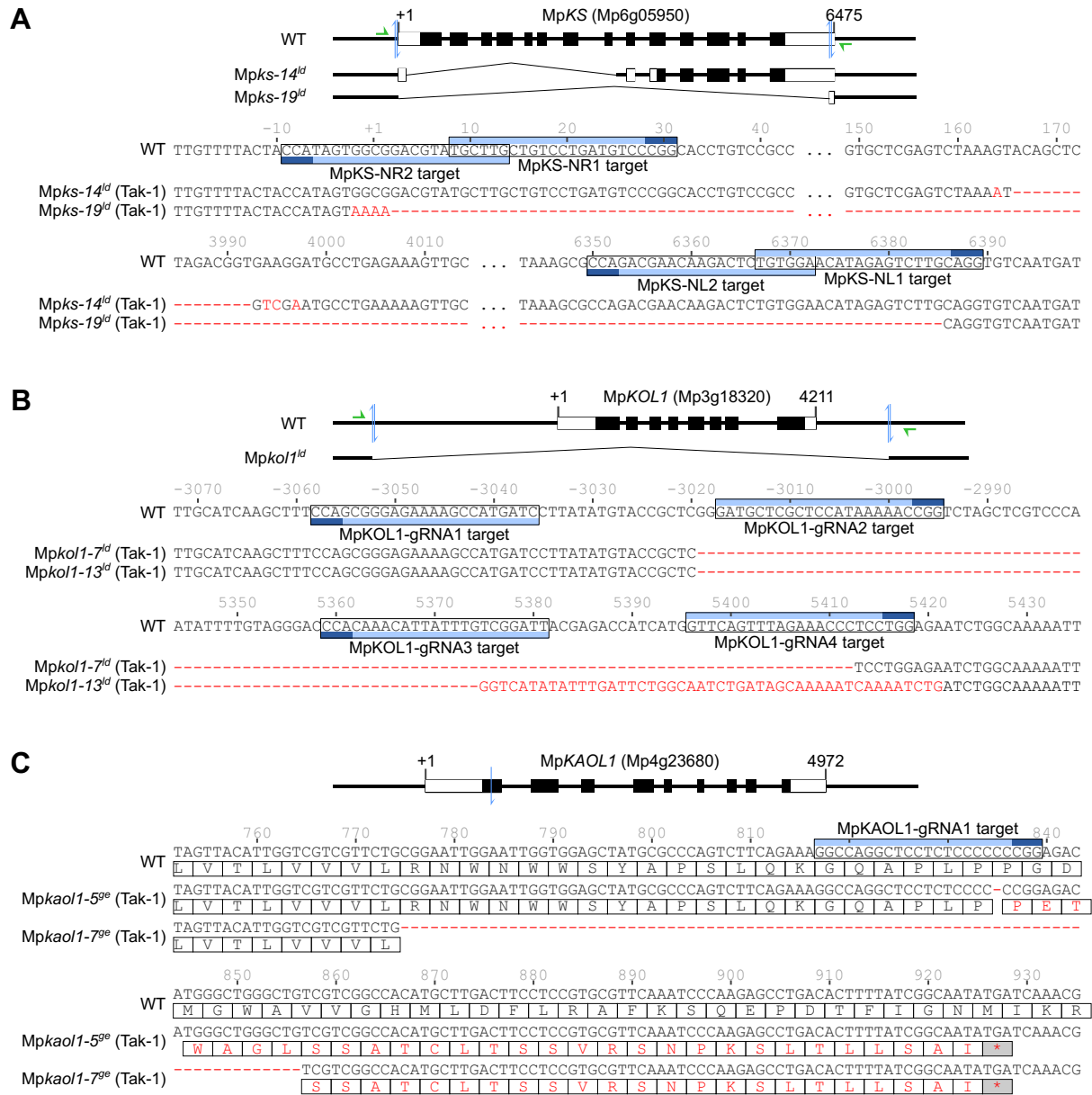


Figure 2-18 Genotype information of *Mpks^{ld}* (A), *Mpkol1^{ld}* (B) and *Mpkao1^{se}* (C) mutants. The reference sequence (WT) was extracted from the MpTak_v6.1 genome assembly. In the gene structure diagram, untranslated regions in the transcript are depicted as white rectangles, while coding regions of exons are represented by black rectangles. Binding sites for genotyping primers are indicated by green arrows. Target sites for guide RNAs are denoted by blue arrows in the diagram and highlighted in the sequence with frames, with the protospacer adjacent motif (PAM) indicated in dark blue. Numbers above the sequences indicate their positions relative to the transcription start sites (+1). In the alignments, insertions and substitutions are highlighted using red letters. In (D), putative translations are presented using framed letters, with asterisks (*) indicating premature stop codons.

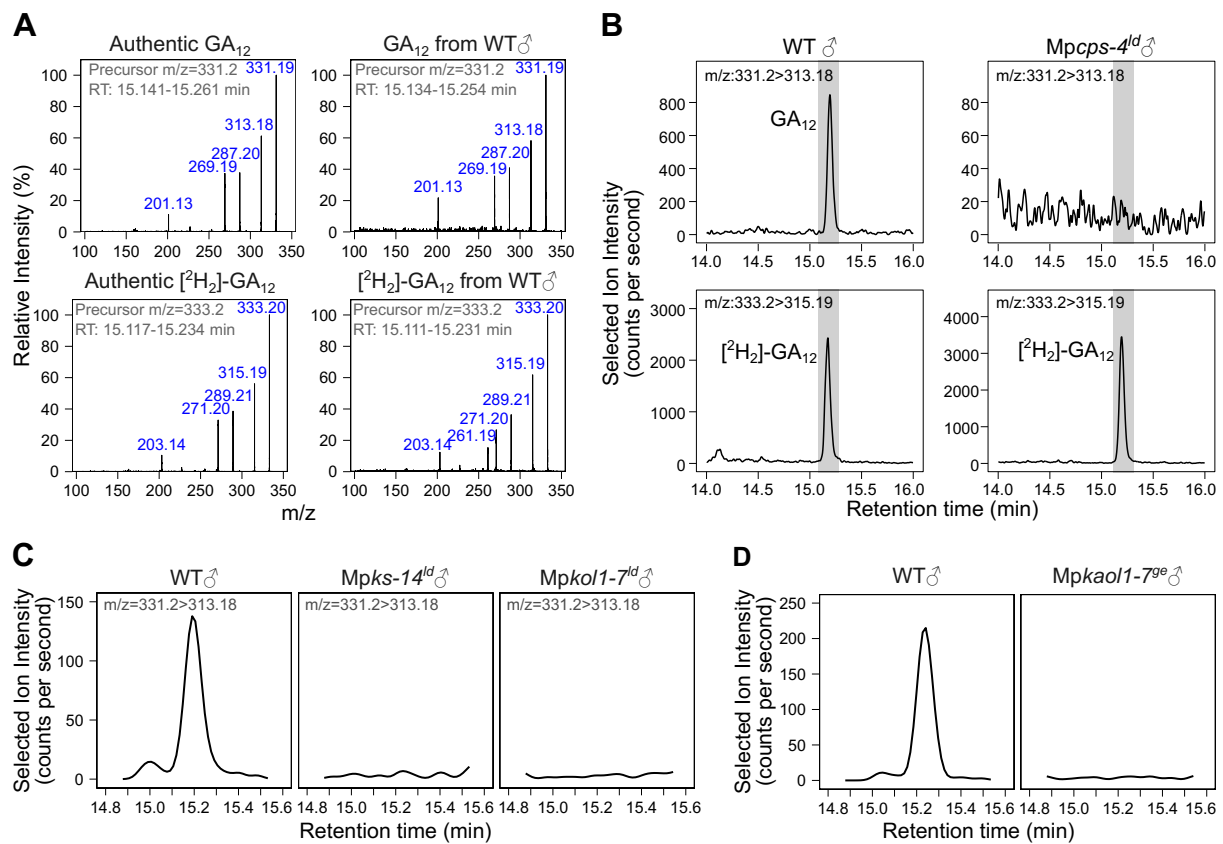


Figure 2-19 Analysis of endogenous GA_{12} in GAM_p biosynthesis mutants by LC-MS/MS. (A) Identification of GA_{12} in wild-type plants by LC-MS/MS, showing identical mass spectra of GA_{12} and $[^2H_2]-GA_{12}$ with authentic compounds. (B) Selected ion chromatograph showing the absence of endogenous GA_{12} in $Mpcps-4^{ld}$. The internal reference compound $[^2H_2]-GA_{12}$ was detected successfully. (C-D) Selected ion chromatograph showing the absence of GA_{12} in $Mpks-14^{ld}$, $Mpkol1-7^{ld}$ or $Mpkaol1-7^{ge}$, analyzed in the multiple reaction monitoring (MRM) mode. All the samples were collected from plants grown under cW for 10 days and then under cW+cFR for 4 days. (Data of this figure is collected by Maiko Okabe).

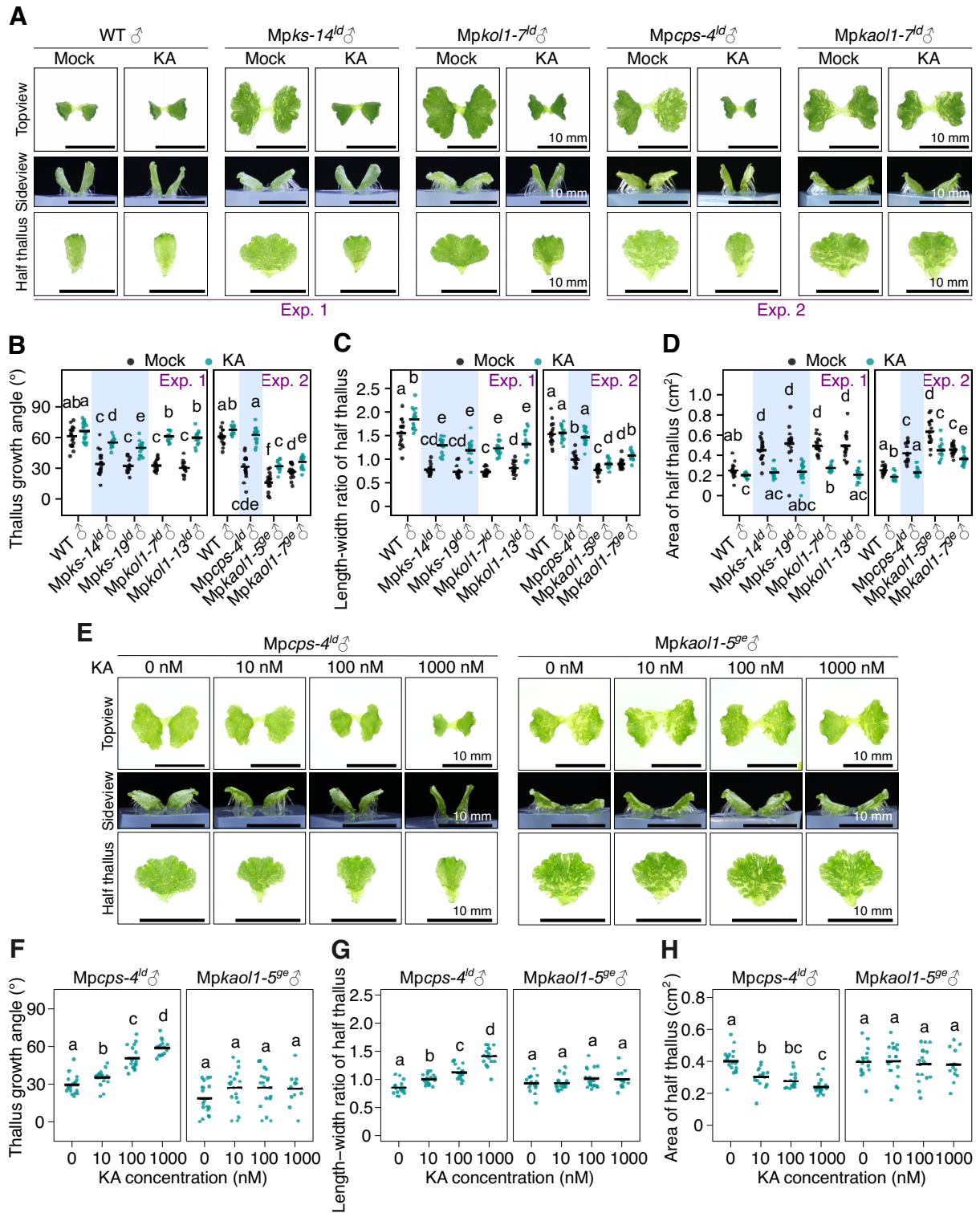


Figure 2-20 Thallus growth response of *Mpkps^{ld}*, *Mpkol^{ld}* and *Mpkao1^{se}* mutants to FR-enrichment and KA. (A) Thallus morphology of 12-day-old plants grown from gemmae under cW+cFR, with or without 2 μ M KA treatment. (B-D) Quantification of thallus hyponasty (B), shape (C) and size (D) for plants shown in (A). (E-H) Thallus morphology (E) and quantifications (F-H) of *Mpcps-4^{ld}* and *Mpkao1-5^{ge}* grown under cW+cFR with different concentrations of KA. Each dot represents data from a half thallus. Horizontal bars represent mean values, and letters represent non-pooled Welch's *t*-test with Benjamini-Hochberg adjustment (adjusted $P < 0.05$ for non-overlapping combinations). $n = 14-18$ for (B-D), $n = 12-18$ for (F-H).

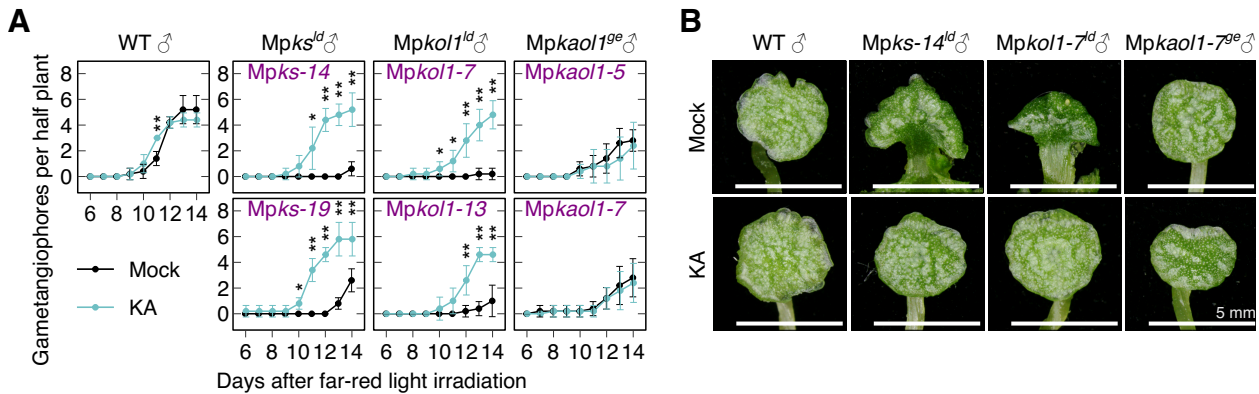


Figure 2-21 Gametangiophore formation of G_{AMp} biosynthesis mutants. (A) Progress of gametangiophore formation. Plants were grown from gemmae under cW for 7 days, then induced under cW+cFR with or without 2 μ M KA. Dots and error bars represent mean \pm SD (n=5). Asterisks indicate statistical difference by Kruskal-Wallis test (*, $P<0.05$; **, $P<0.01$). (B) Morphology of male gametangiophore receptacles.

Genetic redundancy of G_{AMp} biosynthesis enzymes

Compared to other G_{AMp} biosynthesis mutants, *Mpkao1^{ge}* exhibited a relative weak phenotype under FR-enriched conditions, which suggested that it might act redundantly with other genes. Although other KO and KAO homologs failed to show canonical activities in yeast, it is possible that they retain some affinity to GA-related compounds and participate in other steps of G_{AMp} biosynthesis. As a preliminary test for this hypothesis, mutants were generated to disrupt *MpKOL2*, *MpKOL3* and *MpKAOL3* in the Tak-1 background. Since *MpKOL2* and *MpKOL3* locate next to each other in the genome, the genomic fragment containing both genes was deleted at once to create [*Mpkol2 Mpkol3*]^{ld} double mutants. In addition, *MpTPS1* (Mp6g05430) was investigated by genetic mutation. This gene encodes a homolog of MpKS, which exhibited activity to generate *ent*-kaurene as a minor product in a previous study (Kumar et al., 2016) (Figure 2-22).

Similar to other experiments, *Mptps1^{ld}*, [*Mpkol2 Mpkol3*]^{ld} and *Mpkao1^{3ld}* mutants were observed for thallus morphology and sexual reproduction. After 12 days of growth from gemmae, the mutants clearly showed different morphology under cW and cW+cFR conditions. FR enrichment induced hyponastic growth and thallus slenderness in all three types of mutants, similar to the response in wild-type plants (Figure 2-23A-D). Besides, no robust delay in gametangiophore formation or morphological defect in antheridiophores were observed in any of these mutants (Figure 2-23E-F). It appears that these genes may not play significant roles in G_{AMp} biosynthesis, though multiplex mutation experiments are required to figure out if they contributed to the functional redundancy.

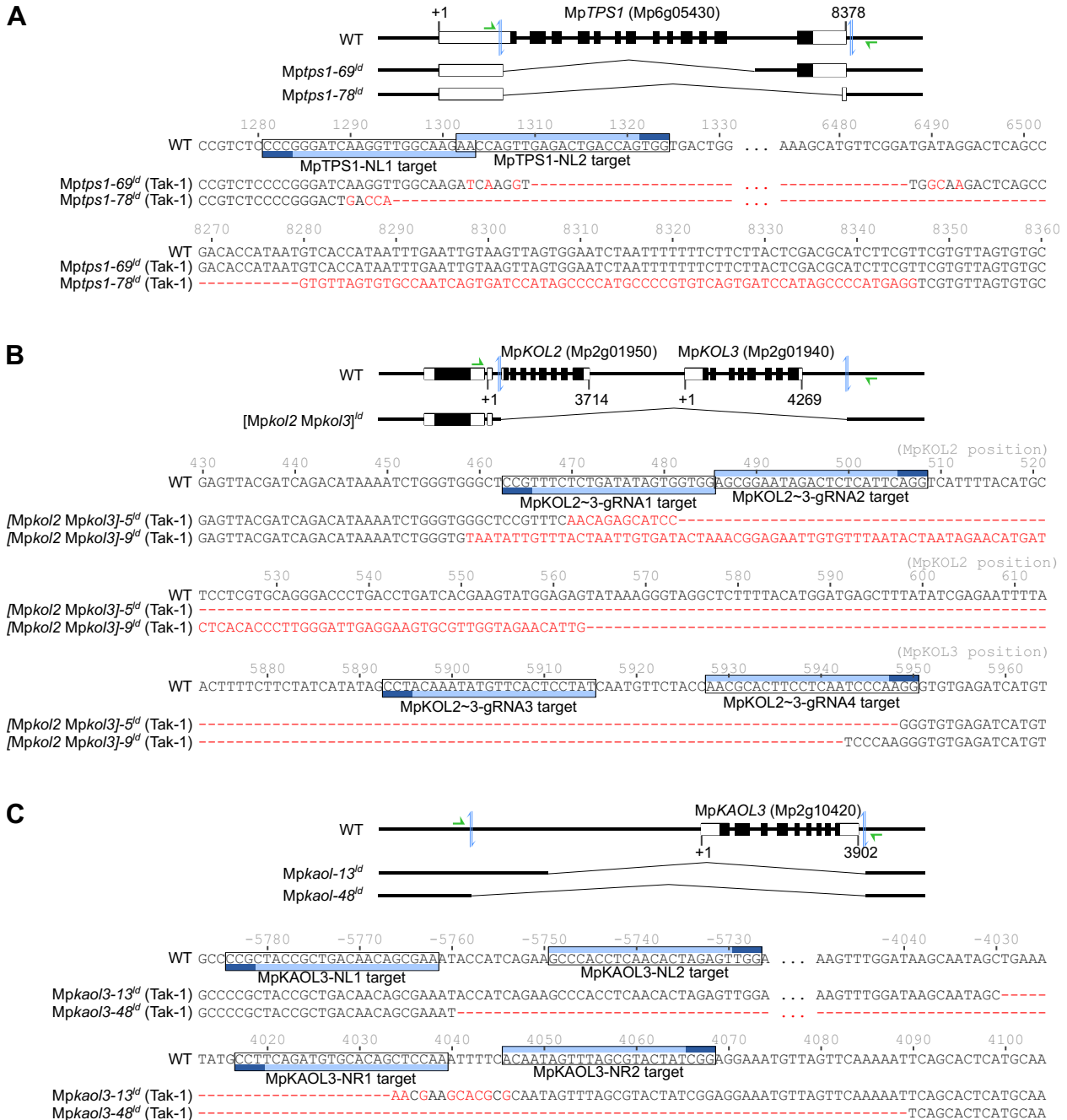


Figure 2-22 Genotype information of *Mptps1*^Δ (A), [Mpkol2 Mpkol3]^Δ (B) and *Mpkaol3*^Δ (C) mutants. The reference sequence (WT) was extracted from the MpTak_v6.1 genome assembly. In the gene structure diagram, untranslated regions in the transcript are depicted as white rectangles, while coding regions of exons are represented by black rectangles. Binding sites for genotyping primers are indicated by green arrows. Target sites for guide RNAs are denoted by blue arrows in the diagram and highlighted in the sequence with frames, with the protospacer adjacent motif (PAM) indicated in dark blue. Numbers above the sequences indicate their positions relative to the transcription start sites (+1). In the alignments, insertions and substitutions are highlighted using red letters.

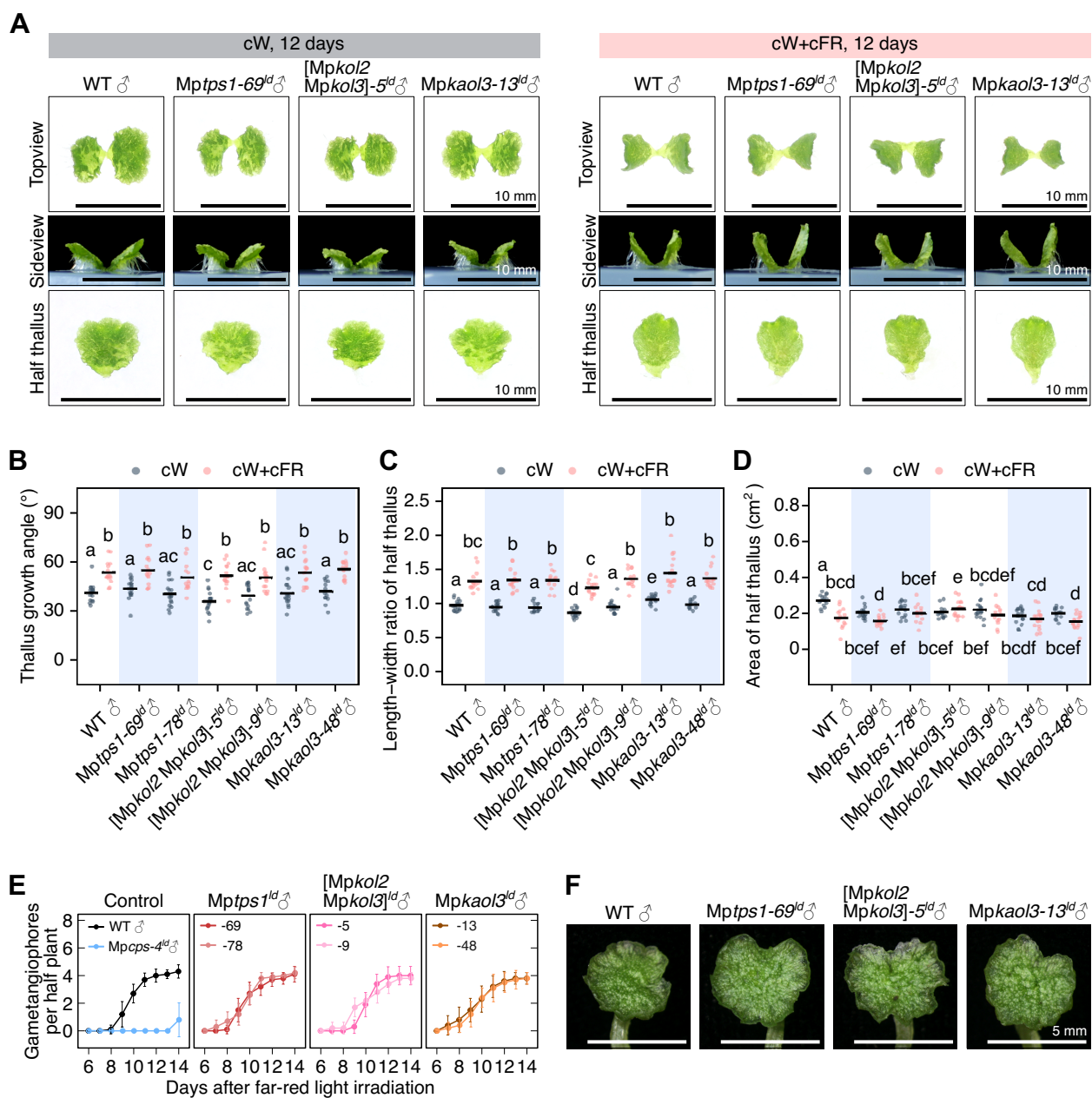


Figure 2-23 Response of *Mptps1^{ld}*, [*Mpkol2 Mpkol3*]^{ld} and *Mpkao13^{ge}* mutants to FR enrichment. (A) Thallus morphology of 12-day-old plants grown from gemmae under cW or cW+cFR. Quantification of thallus hyponasty (B), shape (C) and size (D). Each dot represents data from a half thallus (n=11-18). Horizontal bars represent mean values, and non-overlapping letters represent significant statistical difference (non-pooled Welch's *t*-test with Benjamini-Hochberg adjustment, adjusted *P*<0.05). (E) Progress of gametangiophore formation. Dots and error bars represent mean±SD (n=5). (F) Morphology of male gametangiophore receptacles.

Transcriptional response to FR enrichment is modulated by GA_{Mp}

In addition to morphological observations, gene expression changes related to GA_{Mp} deficiency were investigated with a transcriptome approach. For RNA-sequencing (RNA-seq), whole thallus samples were collected from plants grown from gemmae for 12 days under cW or cW+cFR. Under each condition, *Mpcps-4^{ld}* mutants treated with 0 or 2 μM KA was compared with Tak-1 wild-type plants (Table 2-1).

Table 2-1 List of samples used for transcriptome analysis

Genotype	Growth condition	Chemical treatment	# of replicates
WT ♂	cW, 12 days	Mock	3
<i>Mpcps-4^{ld}</i> ♂	cW, 12 days	Mock	3
<i>Mpcps-4^{ld}</i> ♂	cW, 12 days	KA (2 μM)	3
WT ♂	cW+cFR, 12 days	Mock	3
<i>Mpcps-4^{ld}</i> ♂	cW+cFR, 12 days	Mock	3
<i>Mpcps-4^{ld}</i> ♂	cW+cFR, 12 days	KA (2 μM)	3

Under the cW condition, only a small number of genes exhibited differential expression between *Mpcps-4^{ld}* and wild-type plants. The pairwise analysis identified 7 genes with reduced expression and 14 genes with increased expression in *Mpcps-4^{ld}*, among which only 3 down-regulated genes and 4 up-regulated genes showed an opposite response to KA treatment (Figure 2-24A). Remarkably, the expression of *MpTPS6* significantly decreased in *Mpcps-4^{ld}* but was restored by 2 μM KA. Previous research suggested that this gene encodes an enzyme that catalyzes the conversion of GGDP to *cis*-kolavenol (Jia et al., 2022).

In contrast, 780 down-regulated genes and 257 up-regulated genes were influenced by *Mpcps-4^{ld}* under cW+cFR conditions (Figure 2-24A). The increased number of differentially expressed genes (DEGs) suggested an active role of GA_{Mp} under the FR-enriched condition, which was consistent with the prominent morphological change caused by GA_{Mp} deficiency under this condition. When the expression patterns of these genes were examined across all samples, most of them exhibited a clear response to FR enrichment in the wild-type plants. Essentially, the differential expression in *Mpcps-4^{ld}* reflected the reduction of transcriptional response induced by FR enrichment (Figure 2-24B). When FR-induced DEGs were extracted from the comparison between cW+cFR and cW samples, the number of up-regulated genes decreased from 1326 in wild-type to 445 in *Mpcps-4^{ld}*, and the number of down-regulated genes decreased from 1252 in wild-type to 500 in *Mpcps-4^{ld}*, confirming that *Mpcps-4^{ld}* suppressed the response to FR enrichment (Figure 2-24C).

To capture the biological function beneath the gene expression changes, gene ontology (GO) enrichment analysis was performed for *Mpcps^{ld}*- and KA-induced DEGs under cW+cFR. As yet no comprehensive genome-wide functional annotations were established from experimental data in *M. polymorpha*, the Blast2GO algorithm was used to generate a fussy set of biological process GO annotations for predicted genes in the *M. polymorpha* genome based on protein similarity (Conesa and Götz, 2008; Hernández-García et al., 2021). While KA application only partially restored gene expression changes in *Mpcps-4^{ld}*, there was a significant overlap in the top-ranked GO terms enriched from the genes that showed opposite responses to *MpCPS* loss-of-function and the KA treatment (Figure 2-25).

Generally, GO terms related to secondary metabolism and stress responses were highlighted in all four gene sets. The phenylpropanoid metabolic process seemed to be enriched in all four comparisons, with the highest level of statistical significance shown in genes down-regulated by *Mpcps-4^{ld}*. Through careful examination of gene homologs, 23

genes that are putatively involved in the biosynthesis of lignin monomers, auronidins, or bibenzyls (Berland et al., 2019; Zhu et al., 2023) exhibited MpCPS-dependent positive expression response to FR enrichment (Figure 2-26A). The enrichment of phenylpropanoid metabolism in *Mpcps-4^{ld}*-up-regulated genes and KA-down-regulated genes were largely contributed by peroxidases (PODs), which potentially use lignin monomers as substrates for reaction. While 17 PODs were down-regulated in *Mpcps-4^{ld}*, the other 22 family members showed opposite responses to FR enrichment and *Mpcps-4^{ld}* (Figure 2-26B). A similar pattern of both up-regulation and down-regulation was observed in other cell-wall associated enzymes, suggesting a sophisticated remodeling of cell wall function during FR response (Figure 2-26C). Besides, 7 members of uridine 5'-diphospho-glucuronosyltransferases (UGTs), 30 members of CYPs and 12 members of 2ODDs were down-regulated in *Mpcps-4^{ld}* under cW+cFR. Most of these genes belong to subfamilies specifically expanded in *M. polymorpha*, which might be related to lineage-specific secondary metabolism (Figure 2-26D-F).

FR enrichment triggered gene expression changes related to several phytohormone pathways in a MpCPS-dependent manner. Three genes related to cytokinin (CK) metabolism were induced by FR enrichment and down-regulated by *Mpcps-4^{ld}*, namely the biosynthesis enzymes MpISOPENTENYLTRANSFERASE2 (MpIPT2) and MpLONELY GUY (MpLOG), as well as the deactivation enzyme MpCYTOKININ OXIDASE2 (MpCKX2) (Figure 2-26G). Given that CK negatively regulates thallus hyponasty in *M. polymorpha* (Aki et al., 2019), it is reasonable to hypothesize that a relatively high level of CK might contribute to the flat thallus phenotype of *Mpcps-4^{ld}* under cW+cFR. For abscisic acid (ABA), the expression of three metabolic genes and more than 40 LATE EMBRYOGENESIS ABUNDANT-like (LEA-like) genes were down-regulated by *Mpcps-4^{ld}* under cW+cFR, which contributed to the enrichment of stress response terms in the GO analysis (Figure 2-26H).

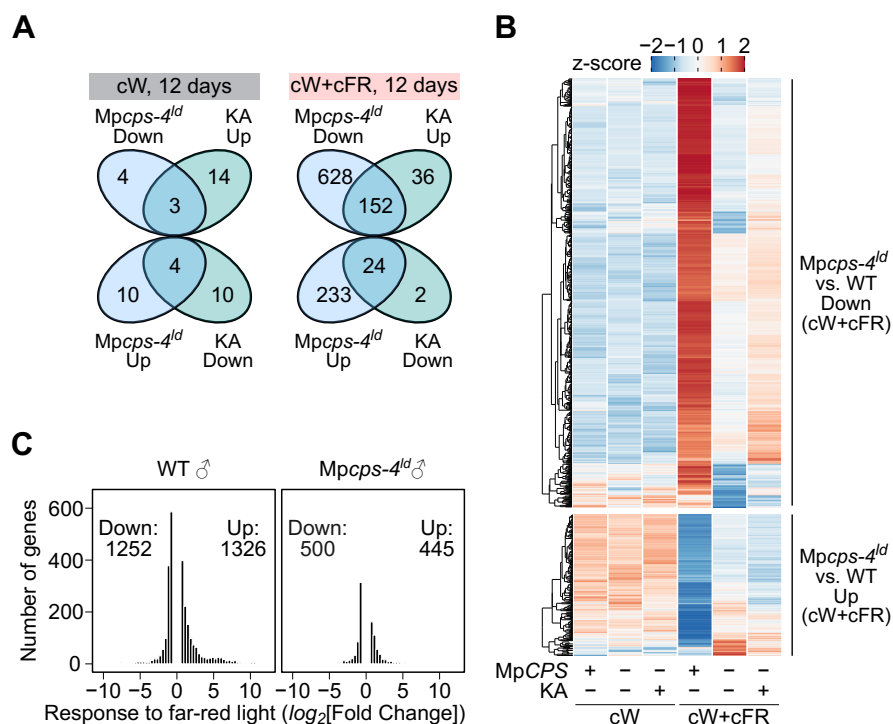


Figure 2-24 DEGs related to GA_{Mp} deficiency under different conditions. (A) Venn diagram showing the overlaps of DEGs between *Mpcps-4^{ld}* and Tak-1 plants, and those evoked by KA treatment in *Mpcps-4^{ld}*. (B) Heatmap showing the expression pattern of DEGs observed in *Mpcps-4^{ld}* under cW+cFR. (C) Distribution of DEGs in response to FR enrichment, compared between Tak-1 and *Mpcps-4^{ld}* plants.

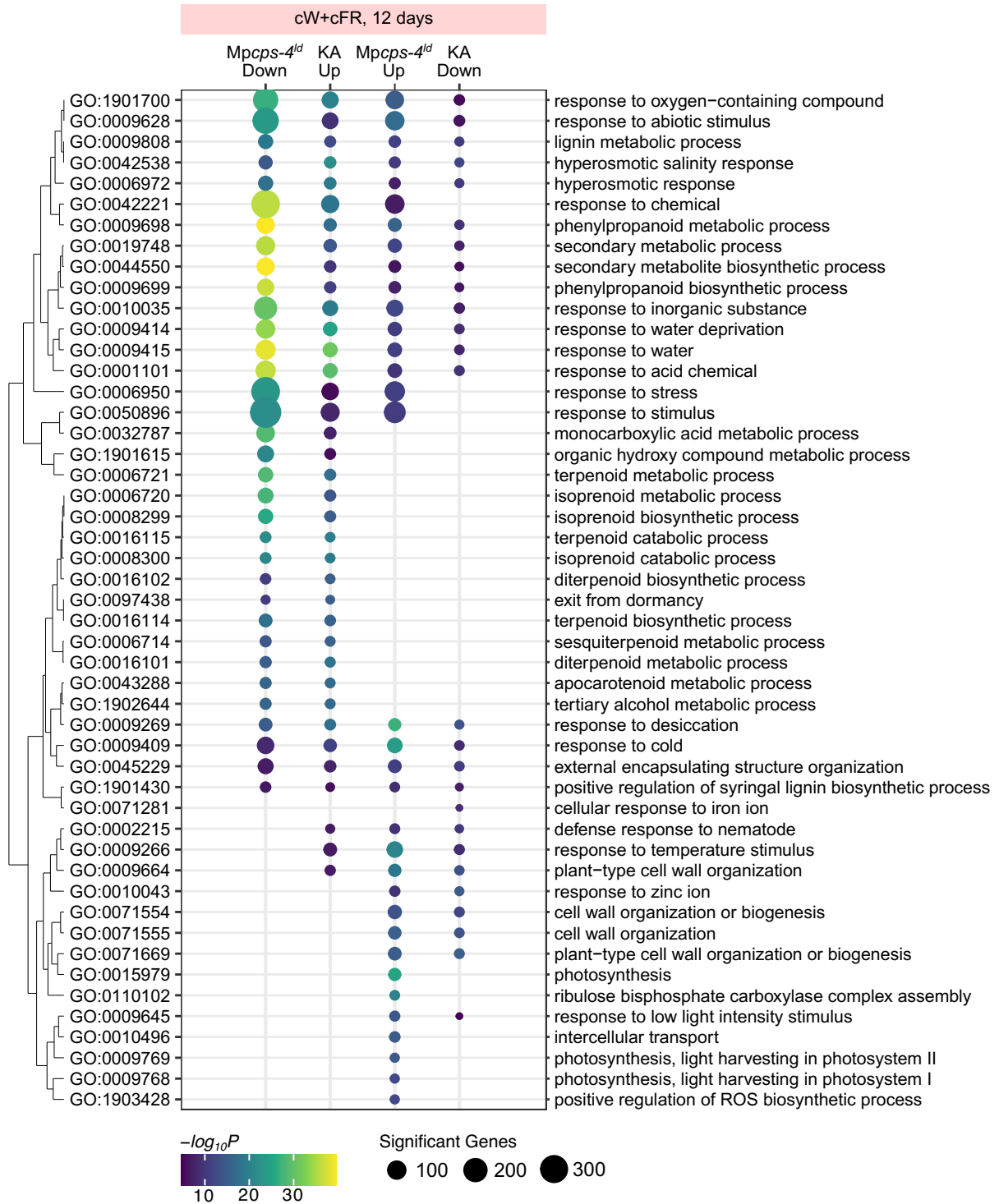
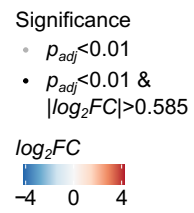
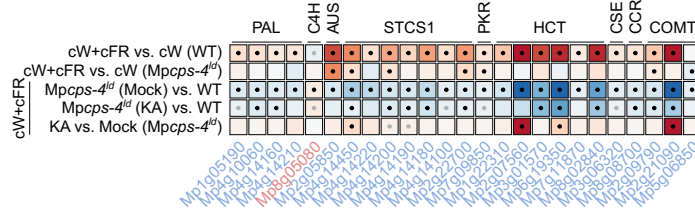
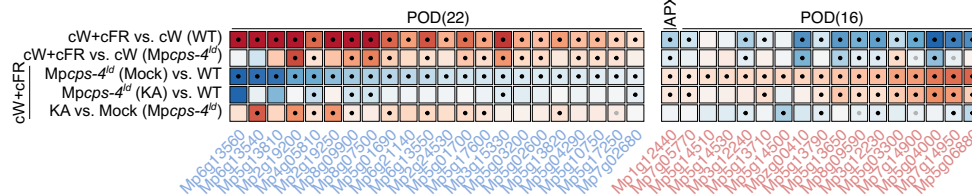


Figure 2-25 GO enrichment analysis of DEGs observed under cW+cFR. The GO terms shown here were collectively selected from the top 20 terms enriched in each DEG set, which were calculated by Fisher's exact tests without adjustment. GO terms in the diagram were clustered based on their statistical significance of enrichment in different DEG sets. ROS, reactive oxygen species.

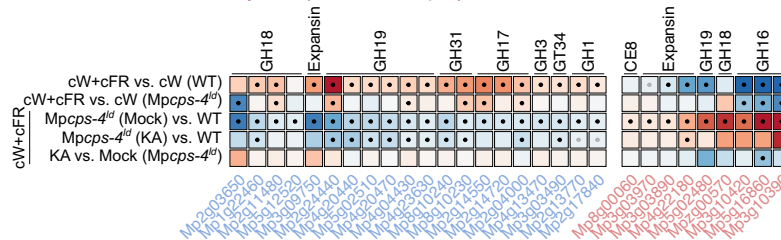
A Phenylpropanoid biosynthesis (Down: 24; Up: 1)



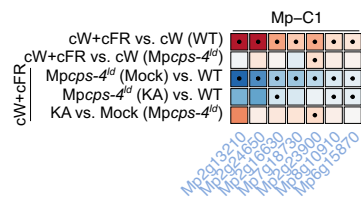
B Peroxidases (Down: 22; Up: 17)



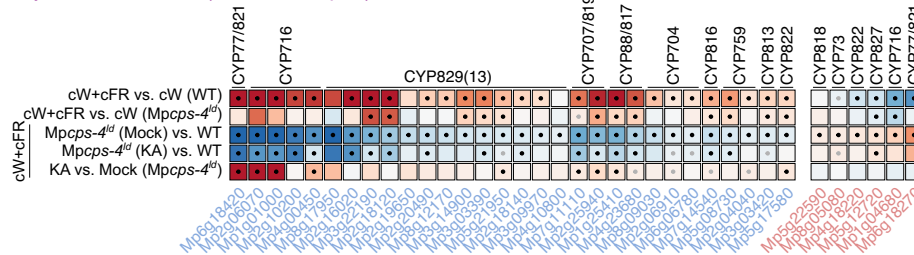
C Cell-wall associated enzymes (Down: 20; Up: 9)



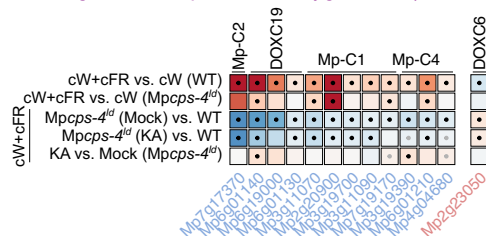
D UDP-glucuronosyltransferases (Down: 7; Up: 0)



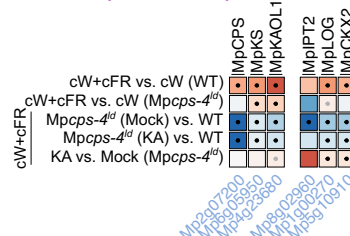
E Cytochrome P450s (Down: 30; Up: 6)



F 2-Oxoglutarate-dependent dioxygenases (Down: 12; Up: 1)



G GA and cytokinin biosynthesis



H ABA biosynthesis and response (Down: 54; Up: 1)

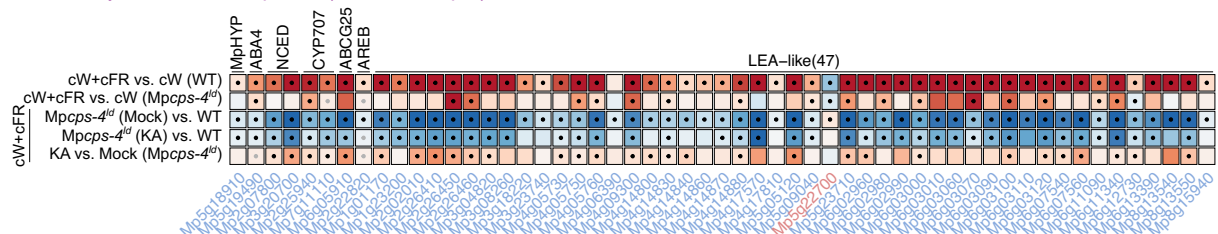


Figure 2-26 Heatmaps showing gene expression changes in selected gene families or pathways. FC, fold change. P_{adj} , adjusted p -value.

Last but not least, under the cW+cFR condition, *Mpcps^{ld}* reduced the expression of *MpKS* and *MpKAOL1*, two enzymes responsible for GA_{Mp} biosynthesis (Figure 2-26G). RT-qPCR experiments were performed to validate this observation. Indeed, in the plants cultured under cW for 11 days and then induced under cW+cFR for 3 days, *MpKS* and *MpKAOL1* expression was significantly decreased in *Mpcps-4^{ld}* and partially restored by 2 μ M KA treatment (Figure 2-27). Such a phenomenon could be explained as a consequence of overall reduction in FR response in *Mpcps-4^{ld}*, or it might imply that GA_{Mp} biosynthesis is modulated through a mechanism of positive feedback. *MpKOL1* did not show the same response as *MpKS* or *MpKAOL1*, which supported the hypothesis that this gene is regulated by a different mechanism.

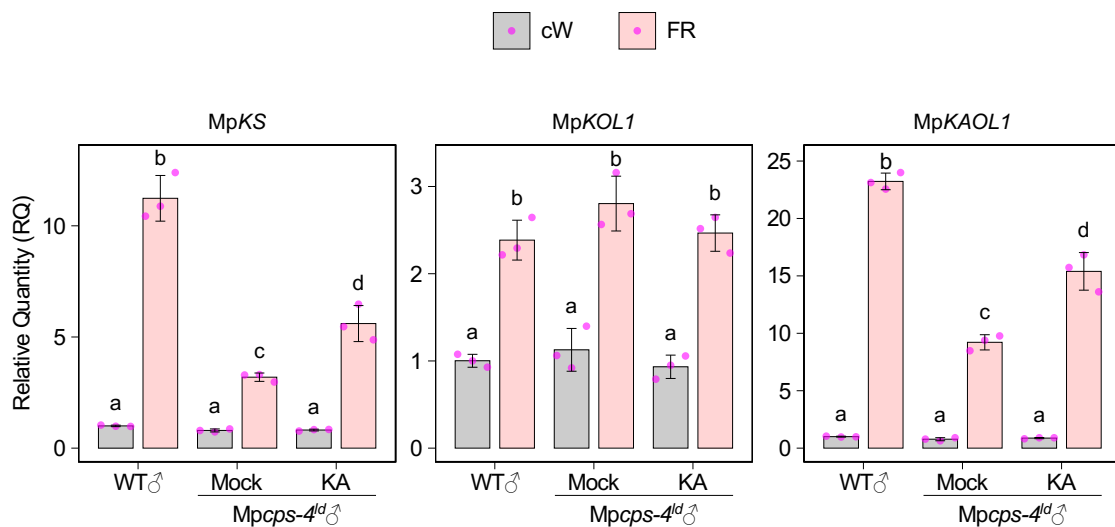


Figure 2-27 Relative expression levels of GA_{Mp} biosynthesis genes in *Mpcps^{ld}* in response to FR enrichment and KA treatment. Plants were cultured under cW for 11 days, then transferred onto fresh medium containing 0 or 2 μ M KA and cultured under cW+cFR for 3 days. For each group, whole thallus tissues collected from different plants were treated as a biological replicate (n=3, represented by dots). Bars and error bars represent mean \pm SD. Different letters represent significant statistical difference from Tukey's HSD test (adjusted $P < 0.05$).

Chapter 3 Discussion

GA_{Mp} serves as a phytohormone in *M. polymorpha*

In the natural environment, a decrease in the R to FR ratio, or enrichment of FR often indicates the presence of competitive neighboring plants. Both bryophytes and vascular plants have to cope with this threat and optimize their growth and photosynthesis accordingly. With a genetic approach, this study showed that GA precursors synthesized by evolutionarily conserved enzymes are required by the liverwort *M. polymorpha* for various responses to the FR-enriched environment. In the wild-type plants, FR enrichment changes the thallus growth orientation and induces sexual reproduction (Figure 2-9 and Figure 2-13), which is associated with elevated expression of GA biosynthesis genes and GA₁₂ accumulation (Figure 2-7). Multiple genetic mutants of different GA biosynthesis enzymes consistently inhibited hyponastic growth and delayed gametangiophore formation under FR enriched conditions (Figure 2-9, Figure 2-13, Figure 2-20 and Figure 2-21). Moreover, KA treatment rescued several mutants that putatively blocked its biosynthesis, supporting that the observed phenotypes were probably caused by deficiency of certain diterpenoid compound(s) derived from KA, which was named as GA_{Mp}.

GA_{Mp} modulates growth anisotropy in response to FR enrichment

In *M. polymorpha*, the function of GA_{Mp} is most prominent under FR-enriched conditions. The changes in thallus shape and hyponasty both indicate that there is a systematic change in the tissue growth anisotropy, which is induced by FR enrichment and diminished by GA_{Mp} deficiency. From previous research, it seems that FR signal alters both the cell shape and the cell division activity in *M. polymorpha* (Nishihama et al., 2015), both might contribute to the anisotropic growth. In Arabidopsis and other angiosperms, the impact of cell elongation is more evident. GA is required for the hyponastic growth of Arabidopsis petioles triggered by local FR enrichment in the leaf tip, and the cellular response that drives the hyponasty was the excessive cell elongation in the adaxial side (Küpers et al., 2023). Besides, experiments in the hypocotyl showed that a transient GA treatment induced anisotropic cellular expansion (Sauret-Güeto et al., 2012).

Using EdU analysis, this study found that FR-induced anisotropic growth in *M. polymorpha* also involves the spatial change of cell division activity. Under FR-enriched conditions, the hyponastic growth of wild-type thallus was associated with more active cell proliferations in the ventral side, while cell divisions in the flat thallus of *Mpcps^{ld}* mutants were equally active in dorsal and ventral sides (Figure 2-11). Both the hyponasty and the asymmetric patterns of cell division could be restored by *MpCPS* complementation using a *35S* constitutive promoter, which showed no obvious dorsoventral bias in driving gene expression (Althoff et al., 2014). As the asymmetric pattern of cell division does not require spatial specific biosynthesis of GA_{Mp}, it is unlikely that GA_{Mp} directly modulates cell division activity through polar distribution. This is similar to the pattern of GA during the FR-induced hyponasty growth of Arabidopsis petiole. Despite that GA deficiency inhibited the hyponastic response, no adaxial-abaxial spatial pattern was observed in GA signaling, suggesting an even distribution of active GA during the process (Küpers et al., 2023).

The formation of gametangiophores in *M. polymorpha* involves a series of morphological transformation in the thallus, including the reduction of dorsal tissues and elongative growth to form the cylindrical and slender stalks (Cao et al., 2013; Shimamura, 2016; Fisher et al., 2023). Compared to wild-type plants, the short and thick

gametangiophore stalks of *Mpcps^{ld}* mutants developed a higher proportion of dorsal tissue with air chambers (Figure 2-14, Figure 2-15). Such stalk morphology reflected reduction in both elongative growth and dorsoventral growth bias, which essentially resembles the changes observed in thallus morphology under FR enriched conditions.

Interestingly, a functional connection could be made between GA_{Mp} and *MpKANADI* (*MpKAN*), the sole member of the KANADI family TFs in *M. polymorpha*. In Arabidopsis, *KAN* genes are important regulators of organ polarity and determine the fate of abaxial tissues (Kerstetter et al., 2001; Eshed et al., 2001). While *MpKAN* could partially rescue the organ polarity defects of Arabidopsis *kan* mutant, *MpKAN* expression level is similar between the dorsal and ventral thallus tissues of *M. polymorpha*, and the dorsoventral polarity was not affected by *Mpkan* under white light conditions (Briginshaw et al., 2022). Under FR-enriched conditions, intriguing similarity could be found between the phenotype of GA_{Mp} deficient mutants in this research and those previously reported *Mpkan* mutants. Both GA_{Mp} deficiency and *MpKAN* loss-of-function inhibited hyponastic growth of the thallus, delayed gametangiophore formation and altered gametangiophore morphology in a similar manner (Briginshaw et al., 2022). It has been shown that the FR-induced upregulation of GA_{Mp} biosynthesis enzymes was inhibited by *Mpkan*, suggesting that GA_{Mp} might act downstream of *MpKAN* to modulate the tissue growth anisotropy under FR enriched conditions (Briginshaw et al., 2022).

The biosynthetic route of GA_{Mp}

In this research, biochemical and genetic experiments clarified key enzymes responsible for GA_{Mp} biosynthesis. Previous studies showed that *MpCPS* and *MpKS* could catalyze the conversion from GGDP to *ent*-kaurene in vitro (Kumar et al., 2016), here their pivotal roles in GA_{Mp} biosynthesis was confirmed by the phenotypes of genetic mutants (Figure 2-9, Figure 2-10, Figure 2-13, Figure 2-20 and Figure 2-21). Although *MpTPS1* could produce *ent*-kaurene as a minor product, *MpTPS1* loss-of-function did not show any obvious phenotype under FR enriched conditions (Figure 2-23). Among the three KO homologs, both enzymatic assay in the yeast and mutant phenotypes supported that *MpKOL1* catalyzes the conversion from *ent*-kaurene to KA (Figure 2-4, Figure 2-20 and Figure 2-21), while *MpKOL2* and *MpKOL3* seemed to be irrelevant to GA_{Mp} biosynthesis (Figure 2-4 and Figure 2-23). Considering the broad existence of CPS, KS and KO homologs in all major lineages of land plants, it is likely that these enzymatic steps emerged in the common ancestor of land plants and were well preserved throughout evolution.

The presence of endogenous GA_{12} and that *MpKAOL1* catalyzed KA to GA_{12} conversion in the yeast suggested that KA serves as a precursor for GA_{12} production in *M. polymorpha*. However, the phenotype of *Mpkaol1^{se}* mutants suggested that this conversion might not be the only route involved in the final synthesis of GA_{Mp} . LC-MS/MS data confirmed that GA_{12} level in a *Mpkaol1^{se}* mutant is below the detection limit, but the gametangiophore formation was less affected in this mutant than KA-deficient mutants. Besides, the thallus of *Mpkaol1^{se}* mutants showed a mild but significant response to 2 μ M KA under cW+cFR, suggesting that GA_{Mp} biosynthesis downstream of KA was not completely blocked in these mutants. Just like other CYPs, plant KAOs of the CYP88 family are monooxygenases, and it actually takes three steps for these enzymes to accomplish the KA to GA_{12} conversion, generating *ent*-7-hydroxy-kaurenoic acid (7OH-KA) and GA_{12} -aldehyde as intermediates (Helliwell et al., 2001a). Although GA_{12} is an essential intermediate for GA biosynthesis in Arabidopsis and used for long-distance transportation across tissues (Regnault et al., 2015),

its production is largely bypassed in the fungus *F. fujikuroi*. After producing GA₁₂-aldehyde from KA, the enzyme P450-1 in *F. fujikuroi* preferentially converts GA₁₂-aldehyde into GA₁₄ aldehyde, then into GA₁₄ (Hedden et al., 1974; Urrutia et al., 2001; Rojas et al., 2001). GA₁₂ was only produced as a minor product (Rojas et al., 2001). In light of this, it is unjustified to attribute the *Mpkaol1^{ge}* mutant phenotypes solely to deficiency in GA₁₂ biosynthesis. The role of 7OH-KA and GA₁₂-aldehyde in GA_{Mp} biosynthesis should be considered, and their production might be catalyzed redundantly by MpKAOL1 and other enzymes.

Evolution of GA-related phytohormones in land plants

Despite that GA_{Mp} is synthesized from GA precursors, GA_{Mp} appeared to have functions and modes of action distinct to canonical GAs in angiosperms. In angiosperms, GA deficiency leads to reduction in both cell division and cell expansion, which severely inhibits plant growth under regular culture conditions (Cowling and Harberd, 1999; Achard et al., 2009). On the contrary, GA_{Mp} deficiency in *M. polymorpha* greatly promoted thallus growth and cell proliferation under FR-enriched conditions, which seemed to be opposite to the role of canonical GAs. While in *Arabidopsis* GA is required for seed germination (Koornneef and van der Veen, 1980), GA_{Mp} seemed to be negatively regulating gemma dormancy (Figure 2-12), which is consistent with the growth-inhibition function of GA_{Mp}. In addition, GA_{Mp} deficiency showed very limited influence on thallus morphology under cW (Figure 2-9, Figure 2-10), suggesting that GA_{Mp} function was primarily evoked during FR responses. Consistently, gene expression changes under cW+cFR indicated that GA_{Mp} biosynthesis might be regulated by positive feedback (Figure 2-27), which may allow this hormone to quickly accumulate in response to environmental changes, unlike the negative feedback to maintain GA homeostasis in angiosperms (Zentella et al., 2007; Fukazawa et al., 2014).

In vascular plants, *GID1* proteins are the only known receptors that mediate the perception of GA, which function through *DELLA* proteins to evoke transcriptional responses (Peng et al., 1997; Silverstone et al., 1998; Ueguchi-Tanaka et al., 2005). Although the transcriptional regulatory role of MpDELLA is conserved among distant lineages of land plants (Briones-Moreno et al., 2023; Hernández-García et al., 2019), no *GID1* homologs were identified from bryophytes including *M. polymorpha* (Bowman et al., 2017; Hernández-García et al., 2019). In a previous report, MpDELLA was shown to negatively regulate FR responses, as the ectopic overexpression promoted gemma germination and inhibited gametangiophore formation (Hernández-García et al., 2021). However, such phenomenon could be better explained by the physical interaction between MpDELLA and MpPIF, which directly inhibited MpPIF function (Hernández-García et al., 2021). In contrast to growth promotion caused by GA_{Mp} deficiency, MpDELLA over-accumulation inhibited cell division in the apical meristem and the overall thallus growth (Hernández-García et al., 2021), suggesting that GA_{Mp} signaling was not mediated through degradation of MpDELLA.

In the moss *P. patens*, the KA derivative 3OH-KA serves as a diterpenoid hormone to regulate protonema differentiation and blue-light avoidance (Hayashi et al., 2010; Miyazaki et al., 2014). While KA deficiency showed no influence on the growth rate of protonema or gametophores, it delayed the spore germination progress (Hayashi et al., 2010; Vesty et al., 2016). Furthermore, treatment with 3OH-KA induced the up-regulation of a KA 2-oxidase (PpKA2ox), which provided a negative feedback through inactivation of KA (Miyazaki et

al., 2018), revealing distinctive modes of action to either GA_{Mp} or canonical GAs. Similar to the situation in *M. polymorpha*, *Ppdella* mutants accelerated spore germination but did not influence the sensitivity to GA₉-Me, which could function as an analog for 3OH-KA in *P. patens* (Phokas et al., 2023).

Overall, it seems that KA derived compounds were utilized as hormone in both bryophytes and vascular plants, but the bioactive forms and functions was quite diversified in different plant lineages (Figure 3-1). If the biosynthesis pathway and perception mechanisms could be elucidated in bryophytes by future research, it would lead to a more comprehensive understanding of the evolution of plant hormones, i.e., how small chemical molecules are utilized by plants to regulate growth and to cope with environmental challenges.

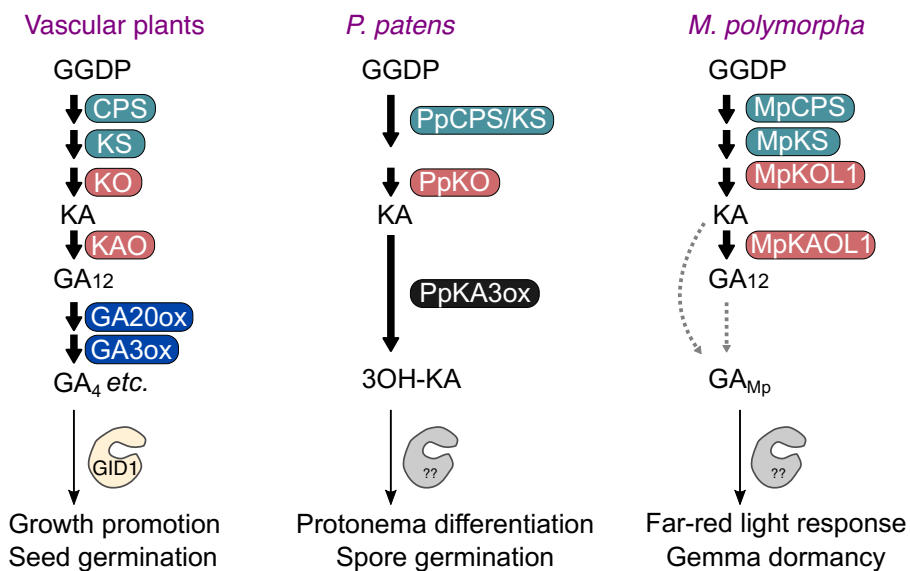


Figure 3-1 Comparison of GA-related hormone pathways in different land plants. The early steps of GA biosynthesis are conserved among land plants, and both the moss *P. patens* and the liverwort *M. polymorpha* use diterpenoid compounds derived from KA as phytohormones. It is likely that the later steps of biosynthesis and physiological functions are diversified in different land plant lineages. Besides, GAs are perceived by GID1 receptors in vascular plants, while the perception mechanisms for 3OH-KA in *P. patens* or GA_{Mp} in *M. polymorpha* is still unknown.

Chapter 4 Materials and Methods

Plant materials and growth conditions

In this research, the following accessions of *M. polymorpha* subsp. *ruderalis* were used as wild-type plants: the male Takaragaike-1 (Tak-1) accession and the female Takaragaike-2 (Tak-2) accession (Ishizaki et al., 2008). *Mppij^{ko}* and *gMpPIF/Mppij^{ko}* refer to *Mppij^{ko}* #1 and *gMpPIF/Mppij^{ko}* #1 plants described in (Inoue et al., 2016), respectively. *MpBNB-Cit* ♂ and *MpBNB-Cit* ♀ knock-in lines are from (Yamaoka et al., 2018).

To maintain the genetic materials, *M. polymorpha* plants were grown at 22 °C on solid medium containing 1% (w/v) agar and a half dose of Gamborg's B5 formulation (Gamborg et al., 1968). Continuous white light (cW) was supplied by cold cathode fluorescent lamps (CCFLs, OPT-40C-N-L from Optrom, Japan) at the intensity of 40-50 $\mu\text{mol photons m}^{-2} \text{s}^{-1}$.

For data collection, the plants were also cultured at 22 °C, either aseptically on half-strength Gamborg's B5 medium containing 1% (w/v) sucrose and 1% (w/v) agar, or on vermiculites in the open air. cW of approximately 40 $\mu\text{mol photons m}^{-2} \text{s}^{-1}$ and continuous far-red light (cFR) of approximately 25 $\mu\text{mol photons m}^{-2} \text{s}^{-1}$ were supplied with various light sources in different experiments. For thallus morphology measurements, plants were cultured in the multichambered incubator (LH-80CCFL-6CT, NK systems, Japan) with CCFLs for cW and light-emitting diodes (LEDs) for cFR. For aseptically gametangiophore formation, plants were grown on shelves in the culture room, with cW supplied by CCFLs (ST-40C-BN, Shinshu Trading, Japan) and cFR supplied by LEDs (IR LED STICK, NAMOTO, Japan). For gametangiophore formation on vermiculites, fluorescent tubes (FLR40SN/M/ 36, Toshiba, Japan) and LEDs (VBL-TFL600-IR730, Valore, Japan) were used to supply cW and cFR, respectively.

Construction of transgenic plants

To generate large-deletion mutants of a specific gene using the CRISPR/Cas9^{D10A} nickase system (Hisanaga et al., 2019; Koide et al., 2020), four guide RNAs (gRNAs) were designed to target sequences flanking the CDS region. DNA oligos carrying the target sequences were annealed and ligated into the BsaI sites of the vectors pMpGE_En04, pBCGE12, pBCGE23, and pBCGE34. Then the gRNA expression cassettes from the pBCGE12-, pBCGE23-, and pBCGE34-backbone plasmids were collectively subcloned into the pMpGE_En04 construct, creating an entry vector carrying all four gRNAs. In the last step of cloning, the gRNAs were integrated into the binary vector pMpGE017 or pMpGE018 (Hisanaga et al., 2019) through recombination with Gateway LR Clonase II (Thermo Fisher Scientific).

To generate the loss-of-function mutation in *MpKAOLI*, a single gRNA that targets a sequence near the start codon was first cloned into pMpGE_En03, then recombined with the binary vector pMpGE011 (Sugano et al., 2018) using Gateway LR reactions.

For promoter activity assays, ~5 kb regulatory regions upstream of the CDS of each gene were amplified from Tak-1 genomic DNA and subcloned into the vector pENTR1a (Thermo Fisher Scientific). The entry clones were then recombined with pMpGWB304 using Gateway LR reactions, to drive the expression of the GUS reporter under the target promoters (Ishizaki et al., 2015).

To complement mutants and observe subcellular localization of proteins, wild-type

CDSs without stop codons were amplified from the complementary DNA (cDNA) of Tak-1 plants and inserted into the pENTR/D-TOPO vector (Thermo Fisher Scientific). Additionally, the gRNA target sites were mutated in pENTR-MpKAOL1-CDS through inverse PCR followed by re-circularization, using back-to-back primers MpKAOL1-mut-F and MpKAOL1-mut-R. All the entry vectors were then recombined with pMpGWB106 or pMpGWB306 using Gateway LR Clonase II, inserting CDS of the target gene between the 35S promoter and the C-terminal Citrine tag to be fused in-frame.

To generate transgenic plants, the binary vectors were introduced into the *Agrobacterium tumefaciens* strain GV2260, which was then used to transform regenerating thalli of *M. polymorpha* as previously described (Kubota et al., 2013). Genotyping PCR was carried out in successful transformants to identify large deletions. Genomic sequences of all mutants were confirmed by Sanger sequencing.

All the transgenic plants constructed in this research are listed in Table 4-1, and Table 4-2 shows the list of DNA oligos and primers used for constructing these materials. The vectors pMpGE018-MpKOL1-LD, pMpGE011-MpKAOL1-gRNA1, and pMpGE018-MpKOL2/3-LD were generated by Ryunosuke Kusunoki in the laboratory.

Table 4-1 Plant materials generated in this research

Name	Genetic background	Sex	Binary vector
<i>pro</i> MpCPS:GUS #1, #8	Tak-1	Male	pMpGWB304-MpCPS-pro
<i>pro</i> MpKS:GUS #7, #9	Tak-1	Male	pMpGWB304-MpKS-pro
<i>pro</i> MpKOL1:GUS #5	Tak-1	Male	pMpGWB304-MpKOL1-pro
<i>pro</i> MpKAOL1:GUS #3, #23	Tak-1	Male	pMpGWB304-MpKAOL1-pro
Mpcps-4 ^{ld} , Mpcps-27 ^{ld}	Tak-1	Male	pMpGE017-MpCPS-LD
<i>pro</i> 35S:MpCPS-Cit (Mpcps-4 ^{ld}) #6, #7	Mpcps-4 ^{ld}	Male	pMpGWB306-MpCPS-CDS
Mpcps-120 ^{ld} , Mpcps-123 ^{ld}	Tak-2	Female	pMpGE017-MpCPS-LD
<i>pro</i> 35S:MpCPS-Cit (Mpcps-120 ^{ld}) #2, #6	Mpcps-120 ^{ld}	Female	pMpGWB306-MpCPS-CDS
Mpcps-5 ^{ld} (MpBNB-Cit ♂), Mpcps-6 ^{ld} (MpBNB-Cit ♂)	MpBNB-Cit ♂	Male	pMpGE018-MpCPS-LD
Mpcps-2 ^{ld} (MpBNB-Cit ♀), Mpcps-3 ^{ld} (MpBNB-Cit ♀)	MpBNB-Cit ♀	Female	pMpGE018-MpCPS-LD
Mpks-14 ^{ld} , Mpks-19 ^{ld}	Tak-1	Male	pMpGE018-MpKS-LD
<i>pro</i> 35S:MpKS-Cit (Mpks-14 ^{ld}) #13, #14	Mpks-14 ^{ld}	Male	pMpGWB106-MpKS-CDS
Mpkol1-7 ^{ld} , Mpkol1-13 ^{ld}	Tak-1	Male	pMpGE018-MpKOL1-LD
<i>pro</i> 35S:MpKOL1-Cit (Mpkol1-7 ^{ld}) #2, #4	Mpkol1-7 ^{ld}	Male	pMpGWB106-MpKOL1-CDS
Mpkaol1-5 ^{ge} , Mpkaol1-7 ^{ge}	Tak-1	Male	pMpGE011-MpKAOL1-gRNA1
<i>pro</i> 35S:MpKAOL1 ^{mut} -Cit (Mpkaol1-5 ^{ge}) #3, #5	Mpkaol1-5 ^{ge}	Male	pMpGWB106-MpKAOL1-CDSmut
Mptps1-52 ^{ld} , Mptps1-69 ^{ld}	Tak-1	Male	pMpGE018-MpTPS1-LD
[Mpkol2 Mpkol3]-5 ^{ld} , [Mpkol2 Mpkol3]-9 ^{ld}	Tak-1	Male	pMpGE018-MpKOL2/3-LD
Mpkaol3-13 ^{ld} , Mpkaol3-48 ^{ld}	Tak-1	Male	pMpGE018-MpKAOL3-LD

Table 4-2 DNA oligos and primers used for generating transgenic plants

Name	Sequence (5'→3')	Used for
MpCPS-NL1-OligoA	CTCG ATCAACCTTACGAACCGGAC	Large-deletion mutation of MpCPS
MpCPS-NL1-OligoB	AAAC GTCCGGTTCGTAAGTTGAT	Large-deletion mutation of MpCPS
MpCPS-NL2-OligoA	CTCG GATAACTGCCACAGCGAAGC	Large-deletion mutation of MpCPS
MpCPS-NL2-OligoB	AAAC GCTTCGCTGTGGCAGTTATC	Large-deletion mutation of MpCPS
MpCPS-NR1-OligoA	CTCG TTCGGGTACAAGGGTTTGG	Large-deletion mutation of MpCPS
MpCPS-NR1-OligoB	AAAC TCCAAACCTTGTACCCGAA	Large-deletion mutation of MpCPS
MpCPS-NR2-OligoA	CTCG GAATGTCTAGTACGGAGCTT	Large-deletion mutation of MpCPS
MpCPS-NR2-OligoB	AAAC AAGCTCCGTAAGACATTC	Large-deletion mutation of MpCPS
MpCPS-gt-F	GGAACCTATCCGGGGATCCT	Genotyping of <i>Mpcps^{ld}</i>
MpCPS-gt-R	ATGTGACGTTCTGTTGCTGC	Genotyping of <i>Mpcps^{ld}</i>
CACC-MpCPS-CDS-F	CACC <u>AT</u> GGCATTCTCGTTAGCAGGT	Cloning of MpCPS CDS
MpCPS-CDS-R	GGCCACAGGCTCGAAGAGTA	Cloning of MpCPS CDS
MpCPS-pro-IF-F1	AGGAACCAATTCAGTCGAC TGTTTGACAATTCTTTGCAATGA	Cloning of MpCPS promoter
MpCPS-pro-IF-R1	ATATCTCGAGTCCGG AGTCCTAAGAGCTCGACAAA	Cloning of MpCPS promoter
MpKS-NL1-OligoA	CTCG TGTGGAACATAGAGTCTTGC	Large-deletion mutation of MpKS
MpKS-NL1-OligoB	AAAC GCAAGACTCTATGTTCCACA	Large-deletion mutation of MpKS
MpKS-NL2-OligoA	CTCG TCCACAGAGTCTTGTTCGTC	Large-deletion mutation of MpKS
MpKS-NL2-OligoB	AAAC GACGAACAAGACTCTGTGGA	Large-deletion mutation of MpKS
MpKS-NR1-OligoA	CTCG TGCTTGCTGTCCTGATGTCC	Large-deletion mutation of MpKS
MpKS-NR1-OligoB	AAAC GGACATCAGGACAGCAAGCA	Large-deletion mutation of MpKS
MpKS-NR2-OligoA	CTCG CAAGCATACTCCGCCACTA	Large-deletion mutation of MpKS
MpKS-NR2-OligoB	AAAC TAGTGGCGACGTATGCTTG	Large-deletion mutation of MpKS
MpKS-gt-F	ACTGTGAGCTGAAACTGCAGA	Genotyping of <i>Mpks^{ld}</i>
MpKS-gt-R	GGACGGACATGGATCTAGCA	Genotyping of <i>Mpks^{ld}</i>
CACC-MpTPS4-CDS-F	CACC <u>AT</u> GATGATCCATCCAGCTATTGTG	Cloning of MpKS CDS
MpTPS4-CDS-R	GGCCTGTTCACTTTCGATGG	Cloning of MpKS CDS
MpKS-pro-IF-F	AGGAACCAATTCAGTCGAC TGCTTATCTTGGCTGCCGAGAT	Cloning of MpKS promoter
MpKS-pro-IF-R	ATATCTCGAGTCCGG CTTACCCGGAATGCAGTAA	Cloning of MpKS promoter
Mapoly0140s0010-gRNA1-F	CTCG GATCATGGCTTTTCTCCCGC	Large-deletion mutation of MpKOL1
Mapoly0140s0010-gRNA1-R	AAAC GCGGGAGAAAAGCCATGATC	Large-deletion mutation of MpKOL1
Mapoly0140s0010-gRNA2-F	CTCG GATGCTCGCTCCATAAAAAC	Large-deletion mutation of MpKOL1
Mapoly0140s0010-gRNA2-R	AAAC GTTTTTATGGAGCGAGCATC	Large-deletion mutation of MpKOL1
Mapoly0140s0010-gRNA3-F	CTCG ATCCGACAAATAATGTTTGT	Large-deletion mutation of MpKOL1
Mapoly0140s0010-gRNA3-R	AAAC ACAAACATTATTTGTCGGAT	Large-deletion mutation of MpKOL1
Mapoly0140s0010-gRNA4-F	CTCG GTTTCAGTTTAGAAACCCTCC	Large-deletion mutation of MpKOL1
Mapoly0140s0010-gRNA4-R	AAACGGAGGGTTTCTAAACTGAAC	Large-deletion mutation of MpKOL1
Dseq-KOL1-gRNA1~4F	GGATTGATGTACTTGACGAG	Genotyping of <i>Mpkol1^{ld}</i>
Dseq-KOL1-gRNA1~4R	TTCGGCCTGAAGTCTAAGAG	Genotyping of <i>Mpkol1^{ld}</i>
CACC-MpKOL1-CDS-F	CACC <u>AT</u> GAAATGCTTCGGTTTG	Cloning of MpKOL1 CDS
MpKOL1-CDS-ns-R	AATCTTCGCTGGACAG	Cloning of MpKOL1 CDS
MpKOL1-pro-IF-F	AGGAACCAATTCAGTCGAC CGTTGATCGACGAGCGCTAT	Cloning of MpKOL1 promoter
MpKOL1-pro-IF-R	ATATCTCGAGTCCGG ACTCACAGACCGTCCCAGCTCTG	Cloning of MpKOL1 promoter
MpKAO-gRNA1F	CTCG CCAGGCTCCTCTCCCCC	Genome editing of MpKAO1

(Table 4-2, continued)

Name	Sequence (5'→3')	Used for
MpKAO-gRNA1R	AAAC GGGGGGAGAGGAGCCTGG	Genome editing of MpKAOL1
MpKAO-Dseq1-F	GAGGCATTGAGATCGAGAGG	Genotyping of Mpkaol1 ^{ge}
MpKAO-Dseq1-R	ATACTCTCGGCGGTCGTTGC	Genotyping of Mpkaol1 ^{ge}
Mapoly0020s0131-F	CACC ATGTTGGAGATTTCTGCCAC	Cloning of MpKAOL1 CDS
MpKAOL1-CDS-ns-R	CAATCGTGAGAAGTTTATAAGACAG	Cloning of MpKAOL1 CDS
MpKAOL1-mut-F	GCTGCCGCCG GGAGACATGGGCTGG	Site-directed mutagenesis of MpKAOL1
MpKAOL1-mut-R	GGTGCTTGCC TTTTCTGAAGACTGGG	Site-directed mutagenesis of MpKAOL1
MpKAOL1-pro-IF-F	AGGAACCAATTCAGTCGAC AGGCGATTGTTCATACAAACA	Cloning of MpKAOL1 promoter
MpKAOL1-pro-IF-R	ATATCTCGAGTGCGG GTTGCACTGCGGAAAC	Cloning of MpKAOL1 promoter
MpTPS1-NL1-OligoA	CTCG GTTCTTGCCAACCTTGATCC	Large-deletion mutation of MpTPS1
MpTPS1-NL1-OligoB	AAAC GGATCAAGGTTGGCAAGAAC	Large-deletion mutation of MpTPS1
MpTPS1-NL2-OligoA	CTCG AACCAGTTGAGACTGACCAG	Large-deletion mutation of MpTPS1
MpTPS1-NL2-OligoB	AAAC CTGGTCAGTCTCAACTGGTT	Large-deletion mutation of MpTPS1
MpTPS1-NR1-OligoA	CTCG ACGTGACTGTGTTGAGTCTA	Large-deletion mutation of MpTPS1
MpTPS1-NR1-OligoB	AAAC TAGACTCAACACAGTCACGT	Large-deletion mutation of MpTPS1
MpTPS1-NR2-OligoA	CTCG CAGTCACGTCACACTACGAGAC	Large-deletion mutation of MpTPS1
MpTPS1-NR2-OligoB	AAAC GTCTCGTAGTGACGTGACTG	Large-deletion mutation of MpTPS1
MpTPS1-gt-F	GGCCTCTCGTAGCTTTGA	Genotyping of Mptps1 ^{ld}
MpTPS1-gt-R	CAGGAAGGTTTGCTTGCA	Genotyping of Mptps1 ^{ld}
Mapoly0130s0002-0003-gRNA1-F	CTCG CCACCCTATATCAGAGAAA	Large-deletion mutation of MpKOL2 and MpKOL3
Mapoly0130s0002-0003-gRNA1-R	AAAC TTTCTCTGATATAGTGGTGG	Large-deletion mutation of MpKOL2 and MpKOL3
Mapoly0130s0002-0003-gRNA2-F	CTCG AGCGGAATAGACTCTCATTC	Large-deletion mutation of MpKOL2 and MpKOL3
Mapoly0130s0002-0003-gRNA2-R	AAAC GAAATGAGAGTCTATTCCGCT	Large-deletion mutation of MpKOL2 and MpKOL3
Mapoly0130s0002-0003-gRNA3-F	CTCG ATAGGAGTGAACATATTTGT	Large-deletion mutation of MpKOL2 and MpKOL3
Mapoly0130s0002-0003-gRNA3-R	AAAC ACAAATATGTTCACTCCTAT	Large-deletion mutation of MpKOL2 and MpKOL3
Mapoly0130s0002-0003-gRNA4-F	CTCG AACGCACTTCTCAATCCCA	Large-deletion mutation of MpKOL2 and MpKOL3
Mapoly0130s0002-0003-gRNA4-R	AAAC TGGGATTGAGGAAGTGC GTT	Large-deletion mutation of MpKOL2 and MpKOL3
Dseq-KOL2-3_gRNA1~4F	CTCCAAGTGTTGTGTAGCTG	Genotyping of [Mpkol2 Mpkol3] ^{ld}
Dseq-KOL2-3_gRNA1~4R	CTCTTAGCAGATGTGACCAC	Genotyping of [Mpkol2 Mpkol3]
MpKAOL3-NL1-OligoA	CTCG TTCGCTGTTGTCAGCGGTAG	Large-deletion mutation of MpKAOL3
MpKAOL3-NL1-OligoB	AAAC CTACCGCTGACAACAGCGAA	Large-deletion mutation of MpKAOL3
MpKAOL3-NL2-OligoA	CTCG GCCCCACCTCAACACTAGAGT	Large-deletion mutation of MpKAOL3
MpKAOL3-NL2-OligoB	AAAC ACTCTAGTGTTGAGGTGGGC	Large-deletion mutation of MpKAOL3
MpKAOL3-NR1-OligoA	CTCG TGGAGCTGTGCACATCTGA	Large-deletion mutation of MpKAOL3
MpKAOL3-NR1-OligoB	AAAC TCAGATGTGCACAGCTCCAA	Large-deletion mutation of MpKAOL3
MpKAOL3-NR2-OligoA	CTCG ACAATAGTTTAGCGTACTAT	Large-deletion mutation of MpKAOL3
MpKAOL3-NR2-OligoB	AAAC ATAGTACGCTAAACTATTGT	Large-deletion mutation of MpKAOL3
MpKAOL3-gt-F	GGCACACACGAGACTCCC	Genotyping of Mpkaol3 ^{ld}
MpKAOL3-gt-R	TCGCGAGGAGTAGGCTTT	Genotyping of Mpkaol3 ^{ld}

(Adapter sequences are highlighted in red, and underlines are used to denote start codons.)

Phylogenetic analysis

To identify homologs for KO and KAO, sequences of Arabidopsis and rice proteins were queried with BLAST (Camacho et al., 2009) against the bryophyte transcriptomes from the 1000 Plant transcriptomes initiative (1KP) (Leebens-Mack et al., 2019; Carpenter et al., 2019), a set of previously published liverwort transcriptomes (Dong et al., 2022) and the genomes of following species: *Calohyllum plumiforme* (Mao et al., 2020), *Ceratodon purpureus* (Carey et al., 2021), *Fontinalis antipyretica* (Yu et al., 2020), *Funaria hygrometrica* (Kirbis et al., 2020), *Physcomitrium patens* (Lang et al., 2018), *Sphagnum angustifolium* (Healey et al., 2023), *Sphagnum divinum* (Healey et al., 2023), *Syntrochia caninervis* (Silva et al., 2021), *Lunularia cruciata* (Linde et al., 2023), *Marchantia paleacea* (Rich et al., 2021), *Marchantia polymorpha* (Diop et al., 2020), *Anthoceros agrestis* (Li et al., 2020a), *Anthoceros angustus* (Zhang et al., 2020a), *Anthoceros punctatus* (Li et al., 2020a), *Isoetes taiwanese* (Wickell et al., 2021), *Lycopodium clavatum* (Yu et al., 2023), *Selaginella moellendorffii* (Banks et al., 2011), *Adiantum capillus-veneris* (Fang et al., 2022), *Alsophila spinulosa* (Huang et al., 2022), *Azolla filiculoides* (Li et al., 2018), *Ceratopteris richardii* (Marchant et al., 2022), *Marsilea vestita* (Rahmatpour et al., 2023), *Salvinia cucullate* (Li et al., 2018), *Ginkgo biloba* (Liu et al., 2021), *Gnetum montanum* (Wan et al., 2021), *Picea abies* (Nystedt et al., 2013), *Sequoiadendron giganteum* (Scott et al., 2020), *Taxus chinensis var. mairei* (Xiong et al., 2021), *Torreya grandis* (Lou et al., 2023), *Welwitschia mirabilis* (Wan et al., 2021), *Amborella trichopoda* (DOE-JGI, 2022a, 2022b), *Arabidopsis thaliana* (Cheng et al., 2017), *Brachypodium distachyon* (Vogel et al., 2010), *Cinnamomum kanehirae* (Chaw et al., 2019), *Liriodendron chinensis* (Chen et al., 2019), *Nymphaea colorata* (Zhang et al., 2020b), *Oryza sativa* (Kawahara et al., 2013), and *Populus trichocarpa* (Tuskan et al., 2006).

From each genome or transcriptome, the top 20 BLAST hits were collected for an initial analysis. The multiple-sequence alignment was performed with all candidate sequences using MAFFT with the progressive FFT-NS-2 algorithm (Katoh and Standley, 2013), and positions with >80% gaps were stripped from the alignment. The maximum likelihood phylogeny was inferred with the IQ-TREE 2 software, with the substitution model determined by ModelFinder and bootstrap support calculated with 1000 ultrafast bootstrap approximations (UFBoot) (Kalyaanamoorthy et al., 2017; Hoang et al., 2018; Minh et al., 2020). Candidate and outgroup sequences were selected from the initial tree and re-analyzed. MAFFT alignment was carried out using the L-INS-I algorithm (Katoh and Standley, 2013). After positions with >98% gaps were removed, IQ-TREE 2 was used to build the maximum likelihood tree with 1000 standard nonparametric bootstraps (Guindon et al., 2010; Minh et al., 2020). The model LG+I+G4 was selected by ModelFinder for both KOs and KAOs (Kalyaanamoorthy et al., 2017). The final phylogenetic trees were visualized with the ggtree package suite in R (Yu et al., 2017, 2018; Yu, 2020; Xu et al., 2022; Yu, 2022). The sequences, alignments and scripts generated during the analysis were deposited to https://github.com/dorrenasun/Mp_GA_biosynthesis.

Yeast enzymatic assay and GC-MS analysis

For protein expression in the yeast *Pichia pastoris*, the CDSs of MpKOLs and MpKAOLs were amplified from the cDNA of Tak-1 using primers listed in Table 4-3, and recombined into pPICZA using the seamless ligation cloning extract (SLiCE) prepared from *Escherichia coli* (Zhang et al., 2012; Motohashi, 2015). The CDS of the Arabidopsis protein AtKAO1 (AT1G05160) was cloned from the cDNA of Columbia-0 seedlings with the same

approach. The Arabidopsis gene ARABIDOPSIS THALIANA CYTOCHROME REDUCTASE1 (ATR1, AT4G24520) was introduced to the X-33 strain of *Pichia pastoris* in a previous research (Katsumata et al., 2008), which was transformed with pPICZA plasmids carrying the target genes.

For enzymatic assays, yeast transformants were cultured at 30 °C with shaking. Initially the yeasts were grown in 2 mL of BMG medium (1.34% [w/v] yeast nitrogen base [YNB], 100 mM potassium phosphate (pH 6.0), 4×10⁻⁵% [w/v] biotin, 1% [v/v] glycerol) until the OD₆₀₀ value reached 2. The cells were isolated by centrifugation and then transferred into 50 mL of MM medium (1.34% [w/v] YNB, 4×10⁻⁵% [w/v] biotin, 0.5% [v/v] methanol). After 24 h of induction in MM, 7 µg of *ent*-kaurene or 15 µg of KA was added to the medium together with 2.5 mL of methanol. After adding another dose of methanol at the 48-h time point, the medium was collected after a total 72 h of culturing in MM. After vigorous centrifugation to remove cell pellets, the supernatants were extracted with equal volumes of ethyl acetate for two times. The organic extracts were vacuum-concentrated, derivatized with diazomethane in ether solution and injected into GC-MS. The GC-MS analyses was carried out in DB-1 capillary column (15 m/0.25 mm/0.25 µm, Agilent J&W) in the Agilent 6890 GC, which was coupled with a mass selective detector (Agilent 5975C MSD, ionization energy at 70 eV). The program for oven temperature was described previously (Hayashi et al., 2006).

Yeast transformations and GC-MS analyses were performed by Wakako Fukuda at the Tokyo University of Agriculture and Technology.

Table 4-3 Primers used for protein expression in *Pichia pastoris*

Name	Sequence (5'→3')
pPICZA-MpKOL1-IF-F	ATTCGAAACGAGGAA <u>ATG</u> AAATGCTTCGGTTTGTC
pPICZA-MpKOL1-IF-R	CCCAAGCTGGCGGCC AATCTTCGCTGGACAG
pPICZA-MpKOL2-IF-F	ATTCGAAACGAGGAA <u>ATG</u> ACCAGACACTTGGGTGA
pPICZA-MpKOL2-IF-R	CCCAAGCTGGCGGCC AGCTGGCAAAATATTTTCA
pPICZA-MpKOL3-IF-F	ATTCGAAACGAGGAA <u>ATG</u> GAGAGTACAGAGAAATC
pPICZA-MpKOL3-IF-R	CCCAAGCTGGCGGCC AGATGGCAGAACACCTTTGA
pPICZA-AtKAO1-IF-F	ATTCGAAACGAGGAA <u>ATG</u> GCGGAGACAACGAGTTG
pPICZA-AtKAO1-IF-R	CCCAAGCTGGCGGCC CCTGATAACTAATTCTTGCCA
pPICZA-MpKAOL1-IF-F	ATTCGAAACGAGGAA <u>ATG</u> TGGAGATTCGTCCAC
pPICZA-MpKAOL1-IF-R	CCCAAGCTGGCGGCC CAATCGTGAGAAGTTTATAA
pPICZA-MpKAOL3-IF-F	ATTCGAAACGAGGAA <u>ATG</u> GCTGCGATTGTTCTCA
pPICZA-MpKAOL3-IF-R	CCCAAGCTGGCGGCC GCTGCACACACGACGAGT

(Adapter sequences are highlighted in red, and underlines are used to denote start codons.)

LC-MS/MS analysis of endogenous GA₁₂

If not specified, plants used for endogenous GA analysis were grown from gemmae for 10 days under cW and then 4 days under cW+cFR, on half-strength Gamborg's B5 medium containing 1% sucrose and 1% agar (Gamborg et al., 1968). To investigate the influence of FR enrichment, Tak-1 plants were either cultured under the conditions above, or under cW for 14 days. Before extraction, 3 g of whole thallus was collected for each replicate in the analysis, flash-frozen in liquid nitrogen and stored at -80°C. Each frozen sample was homogenized and extracted with 15 mL acetone at 4 °C for 2 h, with the ²H₂-labeled authentic compounds added to the mixture. The acetone extracts were filtered through defatted cotton to remove plant debris and concentrated under nitrogen flow to ~1 mL. After mixing with 1 mL acetonitrile, the solution was extracted with equal volume of hexane for 3 times. The aqueous phase was alkalified with 1 mL of NaHCO₃ saturated solution and washed with 2 mL chloroform for two more times. After purification with a polyvinylpyrrolidone (PVP) cartridge, the pH of the eluate was adjusted to 2-3 with 6M HCl. Then the solution was passed through a reverse-phase cartridge (Oasis HLB 3 cc/60 mg, Waters), an anion-exchange cartridge (Bond Elut DEA 100 mg/1 mL, Agilent), and a silica cartridge (Sep-Pak Silica 1 cc Vac Cartridge, Waters) in sequential order. The eluate from the final step was evaporated in a vacuum centrifuge concentrator and re-dissolved in 1% (v/v) acetic acid before subjected to LC-MS/MS analysis.

The LC-MS/MS analysis was performed in an ultraperformance LC system (ExionLC, Sciex) coupled with a quadrupole time-of-flight mass spectrometer (X500R QTOF, Sciex), using a reverse-phase column (CORTECS UPLC C18+, φ1.6 μm, 2.1 × 100 mm, Waters). For LC separation, the temperature was kept at 40 °C, the flow rate was 0.3 mL/min, and the two solvents used were solvent A (0.05% [v/v] acetic acid in water) and solvent B (0.05% [v/v] acetic acid in acetonitrile). Over the first 17 min, the proportion of solvent B was increased linearly from 3% to 65%. Then the system was eluted with 98% solvent B for 2 min, and washed with 3% B for 3 min. For compound identification, the mass spectrum of GA₁₂ was captured under the TOF-MS/MS mode. While for quantification, the multiple reaction monitoring (MRM) mode was used.

These experiments were performed by the laboratory member Maiko Okabe, with the help of Toshiaki Ishida and Kiyoshi Mashiguchi from Kyoto University.

Subcellular localization of proteins

To examine the subcellular localization of proteins, genetic mutants of each gene was used as the negative control, and the complementation lines expressing the target protein with C-terminal Citrine fusion under the control of a 35S promoter was used for observation. Plant materials were grown from gemmae for 7 days under cW+cFR before the whole thallus pieces were collected and fixed with 4% (w/v) paraformaldehyde (PFA) for 20 min at room temperature. After two times of 5-min washing with phosphate buffer saline (PBS, consisting of 137 mM NaCl, 2.7 mM KCl, 10 mM Na₂HPO₄ and 1.8 mM KH₂PO₄, pH = 7.4), the samples were stained with 1 μg/mL DAPI for 8 h at 4°C, or 1 mg/mL calcofluor white for 10 min at room temperature. After staining, the samples were washed twice with PBS and immersed in 75.5% (w/v) iohexol (GE Healthcare Pharma) for at least 1 h. The iohexol solution was also used as the mounting medium for preparing slides. Confocal microscopy was performed with the Leica TCS SP8X Falcon microscopes using the hybrid detector (HyD) and the HC PL APO CS2 40x/1.30 OIL objective lens. Imaging parameters are listed in Table 4-4.

Table 4-4 Parameters of confocal imaging for protein subcellular localizations

Samples: <i>Mpcps-4^{ld}</i> ♂, <i>pro-35S:MpCPS-Cit</i> (<i>Mpcps-4^{ld}</i> ♂) #6	Channel 1: Calcofluor white	Channel 2: Citrine	Channel 3: Chlorophyll
Laser	Diode 405 nm (UV)	WLL (85%)	WLL (85%)
Laser Wavelength	405 nm	488 nm	592 nm
Laser Intensity	0.0984%	25.9609%	2.1007%
Target Wavelength Begin	425 nm	500 nm	680 nm
Target Wavelength End	435 nm	541 nm	700 nm
Time Gating	OFF	1.8-12 ns	OFF
Gain	29 %	100.1 %	30.3 %
Offset	--	-0.01	--
Samples: <i>Mpks-14^{ld}</i> ♂, <i>pro-35S:MpKS-Cit</i> (<i>Mpks-14^{ld}</i> ♂) #13	Channel 1: Calcofluor white	Channel 2: Citrine	Channel 3: Chlorophyll
Laser	Diode 405 nm (UV)	WLL (87%)	WLL (87%)
Laser Wavelength	405 nm	495 nm	649 nm
Laser Intensity	2.4965%	39.9770%	0.5012%
Target Wavelength Begin	425 nm	500 nm	655 nm
Target Wavelength End	475 nm	530 nm	755 nm
Time Gating	OFF	1.2-6.0 ns	OFF
Gain	204.2 %	260 %	60 %
Offset	--	-0.01	--
Samples: <i>Mpkol1-7^{ld}</i> ♂, <i>pro-35S:MpKOL1-Cit</i> (<i>Mpkol1-7^{ld}</i> ♂) #4	Channel 1: Calcofluor white	Channel 2: Citrine	Channel 3: Chlorophyll
Laser	Diode 405 nm	WLL (85%)	WLL (85%)
Laser Wavelength	405 nm	495 nm	649 nm
Laser Intensity	0.0984%	19.9868%	0.5012%
Target Wavelength Begin	425 nm	500 nm	655 nm
Target Wavelength End	475 nm	530 nm	755 nm
Time Gating	OFF	1.2-6.0 ns	OFF
Gain	10 %	71.4 %	15.5 %
Offset	--	--	-0.01
Samples: <i>Mpkaol1-5^{ge}</i> ♂, <i>pro-35S:MpKAOL1-Cit</i> (<i>Mpkaol1-5^{ge}</i> ♂) #3	Channel 1: DAPI	Channel 2: Citrine	Channel 3: Chlorophyll
Laser	Diode 405 nm (UV)	WLL (85%)	WLL (85%)
Laser Wavelength	405 nm	495 nm	649 nm
Laser Intensity	15.2001%	29.9781%	0.5012%
Target Wavelength Begin	430 nm	500 nm	655 nm
Target Wavelength End	480 nm	530 nm	755 nm
Time Gating	OFF	1.2-6.0 ns	OFF
Gain	66.7 %	294.6 %	31.6 %
Offset	--	-0.01	--

RNA extraction and RT-qPCR

In RT-qPCR experiments, 3 different samples of whole thallus tissue (50–100 mg) from one or more plants were collected as biological replicates for each group. The samples were flash-frozen with liquid nitrogen and homogenized into fine powders by shaking with metal beads in a cell disruption device (BMS-A20TP, Bio Medical Science, Japan), followed by RNA-extraction with the TRIzol reagent (Thermo Fisher Scientific). After digestion with the RQ1 RNase-Free DNase (Promega), cDNAs were synthesized from the total RNAs with ReverTra Ace (Toyobo Life Science) and the (dT)₂₀ oligo.

For qPCR reactions, the Taq polymerase was prepared following (Pluthero, 1993), and the DNA quantity was monitored using the SYBR Green I Nucleic Acid Gel Stain (Lonza). Each reaction was performed with three technical replicates, and the following program was executed in a CFX96 real-time PCR detection system (Bio-Rad): initial denaturation at 95 °C for 30 s, then cycling between 5 s at 95 °C and 30 s at 60 °C for 40 times, reading SYBR signals at the end of each cycle. After finishing all cycles, the standard melting curve was

analyzed for each reaction to reveal the thermodynamic property of amplified products. To quantify the relative gene expressions, *MpELONGATION FACTOR1 α* (*MpEF1 α* , Mp3g23400) was used as the internal reference, and the gene expression changes were calculated following (Hellemans et al., 2008). The qPCR primers were listed in Table 4-5.

Table 4-5 Primers used for RT-qPCR experiments

Name	Sequence (5'→3')	Target gene
MpEF1-qPCR_F	AAGCCGTCGAAAAGAAGGAG	<i>MpEF1α</i> (Mp3g23400)
MpEF1-qPCR_R	TTCAGGATCGTCCGTTATCC	<i>MpEF1α</i> (Mp3g23400)
MpCPSKS_qPCR-F	TCTTACACGGTTCTCGGGATG	<i>MpCPS</i> (Mp2g07200)
MpCPSKS_qPCR-R	GGATTGCGTTTTGAGGAAGATG	<i>MpCPS</i> (Mp2g07200)
MpKS-RT-F	CAAGCAAGGATAGCAATCCAG	<i>MpKS</i> (Mp6g05950)
MpKS-RT-R	TCGCATCATTCCCAACCAG	<i>MpKS</i> (Mp6g05950)
MpKO_qPCR-F1	TGCAGCACTTCGAGTTGACC	<i>MpKOL1</i> (Mp3g18320)
MpKO_qPCR-R1	TGCAGTTTGTTGGGAGGTGAC	<i>MpKOL1</i> (Mp3g18320)
MpKAO_qPCR-F1	GCCCTATGCGTTCAAACCTG	<i>MpKAOL1</i> (Mp4g23680)
MpKAO_qPCR-R1	GCTCGATGCCGATACAACCTC	<i>MpKAOL1</i> (Mp4g23680)

GUS staining

To evaluate GUS activity in whole-mount tissues, fresh plants were infiltrated with the GUS substrate solution (50 mM sodium phosphate buffer [pH 7.2], 0.5 mM $K_3Fe(CN)_6$, 0.5 mM $K_4Fe(CN)_6$, 10 mM EDTA, 0.01% [v/v] Triton X-100, 1 mM 5-bromo-4-chloro-3-indolyl- β -D-glucuronic acid [X-Gluc, Biosynth AG, Switzerland]) in vacuo. After incubating at 37 °C overnight, the reaction was stopped by washing the tissues with 70% (v/v) and 90% (v/v) ethanol solutions. Images were acquired with a stereoscope (Olympus SZX16).

Thallus morphology observation

For quantitative analysis of thallus morphology, plants were grown from gemmae for 12 days under cW or cW+cFR. In the chemical treatment experiments, different compounds were added to the growth medium before gemmae were planted. After taking top-view photos vertically above the plants, individual plants attached to agar medium blocks were cut out and aligned on a staging box with equal distances to a horizontally positioned camera for taking photos from the side view. Finally, the plants were carefully removed from the agar medium for dimensional and size measurements. Generally, the plants consisted of two “half thalli” that were developed from individual apical meristems in the gemmae. These half thalli were separated and placed on a moist filter paper, and photos were taken again vertically from the top. The measurements were carried out on side-view and “half thallus” photos, using in-house macro scripts in Fiji (Schindelin et al., 2012). Data was discarded from a half thallus if its dorsoventral development was defective, or from a whole plant if more than two “half thalli” appeared (Figure 4-1). The scripts are available at https://github.com/dorrenasun/Mp_GA_biosynthesis.

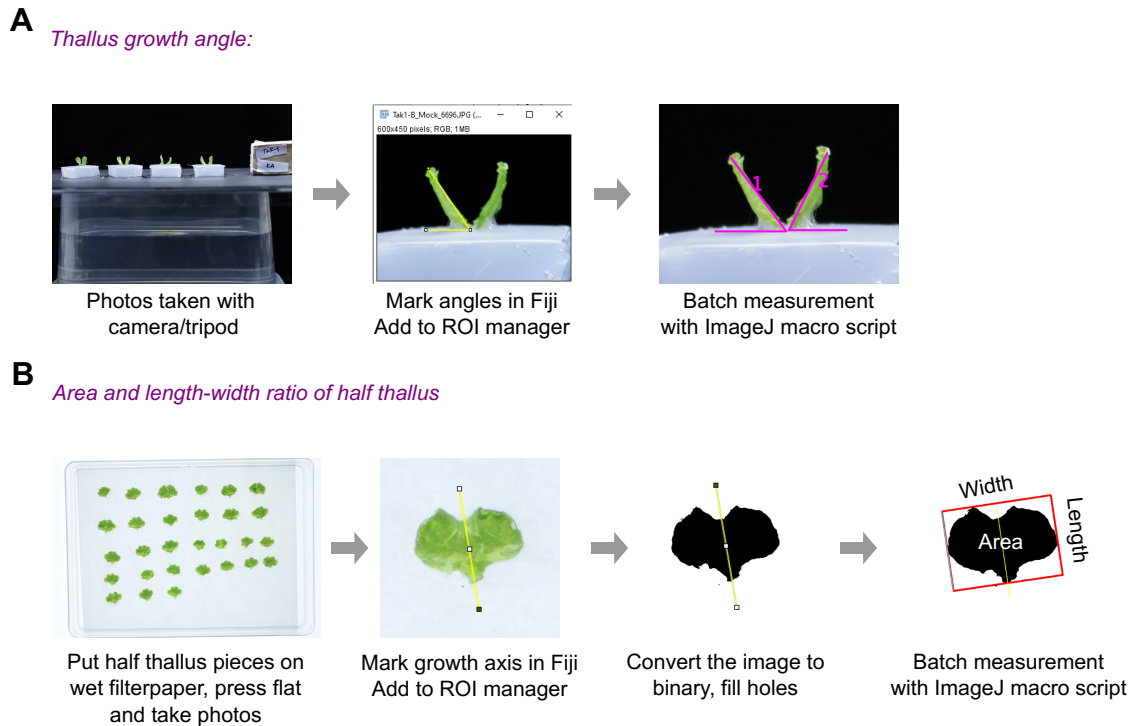


Figure 4-1 Quantitative analysis of thallus morphology. (A) For measuring thallus growth angles, photos were taken horizontally for plants aligned in a row, and the orientation of each plant was adjusted manually before taking the photos. The angles between the thallus and the medium surface were measured in Fiji. (B) For measuring thallus sizes and dimensions, top-view photos of flattened “half thalli” were taken and analyzed in Fiji. An axis that denotes the growth direction was manually marked, and a bounding box was drawn around the thallus to define the maximum dimensions parallel or perpendicular to the growth direction as “length” and “width” of the thallus, respectively.

EdU analysis of cell division

For the EdU assay, 7-day-old plants grown under cW+cFR were harvested from the solid medium and incubated with 20 mM EdU in liquid half-strength Gamborg’s B5 medium for 2 h. After that, the samples were fixed with 3.7% (w/v) formaldehyde for 1 h at room temperature and washed in PBS for two times (5 min each). A 20-min treatment with 0.5% (v/v) Triton X-100 in PBS was performed to permeabilize the samples, followed by two 5-min washes using 3% (w/v) bovine serum albumin in PBS. Then the click reaction was carried out in darkness using the Click-iT EdU Imaging Kit with Alexa Fluor 555 (Thermo Fisher Scientific, #C10338), by incubating the samples with the reaction mixture for 1 h. After washing twice with PBS, the tissues were cleared with the iTOMEI technique (Sakamoto et al., 2022). The chlorophyll was removed from the samples by overnight treatment with 20% (w/v) caprylyl sulfobetaine (#D4246, TCI, Japan). Finally, the samples were washed twice with PBS, and infiltrated with 75.5% (w/v) iohexol (GE Healthcare Pharma) for 1 h before mounted onto slides.

The apical regions of thallus fragments were observed under an Olympus FV1000 confocal laser scanning microscope, and fluorescent images were acquired as z-stacks with 5- μ m intervals. Excitation and emission wavelengths for the EdU signals were 543 nm and 505-605 nm, respectively. The quantitative analysis of EdU-positive nuclei was carried out

with in-house scripts (deposited to https://github.com/dorrenasun/Mp_GA_biosynthesis) in Fiji, with the help of the StarDist plugin (Schindelin et al., 2012; Schmidt et al., 2018).

Observation of gametangiophores

To observe the progress of apical meristem bifurcation and differentiation, plants were grown under aseptic conditions. After 7 d of growth under cW, half thalli were transferred onto fresh medium and induced under cW+cFR. At the second stage, chemical treatments were included in the medium when applicable. Using a stereoscope (Olympus SZX16), the thallus fragments were observed on a daily basis, and the number of meristems and the emergence of gametangiophore primordia (typically with a tiny stalk) was recorded. Images of gametangiophores were also taken with the same microscope.

To observe the gametangiophore morphology, plants were first grown on agar medium for 7 or 14 days, then thallus fragments were transferred onto vermiculites in pots for culturing under cW+cFR in the open air. After gametangiophores were fully developed, images of individual gametangiophores were taken with the Olympus SZX16 stereoscope.

To observe the tissue organization in gametangiophores, stalks or receptacles of gametangiophores were embedded freshly in 5%-6% (w/v) agar. 200- μ m sections for stalks and 70- μ m sections for the receptacle were prepared with a DOSAKA LinearSlicer Pro7 vibratome and observed under the Keyence BZ-X710 microscope.

Microscopic observation of MpBNB-Cit

To monitor the early differentiation of gametangia, Mp*BNB-Cit* knock-in lines with wild-type or disrupted Mp*CPS* alleles were cultured from gemmae under cW+cFR. Male plants were cultured for 11 d, and half thalli derived from single gemma meristems were sampled from different plants. For female plants, two rounds of apical bifurcation already took place in the 14-day-old thalli, thus one of the four branches were selected from each plant for observation in the apical region. The samples were fixed for 1 h with 4% (w/v) PFA, washed for two times with PBS, and cleared with the ClearSeeAlpha solution (Kurihara et al., 2021) for 2 d at room temperature. After two washes with PBS, the samples were stained with 1 mg/mL calcofluor white for 10 min. After another two washes with PBS, the samples were soaked in 75.5% (w/v) iohexol (GE Healthcare Pharma) for 1 h before mounting onto slides.

For fluorescence microscopy, z-stacks of images were acquired at 5- μ m steps with the Keyence BZ-X710 microscope, using the BZ-X DAPI (Excitation: 360 \pm 20 nm; Emission: 460 \pm 25 nm; Dichroic mirror: 400 nm) filter for calcofluor white staining signals, and the customized filter (Excitation: 500 \pm 10 nm; Emission: 535 \pm 15 nm; Dichroic mirror: 515 nm) for Citrine signals. The BZ-X Analyzer software was used to create full-focus projections for image stacks, in which the Citrine-positive nuclei were counted using Fiji (Schindelin et al., 2012).

RNA-seq and data analysis

For RNA-seq, plants were cultured from gemmae under cW or cW+cFR for 12 days on medium containing 0 or 2 μ M of KA, before ~50 mg of whole thallus tissues from one or more plants were collected for RNA extraction. The samples were flash-frozen with liquid nitrogen and homogenized into fine powders by shaking with metal beads in a cell disruption device (BMS-A20TP, Bio Medical Science, Japan), followed by RNA-extraction

with the RNeasy Plant Mini Kit (QIAGEN). After quality check with the Bioanalyzer RNA 6000 pico assay (Agilent), mRNA was enriched from total RNAs with the NEBNext Poly(A) mRNA Magnetic Isolation Module (New England Biolabs, #E7490). The cDNA library was prepared following manufacturer's instructions with the NEBNext Ultra II Directional RNA Library Prep Kit for Illumina (New England Biolabs, #E7760). The NEBNext Multiplex Oligos for Illumina (96 Unique Dual Index Primer Pairs Set 2, New England Biolabs, #E6442) was used for library amplification and indexing. Finally, the library quality was checked with the Bioanalyzer High Sensitivity DNA assay (Agilent) before sequencing in the NextSeq 500 system. Each sample yielded around 7.8 million single-end reads, which were subsequently demultiplexed in the BaseSpace Sequence Hub provided by Illumina.

To analyze the transcriptome data, the Salmon software (v1.9.0) was used to quantify the reads with quasi-mapping to the *M. polymorpha* MpTak_v6.1 genome (Iwasaki et al., 2021). Since all the samples were male, transcripts from the \bar{U} chromosome were removed from the mapping index. Differential gene expression analysis was carried out in R (v4.2.2) with the package DESeq2 (v1.38.3) using the standard pipeline and parameters (Love et al., 2014). For GO enrichment analysis based on previously described annotations (Hernández-García et al., 2021), the R package topGO (v2.50.0) was used to capture the enriched GO terms with the classic Fisher's exact test. Following the package's merit to discover more terms of relevance, the *P*-values were intentionally left unadjusted.

Bibliography

- Achard, P., Gusti, A., Cheminant, S., Alioua, M., Dhondt, S., Coppens, F., Beemster, G.T.S., and Genschik, P.** (2009). Gibberellin signaling controls cell proliferation rate in *Arabidopsis*. *Curr. Biol.* **19** (14): 1188–1193.
- Achard, P., Liao, L., Jiang, C., Desnos, T., Bartlett, J., Fu, X., and Harberd, N.P.** (2007). DELLAs contribute to plant photomorphogenesis. *Plant Physiol.* **143** (3): 1163–1172.
- Aki, S.S., Mikami, T., Naramoto, S., Nishihama, R., Ishizaki, K., Kojima, M., Takebayashi, Y., Sakakibara, H., Kyojuka, J., Kohchi, T., and Umeda, M.** (2019). Cytokinin signaling is essential for organ formation in *Marchantia polymorpha*. *Plant Cell Physiol.* **60** (8): 1842–1854.
- Althoff, F., Kopsischke, S., Zobell, O., Ide, K., Ishizaki, K., Kohchi, T., and Zachgo, S.** (2014). Comparison of the *MpEF1 α* and *CaMV35* promoters for application in *Marchantia polymorpha* overexpression studies. *Transgenic Res.* **23** (2): 235–244.
- Aya, K., Hiwatashi, Y., Kojima, M., Sakakibara, H., Ueguchi-Tanaka, M., Hasebe, M., and Matsuoka, M.** (2011). The gibberellin perception system evolved to regulate a pre-existing GAMYB-mediated system during land plant evolution. *Nat. Commun.* **2** (1): 544–549.
- Bai, M.-Y., Shang, J.-X., Oh, E., Fan, M., Bai, Y., Zentella, R., Sun, T., and Wang, Z.-Y.** (2012). Brassinosteroid, gibberellin and phytochrome impinge on a common transcription module in *Arabidopsis*. *Nat. Cell Biol.* **14** (8): 810–817.
- Banks, J.A. et al.** (2011). The *Selaginella* genome identifies genetic changes associated with the evolution of vascular plants. *Science* **332** (6032): 960–963.
- Beall, F.D., Yeung, E.C., and Pharis, R.P.** (1996). Far-red light stimulates internode elongation, cell division, cell elongation, and gibberellin levels in bean. *Can. J. Bot.* **74** (5): 743–752.
- Berland, H., Albert, N.W., Stavland, A., Jordheim, M., McGhie, T.K., Zhou, Y., Zhang, H., Deroles, S.C., Schwinn, K.E., Jordan, B.R., Davies, K.M., and Andersen, Ø.M.** (2019). Auronidins are a previously unreported class of flavonoid pigments that challenges when anthocyanin biosynthesis evolved in plants. *Proc. Natl. Acad. Sci. U. S. A.* **116** (40): 20232–20239.
- Bömke, C., Rojas, M.C., Gong, F., Hedden, P., and Tudzynski, B.** (2008). Isolation and characterization of the gibberellin biosynthetic gene cluster in *Sphaceloma manihoticola*. *Appl. Environ. Microbiol.* **74** (17): 5325–5339.
- Bömke, C. and Tudzynski, B.** (2009). Diversity, regulation, and evolution of the gibberellin biosynthetic pathway in fungi compared to plants and bacteria. *Phytochemistry* **70** (15–16): 1876–1893.
- Bowman, J.L. et al.** (2017). Insights into land plant evolution garnered from the *Marchantia polymorpha* genome. *Cell* **171** (2): 287–304.
- Brian, P.W. and Hemming, H.G.** (1955). The effect of gibberellic acid on shoot growth of pea seedlings. *Physiol. Plant.* **8** (3): 669–681.
- Briginshaw, L.N., Flores-Sandoval, E., Dierschke, T., Alvarez, J.P., and Bowman, J.L.**

- (2022). KANADI promotes thallus differentiation and FR-induced gametangiophore formation in the liverwort *Marchantia*. *New Phytol.* **234** (4): 1377–1393.
- Briones-Moreno, A., Hernández-García, J., Vargas-Chávez, C., Blanco-Touriñán, N., Phokas, A., Úrbez, C., Cerdán, P.D., Coates, J.C., Alabadí, D., and Blázquez, M.A.** (2023). DELLA functions evolved by rewiring of associated transcriptional networks. *Nat. Plants* **9** (4): 535–543.
- Camacho, C., Coulouris, G., Avagyan, V., Ma, N., Papadopoulos, J., Bealer, K., and Madden, T.L.** (2009). BLAST+: Architecture and applications. *BMC Bioinformatics* **10** (1): 1–9.
- Cannell, N., Emms, D.M., Hetherington, A.J., MacKay, J., Kelly, S., Dolan, L., and Sweetlove, L.J.** (2020). Multiple metabolic innovations and losses are associated with major transitions in land plant evolution. *Curr. Biol.* **30** (10): 1783–1800.
- Cao, J.-G., Wang, Q.-X., Zou, H.-M., Dai, X.-L., and Cao, T.** (2013). New observations on the morphology and structure of *Marchantia polymorpha* gametophores in sexual reproduction adaptation. *Plant Sci. J.* **31** (6): 555.
- Carey, S.B. et al.** (2021). Gene-rich UV sex chromosomes harbor conserved regulators of sexual development. *Sci. Adv.* **7** (27): eabh2488.
- Carpenter, E.J. et al.** (2019). Access to RNA-sequencing data from 1,173 plant species: The 1000 Plant transcriptomes initiative (1KP). *GigaScience* **8** (10): giz126.
- Casey, A. and Dolan, L.** (2023). Genes encoding cytochrome P450 monooxygenases and glutathione S-transferases associated with herbicide resistance evolved before the origin of land plants. *PLOS ONE* **18** (2): e0273594.
- Chaw, S.-M. et al.** (2019). Stout camphor tree genome fills gaps in understanding of flowering plant genome evolution. *Nat. Plants* **5** (1): 63–73.
- Chen, J. et al.** (2019). *Liriodendron* genome sheds light on angiosperm phylogeny and species–pair differentiation. *Nat. Plants* **5** (1): 18–25.
- Chen, Y., Hou, M., Liu, L., Wu, S., Shen, Y., Ishiyama, K., Kobayashi, M., McCarty, D.R., and Tan, B.-C.** (2014). The maize *DWARF1* encodes a gibberellin 3-oxidase and is dual localized to the nucleus and cytosol. *Plant Physiol.* **166** (4): 2028–2039.
- Cheng, C.-Y., Krishnakumar, V., Chan, A.P., Thibaud-Nissen, F., Schobel, S., and Town, C.D.** (2017). Araport11: A complete reannotation of the *Arabidopsis thaliana* reference genome. *Plant J.* **89** (4): 789–804.
- Clack, T., Mathews, S., and Sharrock, R.A.** (1994). The phytochrome apoprotein family in *Arabidopsis* is encoded by five genes: the sequences and expression of PHYD and PHYE. *Plant Mol. Biol.* **25** (3): 413–427.
- Colebrook, E.H., Thomas, S.G., Phillips, A.L., and Hedden, P.** (2014). The role of gibberellin signalling in plant responses to abiotic stress. *J. Exp. Biol.* **217** (1): 67–75.
- Conesa, A. and Götz, S.** (2008). Blast2GO: A comprehensive suite for functional analysis in plant genomics. *Int. J. Plant Genomics* **2008**.
- Cowling, R.J. and Harberd, N.P.** (1999). Gibberellins control *Arabidopsis* hypocotyl growth via regulation of cellular elongation. *J. Exp. Bot.* **50** (337): 1351–1357.

- Devlin, P.F., Yanovsky, M.J., and Kay, S.A.** (2003). A genomic analysis of the shade avoidance response in *Arabidopsis*. *Plant Physiol.* **133** (4): 1617–1629.
- Dill, A., Jung, H.-S., and Sun, T.** (2001). The DELLA motif is essential for gibberellin-induced degradation of RGA. *Proc. Natl. Acad. Sci. U. S. A.* **98** (24): 14162–14167.
- Diop, S.I. et al.** (2020). A pseudomolecule-scale genome assembly of the liverwort *Marchantia polymorpha*. *Plant J.* **101** (6): 1378–1396.
- Djakovic-Petrovic, T., Wit, M.D., Voeselek, L.A.C.J., and Pierik, R.** (2007). DELLA protein function in growth responses to canopy signals. *Plant J.* **51** (1): 117–126.
- DOE-JGI** (2022a). *Amborella trichopoda* var. SantaCruz_75 HAP1 v2.1, <http://phytozome-next.jgi.doe.gov/>.
- DOE-JGI** (2022b). *Amborella trichopoda* var. SantaCruz_75 HAP2 v2.1, <http://phytozome-next.jgi.doe.gov/>.
- Dong, S., Yu, J., Zhang, L., Goffinet, B., and Liu, Y.** (2022). Phylotranscriptomics of liverworts: Revisiting the backbone phylogeny and ancestral gene duplications. *Ann. Bot.* **130** (7): 951–964.
- Duanmu, D. et al.** (2014). Marine algae and land plants share conserved phytochrome signaling systems. *Proc. Natl. Acad. Sci. U. S. A.* **111** (44): 15827–15832.
- Eshed, Y., Baum, S.F., Perea, J.V., and Bowman, J.L.** (2001). Establishment of polarity in lateral organs of plants. *Curr. Biol.* **11** (16): 1251–1260.
- Fang, Y. et al.** (2022). The genome of homosporous maidenhair fern sheds light on the euphyllophyte evolution and defences. *Nat. Plants* **8** (9): 1024–1037.
- Feng, S. et al.** (2008). Coordinated regulation of *Arabidopsis thaliana* development by light and gibberellins. *Nature* **451** (7177): 475–479.
- Fisher, T.J., Flores-Sandoval, E., Alvarez, J.P., and Bowman, J.L.** (2023). PIN-FORMED is required for shoot phototropism/gravitropism and facilitates meristem formation in *Marchantia polymorpha*. *New Phytol.* **238** (4): 1498–1515.
- Fredericq, H.** (1964). Influence formatrice de la lumière rouge-foncé sur le développement des thalles de *Marchantia polymorpha* L. [Formative influence of far-red light on the development of *Marchantia polymorpha* L. thalli]. *Bull. Société R. Bot. Belg.* **98** (1): 67–76.
- Fredericq, H. and de Greef, J.** (1966). Red (R), far-red (FR) photoreversible control of growth and chlorophyll content in light-grown thalli of *Marchantia polymorpha* L. *Naturwissenschaften* **53** (13): 337.
- Fredericq, H. and Greef, J.D.** (1968). Photomorphogenic and chlorophyll studies in the bryophyte *Marchantia polymorpha*. I. Effect of red, far-red irradiations in short and long-term experiments. *Physiol. Plant.* **21** (2): 346–359.
- Fuentes, S., Ljung, K., Sorefan, K., Alvey, E., Harberd, N.P., and Østergaard, L.** (2012). Fruit growth in *Arabidopsis* occurs via DELLA-dependent and DELLA-independent gibberellin responses. *Plant Cell* **24** (10): 3982–3996.
- Fukazawa, J., Teramura, H., Murakoshi, S., Nasuno, K., Nishida, N., Ito, T., Yoshida, M., Kamiya, Y., Yamaguchi, S., and Takahashi, Y.** (2014). DELLAs Function as

- coactivators of GAI-ASSOCIATED FACTOR1 in regulation of gibberellin homeostasis and signaling in *Arabidopsis*. *Plant Cell* **26** (7): 2920–2938.
- Gamborg, O.L., Miller, R.A., and Ojima, K.** (1968). Nutrient requirements of suspension cultures of soybean root cells. *Exp. Cell Res.* **50** (1): 151–158.
- Gilmour, S.J., Zeevaart, J.A.D., Schwenen, L., and Graebe, J.E.** (1986). Gibberellin metabolism in cell-free extracts from spinach leaves in relation to photoperiod. *Plant Physiol.* **82** (1): 190–195.
- Gomi, K., Sasaki, A., Itoh, H., Ueguchi-Tanaka, M., Ashikari, M., Kitano, H., and Matsuoka, M.** (2004). *GID2*, an F-box subunit of the SCF E3 complex, specifically interacts with phosphorylated SLR1 protein and regulates the gibberellin-dependent degradation of SLR1 in rice. *Plant J.* **37** (4): 626–634.
- Griffiths, J., Murase, K., Rieu, I., Zentella, R., Zhang, Z.-L., Powers, S.J., Gong, F., Phillips, A.L., Hedden, P., Sun, T., and Thomas, S.G.** (2006). Genetic characterization and functional analysis of the *GID1* gibberellin receptors in *Arabidopsis*. *Plant Cell* **18** (12): 3399–3414.
- Guindon, S., Dufayard, J.-F., Lefort, V., Anisimova, M., Hordijk, W., and Gascuel, O.** (2010). New algorithms and methods to estimate maximum-likelihood phylogenies: Assessing the performance of PhyML 3.0. *Syst. Biol.* **59** (3): 307–321.
- Harris, B.J., Clark, J.W., Schrepff, D., Szöllösi, G.J., Donoghue, P.C.J., Hetherington, A.M., and Williams, T.A.** (2022). Divergent evolutionary trajectories of bryophytes and tracheophytes from a complex common ancestor of land plants. *Nat. Ecol. Evol.* **6** (11): 1634–1643.
- Hayashi, K., Horie, K., Hiwatashi, Y., Kawaide, H., Yamaguchi, S., Hanada, A., Nakashima, T., Nakajima, M., Mander, L.N., Yamane, H., Hasebe, M., and Nozaki, H.** (2010). Endogenous diterpenes derived from *ent*-kaurene, a common gibberellin precursor, regulate protonema differentiation of the moss *Physcomitrella patens*. *Plant Physiol.* **153** (3): 1085–1097.
- Hayashi, K. ichiro, Kawaide, H., Notomi, M., Sakigi, Y., Matsuo, A., and Nozaki, H.** (2006). Identification and functional analysis of bifunctional *ent*-kaurene synthase from the moss *Physcomitrella patens*. *FEBS Lett.* **580** (26): 6175–6181.
- He, J., Chen, Q., Xin, P., Yuan, J., Ma, Y., Wang, X., Xu, M., Chu, J., Peters, R.J., and Wang, G.** (2019). CYP72A enzymes catalyse 13-hydrolyzation of gibberellins. *Nat. Plants* **5** (10): 1057–1065.
- Healey, A.L. et al.** (2023). Newly identified sex chromosomes in the *Sphagnum* (peat moss) genome alter carbon sequestration and ecosystem dynamics. *Nat. Plants* **9** (2): 238–254.
- Hedden, P., MacMillan, J., and Phinney, B.O.** (1974). Fungal products. Part XII. Gibberellin A14-aldehyde, an intermediate in gibberellin biosynthesis in *Gibberella fujikuroi*. *J. Chem. Soc. Perkin 1* (0): 587–592.
- Hellemans, J., Mortier, G., De Paepe, A., Speleman, F., and Vandesompele, J.** (2008). qBase relative quantification framework and software for management and automated analysis of real-time quantitative PCR data. *Genome Biol.* **8** (2).
- Helliwell, C.A., Chandler, P.M., Poole, A., Dennis, E.S., and Peacock, W.J.** (2001a). The CYP88A cytochrome P450, *ent*-kaurenoic acid oxidase, catalyzes three steps of the

- gibberellin biosynthesis pathway. *Proc. Natl. Acad. Sci. U. S. A.* **98** (4): 2065–2070.
- Helliwell, C.A., Poole, A., James Peacock, W., and Dennis, E.S.** (1999). *Arabidopsis ent-kaurene oxidase catalyzes three steps of gibberellin biosynthesis.* *Plant Physiol.* **119** (2): 507–510.
- Helliwell, C.A., Sheldon, C.C., Olive, M.R., R.Walker, A., Zeevaart, J.A.D., Peacock, W.J., and Dennis, E.S.** (1998). Cloning of the *Arabidopsis ent-kaurene oxidase gene GA3*. *Proc. Natl. Acad. Sci. U. S. A.* **95** (15): 9019–9024.
- Helliwell, C.A., Sullivan, J.A., Mould, R.M., Gray, J.C., James Peacock, W., and Dennis, E.S.** (2001b). A plastid envelope location of *Arabidopsis ent-kaurene oxidase* links the plastid and endoplasmic reticulum steps of the gibberellin biosynthesis pathway. *Plant J.* **28** (2): 201–208.
- Hernández-García, J., Briones-Moreno, A., Dumas, R., and Blázquez, M.A.** (2019). Origin of gibberellin-dependent transcriptional regulation by molecular exploitation of a transactivation domain in DELLA proteins. *Mol. Biol. Evol.* **36** (5): 908–918.
- Hernández-García, J., Sun, R., Serrano-Mislata, A., Inoue, K., Vargas-Chávez, C., Esteve-Bruna, D., Arbona, V., Yamaoka, S., Nishihama, R., Kohchi, T., and Blázquez, M.A.** (2021). Coordination between growth and stress responses by DELLA in the liverwort *Marchantia polymorpha*. *Curr. Biol.* **31** (16): 3678–3686.
- Hirano, K. et al.** (2007). The *GID1*-mediated gibberellin perception mechanism is conserved in the lycophyte *Selaginella moellendorffii* but not in the bryophyte *Physcomitrella patens*. *Plant Cell* **19** (10): 3058–3079.
- Hirose, F., Inagaki, N., Hanada, A., Yamaguchi, S., Kamiya, Y., Miyao, A., Hirochika, H., and Takano, M.** (2012). Cryptochrome and phytochrome cooperatively but independently reduce active gibberellin content in rice seedlings under light irradiation. *Plant Cell Physiol.* **53** (9): 1570–1582.
- Hisamatsu, T., King, R.W., Helliwell, C. a, and Koshioka, M.** (2005). The involvement of gibberellin 20-oxidase genes in phytochrome-regulated petiole elongation of *Arabidopsis*. *Plant Physiol.* **138** (2): 1106–1116.
- Hisanaga, T., Okahashi, K., Yamaoka, S., Kajiwara, T., Nishihama, R., Shimamura, M., Yamato, K.T., Bowman, J.L., Kohchi, T., and Nakajima, K.** (2019). A *cis*-acting bidirectional transcription switch controls sexual dimorphism in the liverwort. *EMBO J.* **38** (6): 1–12.
- Hoang, D.T., Chernomor, O., von Haeseler, A., Minh, B.Q., and Vinh, L.S.** (2018). UFBoot2: Improving the ultrafast bootstrap approximation. *Mol. Biol. Evol.* **35** (2): 518–522.
- Hornych, O., Testo, W.L., Sessa, E.B., Watkins, J.E., Company, C.E., Pittermann, J., and Ekrt, L.** (2021). Insights into the evolutionary history and widespread occurrence of antheridiogen systems in ferns. *New Phytol.* **229** (1): 607–619.
- Hou, X., Lee, L.Y.C., Xia, K., Yan, Y., and Yu, H.** (2010). DELLAs modulate jasmonate signaling via competitive binding to JAZs. *Dev. Cell* **19** (6): 884–894.
- Huang, X. et al.** (2022). The flying spider-monkey tree fern genome provides insights into fern evolution and arborescence. *Nat. Plants* **8** (5): 500–512.

- Huang, X., Tian, H., Park, J., Oh, D.-H., Hu, J., Zentella, R., Qiao, H., Dassanayake, M., and Sun, T.-P.** (2023). The master growth regulator DELLA binding to histone H2A is essential for DELLA-mediated global transcription regulation. *Nat. Plants* **9** (8): 1291–1305.
- Inoue, K., Nishihama, R., Araki, T., and Kohchi, T.** (2019). Reproductive induction is a far-red high irradiance response that is mediated by phytochrome and PHYTOCHROME INTERACTING FACTOR in *Marchantia polymorpha*. *Plant Cell Physiol.* **60** (5): 1136–1145.
- Inoue, K., Nishihama, R., Kataoka, H., Hosaka, M., Manabe, R., Nomoto, M., Tada, Y., Ishizaki, K., and Kohchi, T.** (2016). Phytochrome signaling is mediated by PHYTOCHROME INTERACTING FACTOR in the liverwort *Marchantia polymorpha*. *Plant Cell* **28** (6): 1406–1421.
- Ishizaki, K., Chiyoda, S., Yamato, K.T., and Kohchi, T.** (2008). *Agrobacterium*-mediated transformation of the haploid liverwort *Marchantia polymorpha* L., an emerging model for plant biology. *Plant Cell Physiol.* **49** (7): 1084–1091.
- Ishizaki, K., Nishihama, R., Ueda, M., Inoue, K., Ishida, S., Nishimura, Y., Shikanai, T., and Kohchi, T.** (2015). Development of Gateway binary vector series with four different selection markers for the liverwort *Marchantia polymorpha*. *PLoS ONE* **10** (9): e0138876.
- Itoh, H., Ueguchi-Tanaka, M., Sato, Y., Ashikari, M., and Matsuoka, M.** (2002). The gibberellin signaling pathway is regulated by the appearance and disappearance of SLENDER RICE1 in nuclei. *Plant Cell* **14** (1): 57–70.
- Iwasaki, M. et al.** (2021). Identification of the sex-determining factor in the liverwort *Marchantia polymorpha* reveals unique evolution of sex chromosomes in a haploid system. *Curr. Biol.* **31** (24): 5522–5532.
- Jia, Q., Brown, R., Köllner, T.G., Fu, J., Chen, X., Wong, G.K.S., Gershenzon, J., Peters, R.J., and Chen, F.** (2022). Origin and early evolution of the plant terpene synthase family. *Proc. Natl. Acad. Sci. U. S. A.* **119** (15): 1–9.
- Kalyanamoorthy, S., Minh, B.Q., Wong, T.K.F., von Haeseler, A., and Jermiin, L.S.** (2017). ModelFinder: Fast model selection for accurate phylogenetic estimates. *Nat. Methods* **14** (6): 587–589.
- Kamienska, A., Durley, R.C., and Pharis, R.P.** (1976). Isolation of gibberellins A₃, A₄ and A₇ from *Pinus attenuata* pollen. *Phytochemistry* **15** (3): 421–424.
- Kasahara, H., Hanada, A., Kuzuyama, T., Takagi, M., Kamiya, Y., and Yamaguchi, S.** (2002). Contribution of the mevalonate and methylerythritol phosphate pathways to the biosynthesis of gibberellins in *Arabidopsis*. *J. Biol. Chem.* **277** (47): 45188–45194.
- Katoh, K. and Standley, D.M.** (2013). MAFFT multiple sequence alignment software version 7: Improvements in performance and usability. *Mol. Biol. Evol.* **30** (4): 772–780.
- Katsumata, T., Hasegawa, A., Fujiwara, T., Komatsu, T., Notomi, M., Abe, H., Natsume, M., and Kawaide, H.** (2008). *Arabidopsis* CYP85A2 catalyzes lactonization reactions in the biosynthesis of 2-deoxy-7-oxalactone brassinosteroids. *Biosci. Biotechnol. Biochem.* **72** (8): 2110–2117.
- Kawahara, Y. et al.** (2013). Improvement of the *Oryza sativa* Nipponbare reference

- genome using next generation sequence and optical map data. *Rice* **6** (1): 4.
- Kawaide, H.** (2006). Biochemical and molecular analyses of gibberellin biosynthesis in fungi. *Biosci. Biotechnol. Biochem.* **70** (3): 583–590.
- Kerstetter, R.A., Bollman, K., Taylor, R.A., Bomblied, K., and Poethig, R.S.** (2001). *KANADI* regulates organ polarity in *Arabidopsis*. *Nature* **411** (6838): 706–709.
- Kirbis, A., Waller, M., Ricca, M., Bont, Z., Neubauer, A., Goffinet, B., and Szövényi, P.** (2020). Transcriptional landscapes of divergent sporophyte development in two mosses, *Physcomitrium (Physcomitrella) patens* and *Funaria hygrometrica*. *Front. Plant Sci.* **11**: 747.
- Koide, E., Suetsugu, N., Iwano, M., Gotoh, E., Nomura, Y., Stolze, S.C., Nakagami, H., Kohchi, T., and Nishihama, R.** (2020). Regulation of photosynthetic carbohydrate metabolism by a Raf-like kinase in the liverwort *Marchantia polymorpha*. *Plant Cell Physiol.* **61** (3): 631–643.
- Koornneef, M. and van der Veen, J.H.** (1980). Induction and analysis of gibberellin sensitive mutants in *Arabidopsis thaliana* (L.) Heynh. *Theor. Appl. Genet.* **58** (6): 257–263.
- Kubota, A., Ishizaki, K., Hosaka, M., and Kohchi, T.** (2013). Efficient *Agrobacterium*-mediated transformation of the liverwort *Marchantia polymorpha* using regenerating thalli. *Biosci. Biotechnol. Biochem.* **77** (1): 167–172.
- Kubota, A., Kita, S., Ishizaki, K., Nishihama, R., Yamato, K.T., and Kohchi, T.** (2014). Co-option of a photoperiodic growth-phase transition system during land plant evolution. *Nat. Commun.* **5**: 1–9.
- Kumar, S. et al.** (2016). Molecular diversity of terpene synthases in the liverwort *Marchantia polymorpha*. *Plant Cell* **28** (10): 2632–2650.
- Küpers, J.J. et al.** (2023). Local light signaling at the leaf tip drives remote differential petiole growth through auxin-gibberellin dynamics. *Curr. Biol.* **33** (1): 75–85.
- Kurihara, D., Mizuta, Y., Nagahara, S., and Higashiyama, T.** (2021). ClearSeeAlpha: Advanced optical clearing for whole-plant imaging. *Plant Cell Physiol.* **62** (8): 1302–1310.
- Kurosawa, E.** (1926). 稻馬鹿苗病菌の分泌物に関する実験的研究（予報） [Experimental studies on the nature of the substance excreted by the “bakanae” fungus]. 台湾博物学会会報 *Trans. Nat. Hist. Soc. Formosa* **16** (87): 213–227.
- Lang, D. et al.** (2018). The *Physcomitrella patens* chromosome-scale assembly reveals moss genome structure and evolution. *Plant J.* **93** (3): 515–533.
- Lange, T.** (1994). Purification and partial amino-acid sequence of gibberellin 20-oxidase from *Cucurbita maxima* L. endosperm. *Planta* **195** (1): 108–115.
- Lange, T., Hedden, P., and Graebe, J.E.** (1994). Expression cloning of a gibberellin 20-oxidase, a multifunctional enzyme involved in gibberellin biosynthesis. *Proc. Natl. Acad. Sci. U. S. A.* **91** (18): 8552–8556.
- Lange, T., Krämer, C., and Pimenta Lange, M.J.** (2020). The class III gibberellin 2-oxidases AtGA2ox9 and AtGA2ox10 contribute to cold stress tolerance and fertility.

- Plant Physiol. **184** (1): 478–486.
- Lee, J.W. and Kim, G.H.** (2019). Red and far-red regulation of filament movement correlates with the expression of phytochrome and *FHY1* genes in *Spirogyra varians* (Zygnematales, Streptophyta). J. Phycol. **55** (3): 688–699.
- Leebens-Mack, J.H. et al.** (2019). One thousand plant transcriptomes and the phylogenomics of green plants. Nature **574** (7780): 679–685.
- Leivar, P. and Monte, E.** (2014). PIFs: Systems integrators in plant development. Plant Cell **26** (1): 56–78.
- Lester, D.R., Ross, J.J., Davies, P.J., and Reid, J.B.** (1997). Mendel's stem length gene (*Le*) encodes a gibberellin 3 β -hydroxylase. Plant Cell **9** (8): 1435–1443.
- Lester, D.R., Ross, J.J., Smith, J.J., Elliott, R.C., and Reid, J.B.** (1999). Gibberellin 2-oxidation and the *SLN* gene of *Pisum sativum*. Plant J. **19** (1): 65–73.
- Li, F.-W. et al.** (2020a). *Anthoceros* genomes illuminate the origin of land plants and the unique biology of hornworts. Nat. Plants **6** (3): 259–272.
- Li, F.-W. et al.** (2018). Fern genomes elucidate land plant evolution and cyanobacterial symbioses. Nat. Plants **4** (7): 460–472.
- Li, F.-W., Melkonian, M., Rothfels, C.J., Villarreal, J.C., Stevenson, D.W., Graham, S.W., Wong, G.K.-S., Pryer, K.M., and Mathews, S.** (2015). Phytochrome diversity in green plants and the origin of canonical plant phytochromes. Nat. Commun. **6** (1): 7852.
- Li, J., Li, G., Wang, H., and Wang Deng, X.** (2011). Phytochrome signaling mechanisms. Arab. Book **9**: e0148.
- Li, W., Liu, S.-W., Ma, J.-J., Liu, H.-M., Han, F.-X., Li, Y., and Niu, S.-H.** (2020b). Gibberellin signaling is required for far-red light-induced shoot elongation in *Pinus tabulaeformis* seedlings. Plant Physiol. **182** (1): 658–668.
- Lim, S., Park, J., Lee, N., Jeong, J., Toh, S., Watanabe, A., Kim, J., Kang, H., Kim, D.H., Kawakami, N., and Choi, G.** (2013). ABA-INSENSITIVE3, ABA-INSENSITIVE5, and DELLAs interact to activate the expression of *SOMNUS* and other high-temperature-inducible genes in imbibed seeds in *Arabidopsis*. Plant Cell **25** (12): 4863–4878.
- Linde, A.-M., Singh, S., Bowman, J.L., Eklund, M., Cronberg, N., and Lagercrantz, U.** (2023). Genome evolution in plants: Complex thalloid liverworts (Marchantiopsida). Genome Biol. Evol. **15** (3): evad014.
- Liu, H. et al.** (2021). The nearly complete genome of *Ginkgo biloba* illuminates gymnosperm evolution. Nat. Plants **7** (6): 748–756.
- Lou, H., Song, L., Li, X., Zi, H., Chen, W., Gao, Y., Zheng, S., Fei, Z., Sun, X., and Wu, J.** (2023). The *Torreya grandis* genome illuminates the origin and evolution of gymnosperm-specific sciadonic acid biosynthesis. Nat. Commun. **14** (1): 1315.
- Love, M.I., Huber, W., and Anders, S.** (2014). Moderated estimation of fold change and dispersion for RNA-seq data with DESeq2. Genome Biol. **15** (12): 550.
- de Lucas, M., Davière, J.-M., Rodríguez-Falcón, M., Pontin, M., Iglesias-Pedraz, J.M.,**

- Lorrain, S., Fankhauser, C., Blázquez, M.A., Titarenko, E., and Prat, S.** (2008). A molecular framework for light and gibberellin control of cell elongation. *Nature* **451** (7177): 480–484.
- MacMillan, J.** (2001). Occurrence of gibberellins in vascular plants, fungi, and bacteria. *J. Plant Growth Regul.* **20** (4): 387–442.
- MacMillan, J. and Suter, P.** (1958). The occurrence of gibberellin A₁ in higher plants: isolation from the seed of runner bean (*Phaseolus multiflorus*). *Naturwissenschaften* **45** (2): 46–46.
- Magome, H., Nomura, T., Hanada, A., Takeda-Kamiya, N., Ohnishi, T., Shinma, Y., Katsumata, T., Kawaide, H., Kamiya, Y., and Yamaguchi, S.** (2013). *CYP714B1* and *CYP714B2* encode gibberellin 13-oxidases that reduce gibberellin activity in rice. *Proc. Natl. Acad. Sci. U. S. A.* **110** (5): 1947–1952.
- Mao, L. et al.** (2020). Genomic evidence for convergent evolution of gene clusters for momilactone biosynthesis in land plants. *Proc. Natl. Acad. Sci. U. S. A.* **117** (22): 12472–12480.
- Marchant, D.B. et al.** (2022). Dynamic genome evolution in a model fern. *Nat. Plants* **8** (9): 1038–1051.
- Marín-de la Rosa, N. et al.** (2015). Genome wide binding site analysis reveals transcriptional coactivation of cytokinin-responsive genes by DELLA proteins. *PLoS Genet.* **11** (7): 1–20.
- Marshall, S.D.G., Putterill, J.J., Plummer, K.M., and Newcomb, R.D.** (2003). The carboxylesterase gene family from *Arabidopsis thaliana*. *J. Mol. Evol.* **57** (5): 487–500.
- Martin, D.N., Proebsting, W.M., and Hedden, P.** (1999). The *SLENDER* gene of pea encodes a gibberellin 2-oxidase. *Plant Physiol.* **121** (3): 775–781.
- Minh, B.Q., Schmidt, H.A., Chernomor, O., Schrempf, D., Woodhams, M.D., von Haeseler, A., and Lanfear, R.** (2020). IQ-TREE 2: New models and efficient methods for phylogenetic inference in the genomic era. *Mol. Biol. Evol.* **37** (5): 1530–1534.
- Miyazaki, S., Hara, M., Ito, S., Tanaka, K., Asami, T., Hayashi, K., Kawaide, H., and Nakajima, M.** (2018). An ancestral gibberellin in a moss *Physcomitrella patens*. *Mol. Plant* **11** (8): 1097–1100.
- Miyazaki, S., Katsumata, T., Natsume, M., and Kawaide, H.** (2011). The CYP701B1 of *Physcomitrella patens* is an *ent*-kaurene oxidase that resists inhibition by uniconazole-P. *FEBS Lett.* **585** (12): 1879–1883.
- Miyazaki, S., Kimura, H., Natsume, M., Asami, T., Hayashi, K., Kawaide, H., and Nakajima, M.** (2015a). Analysis of *ent*-kaurenoic acid by ultra-performance liquid chromatography-tandem mass spectrometry. *Biochem. Biophys. Rep.* **2**: 103–107.
- Miyazaki, S., Nakajima, M., and Kawaide, H.** (2015b). Hormonal diterpenoids derived from *ent*-kaurenoic acid are involved in the blue-light avoidance response of *Physcomitrella patens*. *Plant Signal. Behav.* **10** (2): 1–4.
- Miyazaki, S., Toyoshima, H., Natsume, M., Nakajima, M., and Kawaide, H.** (2014). Blue-light irradiation up-regulates the *ent*-kaurene synthase gene and affects the avoidance response of protonemal growth in *Physcomitrella patens*. *Planta* **240** (1): 117–

- Moritz, T.** (1995). Biological activity, identification and quantification of gibberellins in seedlings of Norway spruce (*Picea abies*) grown under different photoperiods. *Physiol. Plant.* **95** (1): 67–72.
- Moritz, T., Philipson, J.J., and Odén, P.C.** (1989). Detection and identification of gibberellins in Sitka spruce (*Picea sitchensis*) of different ages and coning ability by bioassay, radioimmunoassay and gas chromatography–mass spectrometry. *Physiol. Plant.* **75** (3): 325–332.
- Motohashi, K.** (2015). A simple and efficient seamless DNA cloning method using SLiCE from *Escherichia coli* laboratory strains and its application to SLiP site-directed mutagenesis. *BMC Biotechnol.* **15** (1): 47.
- Murase, K., Hirano, Y., Sun, T., and Hakoshima, T.** (2008). Gibberellin-induced DELLA recognition by the gibberellin receptor *GID1*. *Nature* **456** (7221): 459–463.
- Nagashima, F., Kasai, W., Kondoh, M., Fujii, M., Watanabe, Y., Braggins, J.E., and Asakawa, Y.** (2003). New *ent*-kaurene-type diterpenoids possessing cytotoxicity from the New Zealand liverwort *Jungermannia* species. *Chem. Pharm. Bull. (Tokyo)* **51** (10): 1189–1192.
- Nagatani, A., Reed, J.W., and Chory, J.** (1993). Isolation and initial characterization of *Arabidopsis* mutants that are deficient in phytochrome A. *Plant Physiol.* **102** (1): 269–277.
- Nakajima, M. et al.** (2006). Identification and characterization of *Arabidopsis* gibberellin receptors. *Plant J.* **46** (5): 880–889.
- Nelson, D.R.** (2018). Cytochrome P450 diversity in the tree of life. *Biochim. Biophys. Acta BBA - Proteins Proteomics* **1866** (1): 141–154.
- Nelson, D.R.** (2006). Cytochrome P450 nomenclature, 2004. In *Cytochrome P450 Protocols*, I.R. Phillips and E.A. Shephard, eds, *Methods in Molecular Biology*. (Humana Press: Totowa, NJ), pp. 1–10.
- Nett, R.S., Montanares, M., Marcassa, A., Lu, X., Nagel, R., Charles, T.C., Hedden, P., Rojas, M.C., and Peters, R.J.** (2017). Elucidation of gibberellin biosynthesis in bacteria reveals convergent evolution. *Nat. Chem. Biol.* **13** (1): 69–74.
- Ni, M., Tepperman, J.M., and Quail, P.H.** (1999). Binding of phytochrome B to its nuclear signalling partner PIF3 is reversibly induced by light. *Nature* **400** (6746): 781–784.
- Ni, M., Tepperman, J.M., and Quail, P.H.** (1998). PIF3, a phytochrome-interacting factor necessary for normal photoinduced signal transduction, is a novel basic helix-loop-helix protein. *Cell* **95** (5): 657–667.
- Ninnemann, H. and Halbsguth, W.** (1965). Rolle des Phytochroms beim Etiolement von *Marchantia polymorpha*. *Naturwissenschaften* **52** (5): 110–111.
- Nishihama, R., Ishizaki, K., Hosaka, M., Matsuda, Y., Kubota, A., and Kohchi, T.** (2015). Phytochrome-mediated regulation of cell division and growth during regeneration and sporeling development in the liverwort *Marchantia polymorpha*. *J. Plant Res.* **128** (3): 407–421.

- Nomura, T., Magome, H., Hanada, A., Takeda-Kamiya, N., Mander, L.N., Kamiya, Y., and Yamaguchi, S.** (2013). Functional analysis of *Arabidopsis* CYP714A1 and CYP714A2 reveals that they are distinct gibberellin modification enzymes. *Plant Cell Physiol.* **54** (11): 1837–1851.
- Nozaki, H., Hayashi, K.I., Okuda, K., Kuyama, F., Ono, K., and Matsuo, A.** (2007). *ent*-Kaurane-type diterpenoids from a cell suspension culture of the liverwort *Jungermannia subulata*. *Planta Med.* **73** (7): 689–695.
- Nystedt, B. et al.** (2013). The Norway spruce genome sequence and conifer genome evolution. *Nature* **497** (7451): 579–584.
- Ogawa, M., Hanada, A., Yamauchi, Y., Kuwahara, A., Kamiya, Y., and Yamaguchi, S.** (2003). Gibberellin biosynthesis and response during *Arabidopsis* seed germination. *Plant Cell* **15** (7): 1591–1604.
- Oh, E., Yamaguchi, S., Hu, J., Yusuke, J., Jung, B., Paik, I., Lee, H.-S., Sun, T., Kamiya, Y., and Choi, G.** (2007). PIL5, a phytochrome-interacting bHLH protein, regulates gibberellin responsiveness by binding directly to the *GAI* and *RGA* promoters in *Arabidopsis* seeds. *Plant Cell* **19** (4): 1192–1208.
- Oh, E., Yamaguchi, S., Kamiya, Y., Bae, G., Chung, W.I., and Choi, G.** (2006). Light activates the degradation of PIL5 protein to promote seed germination through gibberellin in *Arabidopsis*. *Plant J.* **47** (1): 124–139.
- Okabe, M.** (2022). 質量分析法を用いた苔類ゼニゴケにおけるジベレリン類縁化合物の探索 (Bachelor's thesis, Kyoto University).
- Okada, K., Ito, T., Fukazawa, J., and Takahashi, Y.** (2017). Gibberellin induces an increase in cytosolic Ca²⁺ via a DELLA-independent signaling pathway. *Plant Physiol.* **175** (4): 1536–1542.
- Otto, K.-R. and Halbsguth, W.** (1976). Die Förderung der Bildung von Primärrhizoiden an Brutkörpern von *Marchantia polymorpha* L. durch Licht und IES [Stimulation of primary rhizoid formation on gemmae of *Marchantia polymorpha* L. as caused by light and IAA]. *Z. Für Pflanzenphysiol.* **80** (3): 197–205.
- Parks, B.M. and Quail, P.H.** (1993). *hy8*, a new class of *Arabidopsis* long hypocotyl mutants deficient in functional phytochrome A. *Plant Cell* **5** (1): 39–48.
- Peng, J., Carol, P., Richards, D.E., King, K.E., Cowling, R.J., Murphy, G.P., and Harberd, N.P.** (1997). The *Arabidopsis* *GAI* gene defines a signaling pathway that negatively regulates gibberellin responses. *Genes Dev.* **11** (23): 3194–205.
- Phillips, A.L., Ward, D.A., Uknes, S., Appleford, N.E.J., Lange, T., Huttly, A.K., Caskin, P., Craebe, J.E., and Hedden, P.** (1995). Isolation and expression of three gibberellin 20-oxidase cDNA clones from *Arabidopsis*. *Plant Physiol.* **108** (3): 1049–1057.
- Phinney, B.O.** (1956). Growth response of single-gene dwarf mutants in maize to gibberellic acid. *Proc. Natl. Acad. Sci. U. S. A.* **42** (4): 185–189.
- Phokas, A., Meyberg, R., Briones-Moreno, A., Hernandez-Garcia, J., Wadsworth, P.T., Vesty, E.F., Blazquez, M.A., Rensing, S.A., and Coates, J.C.** (2023). DELLA proteins regulate spore germination and reproductive development in *Physcomitrium*

- patens*. *New Phytol.* **238** (2): 654–672.
- Pluthero, F.G.** (1993). Rapid purification of high-activity Taq DNA polymerase. *Nucleic Acids Res.* **21** (20): 4850–4851.
- Puttick, M.N., Morris, J.L., Williams, T.A., Cox, C.J., Edwards, D., Kenrick, P., Pressel, S., Wellman, C.H., Schneider, H., Pisani, D., and Donoghue, P.C.J.** (2018). The interrelationships of land plants and the nature of the ancestral embryophyte. *Curr. Biol.* **28** (5): 733–745.
- Rahmatpour, N., Kuo, L.-Y., Kang, J., Herman, E., Lei, L., Li, M., Srinivasan, S., Zipper, R., Wolniak, S.M., Delwiche, C.F., Mount, S., and Li, F.-W.** (2023). Analyses of *Marsilea vestita* genome and transcriptomes do not support widespread intron retention during spermatogenesis. *New Phytol.* **237** (5): 1490–1494.
- Reed, J.W., Nagatani, A., Elich, T.D., Fagan, M., and Chory, J.** (1994). Phytochrome A and phytochrome B have overlapping but distinct functions in *Arabidopsis* development. *Plant Physiol.* **104** (4): 1139–1149.
- Regnault, T., Davière, J.-M., Wild, M., Sakvarelidze-Achard, L., Heintz, D., Carrera Bergua, E., Lopez Diaz, I., Gong, F., Hedden, P., and Achard, P.** (2015). The gibberellin precursor GA₁₂ acts as a long-distance growth signal in *Arabidopsis*. *Nat. Plants* **1** (6): 15073.
- Reid, J.B., Botwright, N.A., Smith, J.J., O’Neill, D.P., and Kerckhoffs, L.H.J.** (2002). Control of gibberellin levels and gene expression during de-etiolation in pea. *Plant Physiol.* **128** (2): 734–741.
- Rich, M.K. et al.** (2021). Lipid exchanges drove the evolution of mutualism during plant terrestrialization. *Science* **372** (6544): 864–868.
- Rockwell, N.C., Duanmu, D., Martin, S.S., Bachy, C., Price, D.C., Bhattacharya, D., Worden, A.Z., and Lagarias, J.C.** (2014). Eukaryotic algal phytochromes span the visible spectrum. *Proc. Natl. Acad. Sci. U. S. A.* **111** (10): 3871–3876.
- Rojas, M.C., Hedden, P., Gaskin, P., and Tudzynski, B.** (2001). The *P450-1* gene of *Gibberella fujikuroi* encodes a multifunctional enzyme in gibberellin biosynthesis. *Proc. Natl. Acad. Sci. U. S. A.* **98** (10): 5838–5843.
- Sakamoto, T. et al.** (2004). An overview of gibberellin metabolism enzyme genes and their related mutants in rice. *Plant Physiol.* **134** (4): 1642–1653.
- Sakamoto, Y., Ishimoto, A., Sakai, Y., Sato, M., Nishihama, R., Abe, K., Sano, Y., Furuichi, T., Tsuji, H., Kohchi, T., and Matsunaga, S.** (2022). Improved clearing method contributes to deep imaging of plant organs. *Commun. Biol.* **5** (1): 12.
- Salic, A. and Mitchison, T.J.** (2008). A chemical method for fast and sensitive detection of DNA synthesis *in vivo*. *Proc. Natl. Acad. Sci. U. S. A.* **105** (7): 2415–2420.
- Sasaki, A., Itoh, H., Gomi, K., Ueguchi-Tanaka, M., Ishiyama, K., Kobayashi, M., Jeong, D.H., An, G., Kitano, H., Ashikari, M., and Matsuoka, M.** (2003). Accumulation of phosphorylated repressor for gibberellin signaling in an F-box mutant. *Science* **299** (5614): 1896–1898.
- Sauret-Güeto, S., Calder, G., and Harberd, N.P.** (2012). Transient gibberellin application promotes *Arabidopsis thaliana* hypocotyl cell elongation without maintaining transverse

- orientation of microtubules on the outer tangential wall of epidermal cells. *Plant J.* **69** (4): 628–639.
- Schindelin, J. et al.** (2012). Fiji: an open-source platform for biological-image analysis. *Nat. Methods* **9** (7): 676–682.
- Schmidt, U., Weigert, M., Broaddus, C., and Myers, G.** (2018). Cell Detection with Star-Convex Polygons. In *Medical Image Computing and Computer Assisted Intervention – MICCAI 2018*, A.F. Frangi, J.A. Schnabel, C. Davatzikos, C. Alberola-López, and G. Fichtinger, eds, Lecture Notes in Computer Science. (Springer International Publishing: Cham), pp. 265–273.
- Schneller, J.J.** (2008). Antheridiogens. In *Biology and Evolution of Ferns and Lycophytes*, T.A. Ranker and C.H. Haufler, eds (Cambridge University Press: New York), pp. 134–158.
- Scott, A.D. et al.** (2020). A reference genome sequence for giant sequoia. *G3 GenesGenomesGenetics* **10** (11): 3907–3919.
- Sessa, G., Carabelli, M., Sassi, M., Ciolfi, A., Possenti, M., Mitterpergher, F., Becker, J., Morelli, G., and Ruberti, I.** (2005). A dynamic balance between gene activation and repression regulates the shade avoidance response in *Arabidopsis*. *Genes Dev.* **19** (23): 2811–2815.
- Sharrock, R.A. and Quail, P.H.** (1989). Novel phytochrome sequences in *Arabidopsis thaliana*: structure, evolution, and differential expression of a plant regulatory photoreceptor family. *Genes Dev.* **3** (11): 1745–1757.
- Shimada, A., Ueguchi-Tanaka, M., Nakatsu, T., Nakajima, M., Naoe, Y., Ohmiya, H., Kato, H., and Matsuoka, M.** (2008). Structural basis for gibberellin recognition by its receptor GID1. *Nature* **456** (7221): 520–523.
- Shimamura, M.** (2016). *Marchantia polymorpha*: Taxonomy, phylogeny and morphology of a model system. *Plant Cell Physiol.* **57** (2): 230–256.
- Shinomura, T., Nagatani, A., Chory, J., and Furuya, M.** (1994). The induction of seed germination in *Arabidopsis thaliana* is regulated principally by phytochrome B and secondarily by phytochrome A. *Plant Physiol.* **104**: 363–371.
- Shinomura, T., Nagatani, A., Hanzawa, H., Kubota, M., Watanabe, M., and Furuya, M.** (1996). Action spectra for phytochrome A- and B-specific photoinduction of seed germination in *Arabidopsis thaliana*. *Proc. Natl. Acad. Sci. U. S. A.* **93** (15): 8129–8133.
- Silva, A.T., Gao, B., Fisher, K.M., Mishler, B.D., Ekwealor, J.T.B., Stark, L.R., Li, X., Zhang, D., Bowker, M.A., Brinda, J.C., Coe, K.K., and Oliver, M.J.** (2021). To dry perchance to live: Insights from the genome of the desiccation-tolerant biocrust moss *Syntrichia caninervis*. *Plant J.* **105** (5): 1339–1356.
- Silverstone, A.L., Ciampaglio, C.N., and Sun, T.** (1998). The *Arabidopsis RGA* gene encodes a transcriptional regulator repressing the gibberellin signal transduction pathway. *Plant Cell* **10** (2): 155–169.
- Sousa, F., Foster, P.G., Donoghue, P.C.J., Schneider, H., and Cox, C.J.** (2019). Nuclear protein phylogenies support the monophyly of the three bryophyte groups (Bryophyta Schimp.). *New Phytol.* **222** (1): 565–575.

- Sponsel, V.M.** (2016). Signal achievements in gibberellin research: The second half-century. In *The Gibberellins*, P. Hedden and S.G. Thomas, eds, Annual Plant Reviews. (John Wiley & Sons, Ltd: Chichester,UK), pp. 1–36.
- Streubel, S., Deiber, S., Rötzer, J., Mosiolek, M., Jandrasits, K., and Dolan, L.** (2023). Meristem dormancy in *Marchantia polymorpha* is regulated by a liverwort-specific miRNA and a clade III SPL gene. *Curr. Biol.* **33** (4): 660–674.
- Su, D., Yang, L., Shi, X., Ma, X., Zhou, X., Hedges, S.B., and Zhong, B.** (2021). Large-scale phylogenomic analyses reveal the monophyly of bryophytes and neoproterozoic origin of land plants. *Mol. Biol. Evol.* **38** (8): 3332–3344.
- Sugano, S.S., Nishihama, R., Shirakawa, M., Takagi, J., Matsuda, Y., Ishida, S., Shimada, T., Hara-Nishimura, I., Osakabe, K., and Kohchi, T.** (2018). Efficient CRISPR/Cas9-based genome editing and its application to conditional genetic analysis in *Marchantia polymorpha*. *PLoS ONE* **13** (10): e0205117.
- Sugano, S.S., Shirakawa, M., Takagi, J., Matsuda, Y., Shimada, T., Hara-Nishimura, I., and Kohchi, T.** (2014). CRISPR/Cas9-mediated targeted mutagenesis in the liverwort *Marchantia polymorpha* L. *Plant Cell Physiol.* **55** (3): 475–481.
- Sun, T. and Kamiya, Y.** (1994). The Arabidopsis *GAI* locus encodes the cyclase *ent*-kaurene synthetase A of gibberellin biosynthesis. *Plant Cell* **6** (10): 1509–1518.
- Talon, M., Koornneef, M., and Zeevaart, J.A.D.** (1990). Endogenous gibberellins in *Arabidopsis thaliana* and possible steps blocked in the biosynthetic pathways of the semidwarf *ga4* and *ga5* mutants. *Proc. Natl. Acad. Sci. U. S. A.* **87** (20): 7983–7987.
- Tanaka, J., Yano, K., Aya, K., Hirano, K., Takehara, S., Koketsu, E., Ordonio, R.L., Park, S.-H., Nakajima, M., Ueguchi-Tanaka, M., and Matsuoka, M.** (2014). Antheridiogen determines sex in ferns via a spatiotemporally split gibberellin synthesis pathway. *Science* **346** (6208): 469–473.
- Thomas, S.G., Phillips, A.L., and Hedden, P.** (1999). Molecular cloning and functional expression of gibberellin 2-oxidases, multifunctional enzymes involved in gibberellin deactivation. *Proc. Natl. Acad. Sci. U. S. A.* **96** (8): 4698–4703.
- Toyomasu, T., Yamane, H., Yamaguchi, I., Murofushi, N., Takahashi, N., and Inoue, Y.** (1992). Control by light of hypocotyl elongation and levels of endogenous gibberellins in seedlings of *Lactuca sativa* L. *Plant Cell Physiol.* **33** (6): 695–701.
- Tudzynski, B., Hedden, P., Carrera, E., and Gaskin, P.** (2001). The *P450-4* Gene of *Gibberella fujikuroi* encodes *ent*-kaurene oxidase in the gibberellin biosynthesis pathway. *Appl. Environ. Microbiol.* **67** (8): 3514–3522.
- Tudzynski, B. and Hölter, K.** (1998). Gibberellin biosynthetic pathway in *Gibberella fujikuroi*: Evidence for a gene cluster. *Fungal Genet. Biol.* **25** (3): 157–170.
- Tudzynski, B., Studt, L., and Rojas, M.C.** (2016). Gibberellins in fungi, bacteria and lower plants: biosynthesis, function and evolution. In *The Gibberellins*, P. Hedden and S.G. Thomas, eds, Annual Plant Reviews. (John Wiley & Sons, Ltd), pp. 121–152.
- Tuskan, G.A. et al.** (2006). The genome of black cottonwood, *Populus trichocarpa* (Torr. & Gray). *Science* **313** (5793): 1596–1604.
- Ueguchi-Tanaka, M., Ashikari, M., Nakajima, M., Itoh, H., Katoh, E., Kobayashi, M.,**

- Chow, T., Hsing, Y.C., Kitano, H., Yamaguchi, I., and Matsuoka, M.** (2005). *GIBBERELLIN INSENSITIVE DWARF1* encodes a soluble receptor for gibberellin. *Nature* **437** (7059): 693–698.
- Ulijasz, A.T. and Vierstra, R.D.** (2011). Phytochrome structure and photochemistry: Recent advances toward a complete molecular picture. *Curr. Opin. Plant Biol.* **14** (5): 498–506.
- Urbanova, T. and Leubner-Metzger, G.** (2016). Gibberellins and seed germination. In *The Gibberellins*, P. Hedden and S.G. Thomas, eds, Annual Plant Reviews. (John Wiley & Sons, Ltd), pp. 253–284.
- Urrutia, O., Hedden, P., and Rojas, M.C.** (2001). Monooxygenases involved in GA₁₂ and GA₁₄ synthesis in *Gibberella fujikuroi*. *Phytochemistry* **56** (5): 505–511.
- Varbanova, M. et al.** (2007). Methylation of gibberellins by *Arabidopsis* GAMT1 and GAMT2. *Plant Cell* **19** (1): 32–45.
- Vesty, E.F. et al.** (2016). The decision to germinate is regulated by divergent molecular networks in spores and seeds. *New Phytol.* **211** (3): 952–966.
- Vogel, J.P. et al.** (2010). Genome sequencing and analysis of the model grass *Brachypodium distachyon*. *Nature* **463** (7282): 763–768.
- Wan, T. et al.** (2021). The *Welwitschia* genome reveals a unique biology underpinning extreme longevity in deserts. *Nat. Commun.* **12** (1): 4247.
- Wang, Q., Little, C.H.A., Moritz, T., and Odén, P.C.** (1996). Identification of endogenous gibberellins, and metabolism of tritiated and deuterated GA₄, GA₉ and GA₂₀, in Scots pine (*Pinus sylvestris*) shoots. *Physiol. Plant.* **97** (4): 764–771.
- Wenzel, C.L., Williamson, R.E., and Wasteneys, G.O.** (2000). Gibberellin-induced changes in growth anisotropy precede gibberellin-dependent changes in cortical microtubule orientation in developing epidermal cells of barley leaves. Kinematic and cytological studies on a gibberellin-responsive dwarf mutant, M489. *Plant Physiol.* **124** (2): 813–822.
- Wickell, D. et al.** (2021). Underwater CAM photosynthesis elucidated by *Isoetes* genome. *Nat. Commun.* **12** (1): 6348.
- Williams, J., Phillips, A.L., Gaskin, P., and Hedden, P.** (1998). Function and substrate specificity of the gibberellin 3 β -hydroxylase encoded by the *Arabidopsis* GA4 Gene. *Plant Physiol.* **117** (2): 559–563.
- Willige, B.C., Ghosh, S., Nill, C., Zourelidou, M., Dohmann, E.M.N., Maier, A., and Schwechheimer, C.** (2007). The DELLA domain of GA INSENSITIVE mediates the interaction with the GA INSENSITIVE DWARF1A gibberellin receptor of *Arabidopsis*. *Plant Cell* **19** (4): 1209–1220.
- Xiong, X. et al.** (2021). The *Taxus* genome provides insights into paclitaxel biosynthesis. *Nat. Plants* **7** (8): 1026–1036.
- Xu, S., Li, L., Luo, X., Chen, M., Tang, W., Zhan, L., Dai, Z., Lam, T.T., Guan, Y., and Yu, G.** (2022). Ggtree: A serialized data object for visualization of a phylogenetic tree and annotation data. *iMeta* **1** (4): e56.
- Yamaguchi, S., Smith, M.W., Brown, R.G.S., Kamiya, Y., and Sun Tai-ping** (1998a).

- Phytochrome regulation and differential expression of gibberellin 3 β -hydroxylase genes in germinating *Arabidopsis* seeds. *Plant Cell* **10** (12): 2115–2126.
- Yamaguchi, S., Sun, T., Kawaide, H., and Kamiya, Y.** (1998b). The *GA2* locus of *Arabidopsis thaliana* encodes *ent*-kaurene synthase of gibberellin biosynthesis. *Plant Physiol.* **116** (4): 1271–1278.
- Yamane, H.** (1998). Fern antheridiogens. *Int. Rev. Cytol.* **184**: 1–32.
- Yamane, H., Fujioka, S., Spray, C.R., Macmillan, J., Gaskin, P., and Takahashi, N.** (1988). Endogenous gibberellins from sporophytes of two tree ferns, *Cibotium glaucum* and *Dicksonia antarctica*. *Plant Physiol.* **86**: 857–862.
- Yamane, H., Takahashi, N., Takeno, K., and Furuya, M.** (1979). Identification of gibberellin A₉ methyl ester as a natural substance regulating formation of reproductive organs in *Lygodium japonicum*. *Planta* **147** (3): 251–256.
- Yamane, H., Yamaguchi, I., Kobayashi, M., Takahashi, M., Sato, Y., Takahashi, N., Iwatsuki, K., Phinney, B.O., Spray, C.R., Gaskin, P., and MacMillan, J.** (1985). Identification of ten gibberellins from sporophytes of the tree fern, *Cyathea australis*. *Plant Physiol.* **78** (4): 899–903.
- Yamaoka, S. et al.** (2018). Generative cell specification requires transcription factors evolutionarily conserved in land plants. *Curr. Biol.* **28** (3): 479–486.e5.
- Yamauchi, T., Oyama, N., Yamane, H., Murofushi, N., Schraudolf, H., Pour, M., Furber, M., and Mander, L.N.** (1996). Identification of antheridiogens in *Lygodium circinnatum* and *Lygodium flexuosum*. *Plant Physiol.* **111** (3): 741–745.
- Yasumura, Y., Crumpton-Taylor, M., Fuentes, S., and Harberd, N.P.** (2007). Step-by-step acquisition of the gibberellin-DELLA growth-regulatory mechanism during land-plant evolution. *Curr. Biol.* **17** (14): 1225–1230.
- Yoshida, H. et al.** (2014). DELLA protein functions as a transcriptional activator through the DNA binding of the INDETERMINATE DOMAIN family proteins. *Proc. Natl. Acad. Sci. U. S. A.* **111** (21): 7861–7866.
- Yoshida, H. et al.** (2018). Evolution and diversification of the plant gibberellin receptor *GID1*. *Proc. Natl. Acad. Sci. U. S. A.* **115** (33): E7844–E7853.
- Yoshida, H., Takehara, S., Mori, M., Ordonio, R.L., and Matsuoka, M.** (2020). Evolution of GA metabolic enzymes in land plants. *Plant Cell Physiol.* **61** (11): 1919–1934.
- Yu, G.** (2022). Data integration, manipulation and visualization of phylogenetic trees (Chapman and Hall/CRC: New York).
- Yu, G.** (2020). Using ggtree to visualize data on tree-like structures. *Curr. Protoc. Bioinforma.* **69** (1): e96.
- Yu, G., Lam, T.T.-Y., Zhu, H., and Guan, Y.** (2018). Two methods for mapping and visualizing associated data on phylogeny using ggtree. *Mol. Biol. Evol.* **35** (12): 3041–3043.
- Yu, G., Smith, D.K., Zhu, H., Guan, Y., and Lam, T.T.-Y.** (2017). Ggtree: An R package for visualization and annotation of phylogenetic trees with their covariates and other associated data. *Methods Ecol. Evol.* **8** (1): 28–36.

- Yu, H., Ito, T., Zhao, Y., Peng, J., Kumar, P., and Meyerowitz, E.M.** (2004). Floral homeotic genes are targets of gibberellin signaling in flower development. *Proc. Natl. Acad. Sci. U. S. A.* **101** (20): 7827–7832.
- Yu, J. et al.** (2020). Draft genome of the aquatic moss *Fontinalis antipyretica* (Fontinalaceae, Bryophyta). *Gigabyte* **2020**: 1–9.
- Yu, J.-G., Tang, J.-Y., Wei, R., Lan, M.-F., Xiang, R.-C., Zhang, X.-C., and Xiang, Q.-P.** (2023). The first homosporous lycophyte genome revealed the association between the recent dynamic accumulation of LTR-RTs and genome size variation. *Plant Mol. Biol.* **112** (6): 325–340.
- Zentella, R., Zhang, Z.-L., Park, M., Thomas, S.G., Endo, A., Murase, K., Fleet, C.M., Jikumaru, Y., Nambara, E., Kamiya, Y., and Sun, T.** (2007). Global analysis of DELLA direct targets in early gibberellin signaling in *Arabidopsis*. *Plant Cell* **19** (10): 3037–3057.
- Zhang, J. et al.** (2020a). The hornwort genome and early land plant evolution. *Nat. Plants* **6** (2): 107–118.
- Zhang, L. et al.** (2020b). The water lily genome and the early evolution of flowering plants. *Nature* **577** (7788): 79–84.
- Zhang, Y., Werling, U., and Edlmann, W.** (2012). SLiCE: A novel bacterial cell extract-based DNA cloning method. *Nucleic Acids Res.* **40** (8): 1–10.
- Zhu, T., Sun, C., Liu, X., Zhang, J., Hou, X., Ni, R., Zhang, J., Cheng, A., and Lou, H.** (2023). Interaction of PKR with STCS1: An indispensable step in the biosynthesis of lunularic acid in *Marchantia polymorpha*. *New Phytol.* **237** (2): 515–531.
- Zhu, Y. et al.** (2006). *ELONGATED UPPERMOST INTERNODE* encodes a cytochrome P450 monooxygenase that epoxidizes gibberellins in a novel deactivation reaction in rice. *Plant Cell* **18** (2): 442–456.

Acknowledgments

It has been a long but enlightening journey for me to accomplish this research over the past years at the Laboratory of Plant Molecular Biology, Graduate School of Biostudies, Kyoto University. The path to completion has been paved with the great help and assistance of numerous people to whom I owe a debt of gratitude. First and foremost, I would like to express my deepest appreciation to my advisor, Dr. Takayuki Kohchi, for his continuous support, patience, and invaluable guidance throughout the research. I would like to extend my heartfelt thanks to Dr. Ryuichi Nishihama, Dr. Shohei Yamaoka and Dr. Yoshihiro Yoshitake, who provided insightful feedback and experimental guidance over the years. I would like to thank my sub-supervisors, Dr. Takashi Araki and Dr. Hideya Fukuzawa, for discussions and suggestions.

My sincere thanks go to all the collaborators for their invaluable help on the project. I would like to thank Dr. Toshiaki Ishida, Dr. Kiyoshi Mashiguchi and Dr. Shinjiro Yamaguchi from the Chemical Institute of Kyoto University, Dr. Sho Miyazaki from the Tokyo University of Agriculture and Technology, as well as Dr. Masatoshi Nakajima from the University of Tokyo for their help on the analysis of endogenous GAs in *M. polymorpha*. I am grateful to Ms. Wakako Fukuda and Dr. Hiroshi Kawaide from the Tokyo University of Agriculture and Technology for the enzymatic assay of KO and KAO homologs in the yeast.

I would like to express my most sincere appreciation to people who contributed to the work. Dr. Keisuke Inoue conceptualized the research with initial data. Mr. Ryunosuke Kusunoki constructed several plasmids and confirmed the phenotype of several mutants. Ms. Maiko Okabe performed all the analysis on endogenous GA in *M. polymorpha* that was pivotal in advancing this research. I gratefully acknowledge the technical support from Dr. Takefumi Kondo and Ms. Yukari Sando on RNA-sequencing, and Dr. Megumi Iwano on the help with confocal microscopy.

Lastly, but certainly not least, I wish to express my gratitude to all laboratory members for communication, support and help with experiments. Also, I would like to thank my family and friends, who have always been a support to my life and research.

This thesis is based on material contained in the following research paper.

Rui Sun, Maiko Okabe, Sho Miyazaki, Toshiaki Ishida, Kiyoshi Mashiguchi, Keisuke Inoue, Yoshihiro Yoshitake, Shohei Yamaoka, Ryuichi Nishihama, Hiroshi Kawaide, Masatoshi Nakajima, Shinjiro Yamaguchi, Takayuki Kohchi

Biosynthesis of gibberellin-related compounds modulates far-red light responses in the liverwort *Marchantia polymorpha*

The Plant Cell, 2023, koad216, <https://doi.org/10.1093/plcell/koad216>